# Experimental Investigation on Condensation Heat Transfer Coefficient and Frictional Pressure Drop of Refrigerant R1234yf on Brazed Plate Fin Compact Heat Exchanger Surfaces

A thesis submitted in partial fulfilment of the requirements for the award of the degree of

**Doctor of Philosophy**


Submitted by

**Partha Pratim Kemprai**

(Roll No: 166103003)




**Department of Mechanical Engineering**

**Indian Institute of Technology Guwahati**

**Guwahati - 781039, India**


**April 2025**

**Indian Institute of Technology Guwahati**
**Department of Mechanical Engineering**
**Guwahati – 781039, Assam, India**

## STATEMENT

This is to certify that I have carried out the research work presented in this thesis entitled "Experimental Investigation on Condensation Heat Transfer Coefficient and Frictional Pressure Drop of Refrigerant R1234yf on Brazed Plate Fin Compact Heat Exchanger Surfaces" at the Department of Mechanical Engineering, Indian Institute of Technology Guwahati and Aeronautical Development Agency, Bangalore, under the supervision of Prof. P. Muthukumar and Dr. C. Ranganayakulu.

I hereby confirm that there is no conflict of interest related to the research work and any part of this work has not been earlier submitted to any other Institute or University for the award of any other degree or diploma.

In keeping up with the general practice of reporting scientific observations, due acknowledgements have been made wherever the work described is based on the findings of other investigations.

**(Partha Pratim Kemprai)**

Roll No: 166103003
Department of Mechanical Engineering
Indian Institute of Technology Guwahati
Guwahati - 781039, Assam, India
April 2025

**Indian Institute of Technology Guwahati**
**Department of Mechanical Engineering**
**Guwahati – 781039, Assam, India**

## THESIS CERTIFICATE

This is to certify that the work contained in this thesis entitled "Experimental Investigation on Condensation Heat Transfer Coefficient and Frictional Pressure Drop of Refrigerant R1234yf on Brazed Plate Fin Compact Heat Exchanger Surfaces" submitted by Mr. Partha Pratim Kemprai (Roll. No. 166103003) for the award of Ph.D. degree, is a record of bonafide research carried out by him at the Department of Mechanical Engineering, Indian Institute of Technology Guwahati and Aeronautical Development Agency Bangalore, under our guidance and supervision. The research work in this thesis has not been submitted to any other University or Institute for the award of any other degree or diploma.

**(Prof. P. Muthukumar)**

Professor
Department of Mechanical Engineering
Indian Institute of Technology Guwahati
Guwahati - 781039, Assam, India

Currently at Department of Mechanical Engg.
Indian Institute of Technology Tirupati
Andhra Pradesh - 517619, India
April 2025

**(Dr. C. Ranganayakulu)**

Former Outstanding Scientist, Technology
Director (GS) and Director (MM)
Aeronautical Development Agency
Bangalore - 560017, India

Currently Professor at Mech. Engg. Dept.,
Birla Institute of Technology and Science
Pilani, Rajasthan - 333031, India
April 2025

*Dedicated*

*to*

*my family, friends and colleagues*

# ACKNOWLEDGEMENTS

I am profoundly grateful to my supervisor, Prof. P. Muthukumar whose sincere guidance has been instrumental in my journey of research and in successful completion of my thesis. His invaluable mentorship and unwavering support have continuously motivated me to approach challenges with critical thinking and unwavering dedication. I am fortunate to have been guided in such an academic environment, where he empowered me to explore diverse aspects of my research work. Further, his invaluable insights and ideas have motivated me forward, enabling me to persistently pursue and achieve my research objectives. His wealth of experience generously shared with me will undoubtedly serve as an invaluable asset throughout my career.

I extend my deepest gratitude to my internal research supervisor, Dr. C. Ranganayakulu, former Outstanding Scientist, Technology Director (GS) and Director (MM), ADA, Bangalore and currently Professor at BITS Pilani, for his invaluable guidance throughout my research work. I am sincerely thankful for his generosity in sparing his precious time and for consistently motivating me in successful completion of my thesis work. I also convey my sincere gratitude to Prof. Sachin Singh Gautam, DPPC Secretary (ME), for providing guidance and assistance as a coordinating supervisor.

I am grateful to my doctoral committee members, Prof. Ujjwal Kumar Saha, Prof. Vinayak Kulkarni, Prof. S. Senthilmurugan and chairperson, Prof. Amaresh Dalal for their unwavering support and encouragement throughout my PhD journey. I convey my sincere gratitude to DPPC (ME), DPPC Student rep, DPPC Secretary, members and Chairman. I deeply appreciate the Heads of Departments, past and present Office Bearers in the Department of Mechanical Engineering for providing the necessary facilities and assistance during my thesis work.

I extend my deepest gratitude to the Aeronautical Development Agency (ADA), Bangalore for providing assistance to carry out the present investigations and experiments. Grateful thanks are due to PGD (CA) & DG - ADA and Mr. Sankaraiah Mada, OS, Technology Director (GS) and Director (Admin & HR), ADA, Bangalore for permitting me to carry out the research work. I am deeply indebted to Mr. S.V.S. Srinivas and Mr. C.H. Rambabu of M/s BHEL Visakhapatnam, who has taken keen interest in developing and supplying the brazed plate fin compact heat exchangers for the experiments.

I extend my heartfelt appreciation for the continuous assistance provided to me by reporting officer at ADA, Dr. K.V. Ramana Murthy, Scientist 'F' and DPD (GS-CHE) for his constant support and proving guidance during my thesis work. The invaluable support extended by my present and past colleagues of ADA, Dr. M. Amaranatha Raju, Mr. K. Nagaraja, B. Mahesh, Atmanand C. Mugabast, Akshay Sonawane, Dilip Kumar, Sheik Mohammed Asif are also gratefully acknowledged.

I specially thank present and past fellow researcher of IIT Guwahati. I would like to thank Dr. Maryom Dabi, Dr. Sayantan Jana, Dr. Sunku J Prasad, Dr. Gurpreet Singh Sodhi, Dr. Alok Kumar, Dr. Nithin Narmada, Ms. Juri Sonowal, Ms. Dhanjita Medhi, Mr. Subham Parashar, Mr. Tat Suraj Arjun of IIT Guwahati and Mr. Vinay Negi of BITS Pilani and all the batch mates of in assisting and helping me in many circumstances to complete my thesis work

I extend my special thanks to National Aerospace Laboratories (NAL), Bangalore for granting permission to set up the test facility and enabling me to conduct the experiments effectively. I convey my sincere gratitude to Mr. E. Rajesh, Mr. Janakiram Reddy, Mr. Pandiyan, Mr. Krutik and other members of Propulsion division, NAL for their support in successful completion of experiments.

Lastly, I express my deepest gratitude and unwavering devotion to my family members for their unending support, encouragement, and boundless love. I am immensely thankful to my parents, Mr. Nakul Barman and Mrs. Chinu Barman, my sister, Mrs. Mitali Kemprai and her family, my brother, Mr. Pranab Jyoti Kemprai and his family for their unwavering belief in me and their steadfast support during challenging times. I express my deepest gratitude and thankful to my wife, Dr. Sikha Das for her unconditional support, constant encouragement, motivation, patience and sacrifices she has made throughout my research work. I am also thankful to my wife's family members, father-in-law, Mr. Sarat Chandra Das, mother-in-law, Mrs. Bina Das, brothers-in-law, Mr. Utpal, Mr. Hemen and his family members for their assistance throughout my journey. I extend my appreciation to the rest of my extended family and community outside for their encouragement and solidarity.

Sincerely,

Partha Pratim Kemprai

April 2025

# ABSTRACT

The demand for global energy consumption in the recent years has gained attention towards the enhancement of heat transfer mechanism. The requirement to meet the energy demand and heat transfer enhancement has led to the development of new and optimised heat transfer equipment. One of the major heat transfer equipment is the compact heat exchanger which plays a significant role in the thermal fluid systems of various industries. Among these, brazed plate fin type of compact heat exchanger is widely used, mostly in aerospace application because of their compactness, low weight and high effectiveness. These plate fin compact heat exchangers are also used for the phase change applications, because of their higher heat transfer performance. The advancement on compact condensers and evaporators are the major achievement towards the development of advanced heat transfer equipment. In the design and development of any heat exchanger, the primary criteria are to investigate on heat transfer and pressured drop characteristics.

Many researchers have investigated the boiling and condensation phenomenon of many user-friendly refrigerants in order to estimate their heat transfer coefficient and frictional pressure drop. Experiments on phase change heat transfer in compact heat exchangers are challenging and are also limited in literature. In recent years, many investigators have carried out the condensation experiments using an ozone-friendly refrigerant R134a (hydrofluorocarbon) inside tubes, herringbone fins, helicoidal pipe and plate heat exchangers. The refrigerant R134a is widely used as it has zero ozone depletion potential (ODP). However, due to its higher global warming potential (1400 GWP), many researchers have started switching over to low GWP HFO refrigerant R1234yf and other environmentally friendly refrigerants.

The investigation on condensation heat transfer of R1234yf mostly inside tubes, channels and micro-fins were reported by many investigators. They carried out extensive experiments and further developed suitable correlations for condensation heat transfer coefficient and frictional pressure drop. However, these correlations cannot be used directly wherein the fin geometrical parameters differ and have complex geometries. Literature survey also indicates that the investigation on condensation heat transfer and pressure drop of R1234yf in brazed plate fin compact heat exchangers with serrated and wavy fin surfaces are not available. Thus, the key aim of the present work is to investigate condensation inside the compact condenser (brazed plate fin compact heat exchanger) using suitable refrigerant R1234yf.

The primary objective of this work is to estimate the heat transfer coefficients and frictional pressure drop of refrigerant R1234yf inside a brazed plate fin compact heat exchanger with serrated and wavy fin surfaces. The other objectives are as follows: (i) establishment of test facility to investigate the condensation heat transfer and pressure drop of refrigerants R134a and R1234yf, (ii) to obtain single-phase heat transfer coefficient of water in order to estimate the refrigerant heat transfer coefficient, (iii) to carry out the condensation experiments using refrigerants R134a and R1234yf (as a substitute for R134a) for both serrated and wavy fins test condensers, and further to compare these two refrigerants results, (iv) to study the effects of mass flux and saturation temperatures on condensation heat transfer coefficient and heat flux of R1234yf, (v) to study the effect of mass flux, saturation temperature and specific kinetic energy of R1234yf on frictional pressure drop, (vi) to study the effects of fin geometrical parameters on condensation heat transfer coefficient and frictional pressure drop of R1234yf in serrated fins test condensers and (vii) to develop suitable correlations for heat transfer and pressure drop based on the experimental data of R1234yf.

The experimental investigations on condensation heat transfer and pressure drops of refrigerants R134a and R1234yf were carried out in the vapor compression system test facility. In the present test facility, the test condenser used is the cross-flow brazed plate fin compact heat exchanger. Three test condensers were considered for the present investigation, having two numbers of serrated fins type and one number of wavy fin type surfaces. All the three test condensers have different fin geometrical parameters and are manufactured by a vacuum brazing technique.

In the present investigation, the condensation heat transfer coefficient and frictional pressure drop results of refrigerants R134a and R1234yf are compared and found that the heat transfer coefficient of R134a is higher than that of R1234yf by 10 - 19 % and 9 - 16 % for serrated and wavy fins test condenser, respectively when operated under same condition. The higher thermal conductivity of R134a than that of R1234yf contributes to a higher heat transfer coefficient. It was also observed that the frictional pressure drop of R134a is higher than that of R1234yf by 14 - 19 % and 10 - 17 % for serrated and wavy fins test condenser, respectively. The lower reduced pressure of R134a than that of R1234yf contributes to a higher frictional pressure drop. In addition, the higher viscosity of the saturated liquid R134a than that of R1234yf also contributes to the higher frictional pressure drop.

# Nomenclature

| | |
|---|---|
| $A$ | heat transfer area ($m^2$) |
| $a$ | fin area to total area ratio / wave amplitude (m) |
| $C_p$ | specific heat capacity (J/kg/K) |
| $D_h$ | hydraulic diameter (m) |
| $f$ | friction factor |
| $G$ | mass flux ($kg/m^2/s$) |
| $h$ | fin height (m) / heat transfer coefficient ($W/m^2/K$) |
| $j$ | Colburn factor |
| $l$ | serration length (m) |
| $L_f$ | flow length (m) |
| $\dot{m}$ | mass flow rate (kg/s) |
| Nu | Nusselt number |
| $P$ | pressure (bar) |
| $Pr$ | Prandtl number, $Pr = \frac{\mu C_p}{\lambda}$ |
| $\dot{Q}$ | heat transfer rate (W) |
| $\dot{q}$ | heat flux ($W/m^2$) |
| $Re$ | Reynolds number, $Re = \frac{GD_h}{\mu}$ |
| $s$ | fin spacing (m) |
| $T$ | temperature (°C) |
| $t$ | fin thickness (m) |
| $U$ | overall heat transfer coefficient ($W/m^2/K$) |
| $v$ | velocity (m/s) |
| W | width |
| $x$ | vapor quality |

***Greek Symbols***

| | |
|---|---|
| $\Delta$ | difference |
| $\Delta H$ | change in enthalpy (J/kg) |
| $\beta$ | surface area density ($m^2/m^3$) |
| $\lambda$ | thermal conductivity (W/m/K) / wave length (m) |

| | |
|---|---|
| $\mu$ | dynamic viscosity (kg/m/s) |
| $\gamma$ | specific kinetic energy (J/m$^3$) |
| $\upsilon$ | specific volume (m$^3$/kg) |
| $\rho$ | density (kg/m$^3$) |
| $\eta$ | efficiency |

***Subscripts***

| | |
|---|---|
| *a* | momentum |
| *avg* | average |
| *c* | ports and manifold / cold |
| *eq* | equivalent |
| *f* | fin / frictional |
| *g* | vapor / gravity |
| *h* | hot |
| *i* | inlet |
| *l, L* | liquid |
| *m* | mean |
| *o* | outlet / overall |
| *p* | plate |
| *r* | refrigerant |
| *s* | saturation |
| *t* | total |
| *w* | water |

***Abbreviations***

| | |
|---|---|
| ASTM | American society for testing and materials |
| *avg* | average |
| CFC | chlorofluorocarbon |
| CFD | computational fluid dynamics |
| DAS | data acquisition system |
| DM | de-mineralized |
| Eq | equation |
| EEV | electronic expansion valve |

| | |
|---|---|
| FPI | fins per inch |
| FS | full scale |
| GWP | global warming potential |
| HCFC | hydro-chlorofluorocarbon |
| HFC | Hydrofluorocarbon |
| HFO | Hydrofluoroolefin |
| LMTD | logarithm mean temperature difference |
| MCB | miniature circuit breaker |
| NTU | number of transfer units |
| ODP | ozone depletion potential |
| PHE | plate heat exchanger |
| PLC | programable logic controller |
| RTD | resistance temperature detector |
| SCADA | supervisory controller and data acquisition |
| TC | test condenser |
| TEWI | total equivalent warming index |
| VFD | variable frequency drive |

# Contents

# List of figures

# List of tables

# Chapter 1

# Introduction

## 1.1 Preface

The demand for the energy has led to the exploration of various enhancement of heat transfer techniques and devices in many fields and applications. A heat exchanger is a device that is used to transfer or exchange heat between two or more fluids which are at different temperatures. The heat transfer mechanism in a heat exchanger is usually a convection in the fluid domain and conduction heat transfer in the wall separating the fluids. There are usually no external heat and work interactions that can occur in a heat exchanger. The applications of heat exchangers involve heating or cooling of a single or multi fluid streams. Heat exchangers are widely used in automobile, aerospace, cryogenic, chemical industries, process industries, oil and gas industries. Compact heat exchangers are one of the major heat transfer equipment which plays a significant role in the thermal fluid systems of various industries. Among the compact heat exchangers, brazed plate fin type is mostly preferred and widely used in aerospace application because of their compactness, low weight and high effectiveness. These types of brazed plate fin compact heat exchangers are also employed for the phase change applications. The advancement towards compact condensers and evaporators are the major development of heat transfer equipment. These phase change compact heat exchangers gained wide popularity and are employed in many industrial applications. In this chapter, the classification of heat exchangers based on various configurations are presented. The different types of heat transfer fins, material used and general manufacturing process of brazed plate fin compact heat exchangers are also described.

## 1.2 Classification of heat exchangers

Heat exchangers are classified based on the different parameters such as transfer processes, degree of compactness, flow arrangements and construction features. Based on the various requirements and applications, heat exchangers are classified (Mueller, 1973) as follows:

1) Classification according to the transfer process:
    a) Indirect contact type
    b) Direct contact type
2) Number of fluids:
    a) Two fluids
    b) Three fluids
    c) N-fluids ($N > 3$)
3) Construction features:
    a) Tubular
        i) Double pipe
        ii) Shell and tube
        iii) Spiral tube
    b) Plate type
    c) Extended surface
        i) Plate fin type
        ii) Tube fin
    d) Regenerative
4) Surface compactness:
    a) Compact
    b) Non compact
5) Flow arrangements
    a) Single pass
        i) Parallel flow
        ii) Counter flow
        iii) Cross flow
    b) Multi-pass
        i) Extended surfaces
        ii) Shell and tube

As weight, size and space remains the main constraint mostly for the various industrial applications, like automobile and aerospace sectors, compact heat exchangers are widely preferred because of their compactness as compared to other conventional heat exchangers. The design and development of compact heat exchanger strongly depends on the heat transfer and pressure drop characteristics. Many investigators have expressed these characteristics in terms of Colburn factor *'j'* and Fanning friction *'f'* factor, for the suitable range of Reynolds number (*Re*). Decades ago, the availability of Colburn factor *'j'* and friction *'f'* factor data for the various fin geometries of heat exchanger and for different fluids medium were limited in open literature though Kays and London (1964), Shah and Sekulic (2003) and London and Shah (1968) carried out extensive research work and developed the suitable correlations for many fin geometries. But in recent years, Hwang et al. (2006), Kim et al. (2006), Sheik Ismail et al. (2009), Chennu and Paturu (2011), Fernández-Seara et al. (2013), Ramana Murthy et al. (2015), Amaranatha Raju et al. (2015) and many others have derived generalised correlations for the various fin geometries for single-phase heat transfer applications, which have made the development of compact heat exchanger more practical.

Furthermore, in the last few years, phase change application that involves boiling and condensation heat transfer are significantly growing and have received more attention due to the higher effectiveness as compared to single-phase heat transfer mechanism. There has been increasing interest to characterize the boiling and condensation heat transfer and their pressure drops in different types of heat exchangers for various thermal fluid system in refrigeration, air-conditioning, and cryogenic applications. It was found that only limited studies were reported on phase change boiling and condensation, when compared to the single-phase heat transfer mechanism. Further, studies reported on the compact heat exchangers like compact evaporators and condensers are also very limited in the literature. The development of any design correlations for the compact heat exchangers require an accurate data base for the various geometrical surfaces and fins configuration. The unavailability of correlations for various fins geometries and fluid mediums are the reason for limited usage of compact heat exchangers in various applications.

In the phase change heat transfer mechanism and also towards the environmentally friendly aspect, the selection of refrigerant plays a significant role. Many researchers have used various refrigerants to best suit their applications. The environmental concerns imposed over ozone layer depletion and global warming have brought the refrigeration industries to come up with environmentally friendly refrigerants. The refrigerant R134a is widely employed which have

zero Ozone Depletion Potential (ODP). However, due to the higher Global Warming Potential (GWP) features of R134a, many other friendly refrigerants with lesser GWP are being considered in many industries. The HFO refrigerants like R1234yf and R1234ze have relatively lower GWP. The other important parameters that are considered while selecting a suitable refrigerant are the Total Equivalent Warming Impact (TEWI), toxicity, flammability, compatibility, leak detection, etc.

## 1.3 Compact heat exchanger

A heat exchanger that has heat transfer surface area per unit volume (surface area density, $\beta$) greater than 700 $m^2/m^3$ is called as compact heat exchanger (Shah and Sekulic, 2003). As a result of the compactness, compact heat exchangers have reduced size, weight, supporting structure, lower space requirement for installation and also a lower manufacturing cost comparatively in some cases. In general, the shell and tube have a lower surface area density, typically less than 100 $m^2/m^3$ (Shah and Sekulic, 2003). The type of compact heat exchangers can be of plate fin type, tube fin or matrix type. The design and development of compact heat exchanger strongly depends on the heat transfer and pressure drop characteristics.

Many investigators (Kays and London, 1964; Manglik and Bergles, 1995; London and Shah, 1968) have expressed the heat transfer and pressure drop characteristics in terms of Colburn factor *'j'* and friction *'f'* factor, respectively for the suitable range of Reynolds number (*Re*). The extensive research work on Colburn factor *'j'* and friction *'f'* factors for the various fin geometrical parameters of heat exchanger were carried out by authors (Kays and London, 1964; London and Shah, 1968). They also developed and reported the suitable correlations for various fin geometries. Further the availability of these generalised correlations for various fin geometrical parameters have made the development of compact heat exchanger more practical. Additionally, in recent years, there have been increasing interest by many researchers (Ranganayakulu and Kabelac, 2015; Vaisi et al., 2022; Amaranatha Raju et al., 2017; Ramana Murthy et al., 2017 and many others) to investigate phase change boiling and condensation heat transfer in brazed plate fin compact heat exchangers. Boiling and condensation heat transfer as compared to single-phase heat transfer in plate fin compact heat exchangers have received more attention in thermal fluid systems of many industries due to the higher effectiveness. The design data on boiling and condensation heat transfer inside a brazed plate fin compact heat exchanger is also limited in literature as compared to the single-phase heat transfer mechanism in these type of heat exchangers.

In the phase change heat transfer mechanism, selection of refrigerant plays a significant role in the thermal fluid system and also towards the environment. For many years, use of chlorofluorocarbons (CFCs) and hydro-chlorofluorocarbons (HCFCs) as refrigerants were found extensively in various heat transfer applications across the world. However, the use of these refrigerants has been barred according to the Montreal Protocol and were later replaced by hydro-fluorocarbons (HFCs) that has zero ozone depletion potential (ODP). The HFC refrigerant R134a was then considered as a long-term substitute for CFC refrigerant R12. However, due to the higher Global Warming Potential (GWP) of R134a, it is being replaced by hydrofluoroolefin (HFO) refrigerant R1234yf and other natural refrigerants like ammonia and hydrocarbons. There have been studies on condensation of HFO refrigerant R1234yf in tubes, channels, micro-channels and plate heat exchangers. However, there is a lack of design data and its correlations for brazed plate fin compact evaporators and condensers using HFO refrigerant R1234yf. Therefore, in the present study, the primary focus is on the generation of design data and development of suitable correlations for the brazed plate fin compact heat exchangers using refrigerant R1234yf for the various fin configurations.

## 1.4 Plate fin compact heat exchanger

Plate fin type compact heat exchanger consists of corrugated fin layers, separating / parting sheets, headers and sidebars as shown in Fig. 1.1. The hot and cold fluids passing through the corrugated fins exchange heat through the separating sheets. The end parts of the corrugated fin layers are covered by the sidebars. In generally, these fin corrugations, sidebars and separating / parting sheets are brazed together to formed the heat exchanger core. The header, inlet and outlet connectors / ports are then welded to the brazed core to obtained a full size assembled heat exchanger. A schematic representation of plate fin compact heat exchanger is illustrated in Fig. 1.1 below.

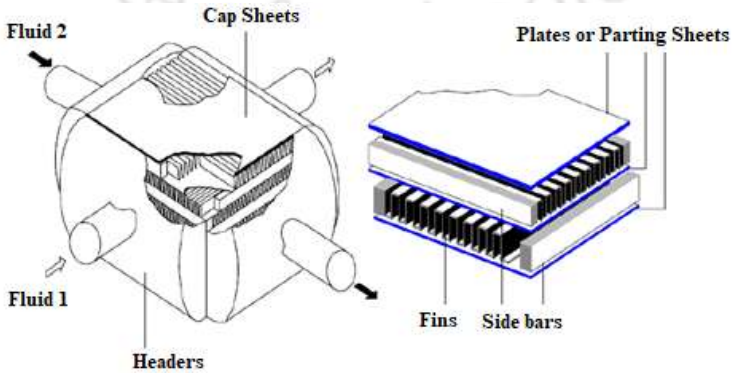


Fig. 1.1. Plate fin heat exchanger assembly (Maiti, 2002)

### 1.4.1 Fin geometries

The different types of fin geometries used in a plate fin compact heat exchanger is illustrated in Fig. 1.2. The most common fin configurations of plate fin compact heat exchanger used are plain rectangular fins, plain triangular fins, trapezoidal fins, wavy fins, serrated or offset strip fins, louvered fins and perforated fins (Maiti, 2002).

1. Uninterrupted fins
   a) Plain fins
      i) Rectangular fins, ii) Triangular fins and iii) Trapezoidal fins
   b) Wavy fins
2. Interrupted fins
   a) Serrated or offset strip fins, b) Louvered fins, c) Perforated fins and d) Pin fins

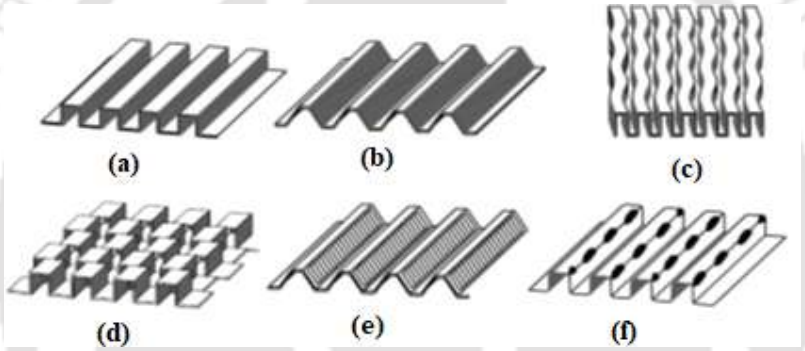


Fig. 1.2. Types of fin geometries: a) Plain rectangular fin, b) Plain trapezoidal fin, c) Wavy fin, d) Serrated or offset strip fin, e) Louvered fin, and f) Perforated fin (Maiti, 2002)

Plain fins are straight rectangular, triangular or trapezoidal fins that are continuous in the fluid flow direction. Typically, these types of fins having rectangular, trapezoidal or triangular shapes are less critical during manufacturing and not that challenging. Plain fins have lower heat transfer performance and lower core pressure drop. Wavy fins are uninterrupted type of fin surfaces which are closely similar to those of plain fins. However, along the fluid flow direction, the geometry of these fins is wavy. This nature of wavy geometry creates disturbance along the fluid path and have better performance than plain fins. Serrated fins surfaces are defined by the interrupted fluid flow surfaces along the fluid flow path. These types of interrupted serrated fins are widely used in many heat exchangers. Serrated fins have very high heat transfer performance and also have a relatively higher pressure drop as compared to wavy and plain types of fins due to their periodic nature of interruptions in the fluid flow direction.

Further, the louvered fin geometry behaves quite similar to the serrated fins. In this type of fin, small segments of the fins are slit at an angle of 20 to 45 degrees relative to the fluid flow direction. The base surface of the louvered fin geometry is generally triangular or rectangular in shape. Louvered type of fins are also extensively used in automobiles sectors. One more type of interrupted fins is perforated fins that have pattern of spaced holes in the fin along the flow path directions. The shape of the perforated channels is either triangular or rectangular. Perforated fins have the heat transfer performance relatively better than that of plain fins.

### 1.4.2 Flow arrangement

In the brazed plate fin compact heat exchangers, various flow arrangements are considered which can be either single pass or multi pass fluid streams. The direction of fluid flow passage in the heat exchanger can be parallel or perpendicular to each other and depends on various factors and parameters like performance, pressure drop, size and accessibility. The different types of flow arrangements considered in the plate fin heat exchangers are: (i) parallel flow (ii) counter flow, (iii) cross flow and (iv) cross-counter flow. Among these heat exchangers, the counter flow arrangement has the highest effectiveness while the parallel flow arrangement has the lowest heat transfer performance. However, the cross-counter flow arrangement has relatively higher core pressure drop across the heat exchanger as compare to the parallel flow arrangement. The cross flow arrangement has the intermediate performance in terms of heat transfer and also provides easier structural accessibility as compared to other types of arrangement. Thus, the optimum selection of any type of flow arrangement is based on the user requirement and its application. The schematic of different types of flow arrangements are shown in Fig. 1.3.

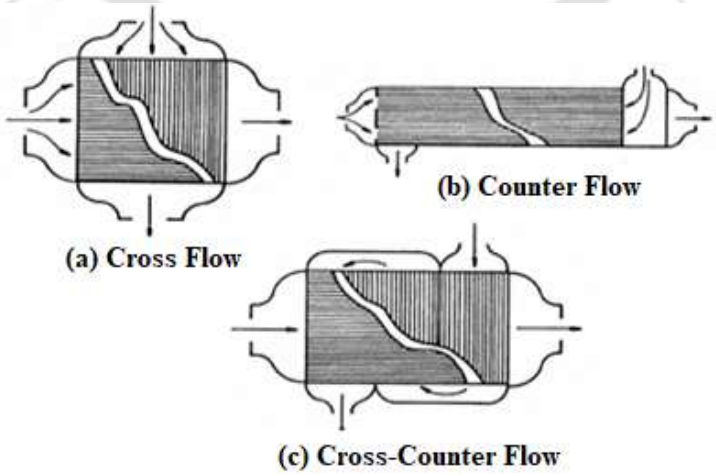


Fig. 1.3. Heat exchanger flow arrangements (Maiti, 2002)

### 1.4.3 Materials selection

Aluminium is the most preferred material for heat exchanger manufacturing, in the cryogenic and aerospace applications because of its low density, high thermal conductivity and higher strength at low temperature. The materials preferred for the application in higher temperature range up to 600 °C are stainless steels, inconel, nickel and copper alloys. The material selection of plate fin compact heat exchanger is based on many factors, as listed below:

a) Operating temperature
b) Operating pressure
c) Operating environment
d) Easy fabrication
e) Corrosion resistance
f) Mechanical strength
g) Physical properties
h) Surface aspects
i) Availability
j) Applicable cost

### 1.4.4 Manufacturing process

The basic manufacturing processes of brazed plate fin heat exchanger are same for all the sizes, materials and applications. The fin corrugations, sidebars, separating sheets are held together in a dedicated fixture under a predefined load and place inside the furnace. The assembly is then brazed together to obtain the heat exchanger core. The header, inlet and outlet connectors are then welded to the core to obtain the full-size heat exchanger. The common brazing process used are salt bath brazing and vacuum brazing (Maiti, 2002).

In salt bath brazing process, the stacked assembly is preheated in a furnace and then dipped into a bath of fused salt, mainly composed of fluorides or chlorides of alkali metals. The bath temperature is raised above the melting point of the brazing alloy that leads to the brazing of the heat exchanger. In the vacuum brazing process, no flux or separate pre-heating furnace is required. The assembled stacked is heated to brazing temperature in the vacuum brazing furnace to obtain the heat exchanger core. The absence of oxygen in the furnace is ensured by maintaining the pressure of $10^{-6}$ mbar approximately. Many materials, such as aluminium, stainless steel, copper and nickel alloys can be brazed satisfactorily using vacuum brazing.

### 1.4.5 Applications

Brazed plate fin compact heat exchangers are widely used in various thermal fluid system due to their compact size and higher performance, as compared to other conventional heat exchangers. Phase change compact condensers and evaporators are also being used in various industries and have a widespread application from the user perspective. There are various advantages of using brazed plate fin compact heat exchangers and the significant parameters commonly considered are as follows:

1. Large heat transfer surface area per unit volume
2. High thermal effectiveness
3. Low weight and reduced space
4. Multi-stream operation

The disadvantages of the brazed plate fin compact heat exchanger are as follows:

1. Limited range of temperature and pressure.
2. Difficulty to clean the flow passages, which limits its application.
3. Difficulty to repair in case of failure or even leakage, which is costly aspect.

## 1.5 Single-phase heat transfer

In the literature, it was observed that significant single-phase data are available on the design and performance of brazed plate fin compact heat exchangers for various fin configurations. The single-phase parameters available are in terms of Colburn factor *'j'* and fanning friction *'f'* factor for heat transfer and pressure drop, respectively in these plate fin compact heat exchangers. One of the earliest established findings is reported by Kays and London (1964) on the experimental Colburn factor *'j'* and friction *'f'* factor data of plate fin compact heat exchangers. They performed the single-phase experiments and reported the results for 3 wavy fins and 21 strip fins configurations. Their empirical correlations have been extensively used for various applications, which involves lesser critical designs.

However, in the recent trends, it is being noticed that the phase change heat transfer in brazed plate fin compact heat exchanger is gaining popularity as the effectiveness and performances are higher. However, there has been still single-phase plate fin compact heat exchangers, that has been preferred and employed in many areas. The usage and mechanism of single-phase applications are much simpler when compared to the phase change applications.

## 1.6 Phase change heat transfer

Boiling and condensation have the convective heat transfer mechanism that comprise of phase change from liquid to vapour and vapour to liquid, respectively. For a given pressure, boiling phenomena occurs as the temperature of a liquid is raised to the saturation temperature of the liquid and condensation occurs as the temperature of a vapor is lowered to the saturation temperature. Both boiling and condensation phenomena exhibit large heat transfer rates. Typically, heat transfer rates associated with phase change boiling and condensation are much higher than with single-phase heat transfer rates. In the literature, decades ago, available design data on boiling and condensation were much limited, when compared to the data of single-phase mechanism. However, in recent years, there has been numerous studies where phase change applications are widely preferred. The usage of compact heat exchanger in phase change applications is also witnessed in recent trends, which leads to the development of compact evaporators and condenser. In the phase change application, towards the development of evaporators and condensers, many investigators have used various refrigerants as fluid medium to carry out their investigation on boiling and condensation. One of the primary objectives of this present study is to contribute towards the development of compact condenser using a suitable refrigerant. The estimation of heat transfer coefficient and frictional pressure drop during condensation of refrigerant constitutes the important parameters towards the design and development of compact condenser.

Condensation heat transfer is described generally as follows: i) film condensation and ii) dropwise condensation. In general, condensation heat transfer that normally occurs in nature are described by film condensation. In the event of film condensation, the condensate forms a liquid film on the surface and then slides down along the surface under the effect of gravity. As a result of continuous condensed vapor, the thickness of the liquid film increases in the flow direction. The surface during film condensation is covered by a liquid film of increasing thickness and this film thickness acts as a resistance to heat transfer. However, in the dropwise condensation, the condensed vapor forms liquid droplets on the surface. As a results, the size of the droplets grow at the surface as more vapour condenses. After certain time, when droplet attains maximum size, it gets separated from the surface and in the process removes the other droplets of smaller sizes from the surface. This continuously expose the surface to the vapor instead of liquid film and thus heat transfer resistances are lower. As a result, the dropwise condensation heat transfer rates are much higher than film condensation. However, in practice,

dropwise condensation is much more difficult and challenging to achieve. Therefore, typically, during the design of heat transfer equipment, film condensation phenomena is assumed and considered.

## 1.7 Refrigerants

Refrigerants have been playing a significant role in thermal fluid systems for many industries. It has been continuously evolving based on the various guidelines and protocols. Decades ago, the chlorofluorocarbons (CFCs) refrigerants like R12 have been very popular and widely used due to their stability, low toxicity, and low flammability. However, these types of refrigerants have a very high ozone depletion potential (ODP), although they have the excellent thermal properties. Eventually, CFC refrigerants were phased-out as these caused depletion of the ozone layer. Later, hydrochlorofluorocarbons (HCFCs) like R22 have evolved as they have a smaller effect on the ozone layer. But HCFCs have other issue like the growing of global warming potential (GWP) of these fluids. Subsequently, hydrofluorocarbons (HFCs) refrigerants like R134a have been developed but eventually eliminated due to their high GWP. Due to these various factors, natural refrigerants are being considered again as a suitable alternative. Toxicity and flammability of these refrigerants are the major concerns, for which various approaches are being employed. Further, HFO refrigerant like R1234yf plays an emerging role in recent years, as this refrigerant has a very low GWP value and tend to be environmentally friendly refrigerant. These HFO refrigerants are already in use in many countries, basically in the automobile sectors. These refrigerants play an effective role in meeting the global energy demand and scope in many industries.

In the literature, there has been works reported on condensation and boiling of the refrigerant R134a inside tube, helicoidal pipes, mini-channels and plate heat exchanger. Further, it is also observed that the studies on condensation heat transfer are more limited as compared to the boiling in brazed plate fin compact heat exchanger. In addition, the condensation study of low GWP refrigerant R1234yf is also limited in compact heat exchangers design and the works available are mostly for the tubes, channels and micro-fins. The condensation experiments using refrigerant R1234yf in the test sections were performed by many investigators and they developed empirical correlations for refrigerant heat transfer coefficient and frictional pressure drop. However, these condensation and pressure drop correlations cannot be used directly wherein the fin geometries and parameters are different. Literature survey also indicates that the work reported on condensation heat transfer of refrigerant R1234yf inside a brazed plate

fin compact heat exchangers with serrated and wavy fin surfaces are not available. Based on this limitation and literature gaps, the condensation study has been conducted to estimate the heat transfer coefficient and frictional pressure drop of R1234yf in a brazed plate fin compact heat exchanger. The heat transfer and pressure drop characteristics are the important parameters towards the design and development of any compact condenser.

## 1.8 Motivation of the thesis work

The development and evolution of heat transfer equipment plays a significant role in meeting the global energy demand. The phase change application using conventional condenser and evaporators are evident in extracting maximum energy in thermal fluid systems of refrigeration industries. Further, there is a need to develop compact condenser and evaporator using suitable environment friendly refrigerant, to obtain the optimum outcome that can be used in wide areas of industries. The enhancement of heat transfer in compact heat exchangers also depends on the types of fin geometries used. In the present work, the primary aim is to conduct condensation experiments using the low GWP refrigerant R1234yf inside a plate fin compact heat exchanger with serrated and wavy fins.

Further, in the development of any heat exchanger, the main criteria is the generation of design parameters in terms of heat transfer coefficient and frictional pressure drop. Literature survey indicates that works reported on condensation heat transfer of R1234yf in a brazed plate fin compact heat exchangers are not available with serrated and wavy fin surfaces. Thus, considering many important aspects and gap from the literature, the objective of the present thesis work is focussed on the estimation of condensation heat transfer coefficient and frictional pressure drop of R1234yf inside brazed plate fin compact heat exchangers with serrated and wavy fins surfaces.

## 1.9 Thesis structure

The main scope of the present thesis is the experimental investigation on condensation heat transfer and pressure drop inside a brazed plate fin compact heat exchanger with serrated and wavy fin surfaces. The thesis is organized into seven chapters.

Chapter 1 starts with the brief introduction of heat exchanger, its classification and applications. In this chapter, brief explanation of compact heat exchangers, condensation heat transfer techniques and explanation on present scope of work are presented. This chapter also presents the various types of fin geometries used in compact heat exchangers. The heat transfer

mechanism used for the single-phase and phase change applications are discussed. The various types of refrigerants used and their advantages are also presented. The evolution of compact condensers in the refrigeration industries are also discussed.

Chapter 2 presents the state-of-art on single-phase heat transfer and pressure drop characteristics in compact heat exchangers. The phase change heat transfer and pressure drop characteristics of various refrigerants in tubes, mini-channels, micro-fins, pipes and compact heat exchangers are presented. Further, the correlations proposed and reported by many investigators related to single-phase and phase change applications are presented. The various gaps found in the literature on condensation research are also discussed and the primary objectives of the present investigations are presented in this chapter.

Chapter 3 describes the numerical analysis performed using ANSYS Fluent to estimate the single-phase heat transfer coefficient of water ($h_w$) for both serrated and wavy fin surfaces. Based on the numerical data, the suitable correlations for the heat transfer coefficients of water are derived and presented in this chapter for both serrated and wavy fin surfaces. Further, the single-phase water to water experiments were performed to estimate the heat transfer coefficient of water in two test sections, one with serrated fins and other with wavy fins. The estimated heat transfer coefficient of water was further used to estimate the refrigerant heat transfer coefficient ($h_r$). The single-phase energy balance is also described in this chapter.

Chapter 4 presents the establishment of experimental facility, which is used to investigate the condensation heat transfer and pressure drop characteristics of refrigerants R134a and R1234yf inside test condenser with serrated and wavy fin surfaces. This chapter also describes the various circuits that are used to circulate refrigerant and DM water. It also discusses the description of all the other major components and measuring instruments, integrated in the test facility. The experimental procedures and approach to carry out the condensation experiments are also described in this chapter.

Chapter 5 describes the data reduction and methodology employed, to estimate the condensation heat transfer coefficient ($h_r$) and frictional pressure drop ($\Delta P_f$) of refrigerants R134a and R1234yf inside a brazed plate fin compact heat exchanger with serrated and wavy fins. The experiments were carried out for the saturated vapour conditions of refrigerant at different refrigerant mass flux and saturation temperatures.

Chapter 6 presents the experimental results obtained on the condensation heat transfer coefficient and frictional pressure drop of refrigerant inside brazed plate compact heat

exchanger with serrated and wavy fin surfaces. The experimental investigations were performed on three test condensers, having two with serrated fins and one with wavy fin surfaces. Further, the effects of mass flux ($G_r$) and saturation temperature ($T_s$) on condensation heat transfer coefficient and frictional pressure drop of refrigerant R1234yf are presented in this chapter. The suitable heat transfer coefficient and frictional pressure drop correlations for serrated and wavy fins surfaces were proposed for refrigerant R1234yf. This chapter also describes the significance of fin geometrical parameters on condensation heat transfer coefficient and frictional pressure drop of R1234yf.

Chapter 7 brings the major conclusions achieved from the present investigation on condensation heat transfer and pressure drop of refrigerants R134a and R1234yf in brazed plate fin compact heat exchanger with serrated and wavy fin surfaces. The effect of refrigerant mass flux, saturation temperatures and hydraulic diameters on condensation heat transfer coefficient and frictional pressure drop are presented. The scope of future work and recommendations are also presented in this chapter.

## 1.10 Summary

The chapter started with brief introduction which describes the enhancement of heat transfer mechanism and various types of heat transfer equipment. The main emphasis was made on the compact heat exchangers and their application in various industries. The heat transfer mechanism that involves single-phase and phase change applications are discussed. In this chapter, the evolution of various heat transfer equipment, compact condensers and usage of various refrigerants in thermal fluid systems are also discussed. This chapter further presents the various fin geometries employed in the brazed plate fin type compact heat exchangers. Finally, the motivation of the thesis work, thesis structure and its main objectives are discussed and presented in this chapter.

# Chapter 2

# State of the Art: Literature Review

## 2.1 Preface

In recent years, the development of compact heat exchangers has evolved comprehensively for different fluid medium with improved process, techniques, applications and materials. The primary idea remains the enhancement of heat transfer to meet the rising global energy demand. Due to its compactness, the compact heat exchangers are preferably used in variety of industries, especially in automobile and aerospace sectors. The usage of these compact heat exchangers in any system leads to reduce weight, size and shape. In contemporary times, compact heat exchangers like compact condensers and evaporators are preferred in the phase change applications, mainly due to their higher effectiveness, higher thermal efficiencies, small sizes, low weight, design flexibility and energy savings. Brazed plate fin compact heat exchangers are highly compact in nature, thus the required heat transfer surface area is smaller than those required by other conventional heat exchangers.

Several studies on single-phase heat transfer are reported in the literature, while studies on phase change heat transfer are limited for various heat transfer equipment. It is more challenging to obtain the design parameters and to develop suitable correlation for phase change heat transfer as compared to the single-phase heat transfer. Due to the adverse effects caused by the chlorofluorocarbons (CFC) refrigerants to the ozone layer, and due to the higher global warming potential (GWP) caused by hydrofluorocarbons (HFC) refrigerants, many researchers are looking forward to the environmentally friendly refrigerants and natural refrigerants. However, it has also been observed that there have been very few studies in the

literature reporting on phase change heat transfer in compact heat exchangers. In this chapter, a detailed literature survey has been carried out on the single-phase heat transfer and pressure drop characteristics in compact heat exchangers. In addition, this chapter also presents the phase change heat transfer and pressure drop characteristics of various refrigerants employed in compact heat exchangers, tubes, mini-channels and micro-channels.

## 2.2 Single-phase heat transfer and friction factor

There have been numerous numerical as well as experimental research works on single-phase heat transfer in compact heat exchangers reported in the literature. The Colburn *'j'* factor and fanning friction *'f'* factor are the parameters that predicts the heat transfer and pressure drop characteristics, respectively. In the literature, significant single-phase data are available on the design and performance of plate fin compact heat exchangers for various fin configurations. One of the earliest established findings was reported by Kays and London (1964) on the experimental Colburn *'j'* factor and friction factor *'f'* data of plate fin compact heat exchangers. They performed the single-phase heat transfer experiments and presented the results for 3 wavy fins and 21 strip fins configurations. Their empirical correlations have been extensively adopted in the industry, particularly that requires lesser critical designs.

Kays (1972) reported an analytical model using air medium that was carried out to estimate the heat transfer and friction loss in offset strip fins. He proposed a laminar boundary layer solution that includes the finite drag contribution of the blunt fin edges. However, his correlations take the effects of fin thickness ($t$) and serration length ($l$) but does not take into consideration the fin spacing ($s$) and fin height ($h$). He proposed the following correlations for Colburn *'j'* factor and friction *'f'* factor in terms of Reynolds number ($Re_l$), which was estimated based on fin length:

$$j = 0.665(Re_l)^{-0.5} \tag{2.1}$$

$$f = 0.44\left(\frac{t}{l}\right) + 1.328Re_l^{-0.5} \tag{2.2}$$

Wieting (1975) proposed an empirical relation by correlating the experimental heat transfer and flow friction data for 22 offset-fin plate fin configurations over the range of two Reynolds number, $Re_{Dh} < 1000$ and $Re_{Dh} > 2000$. He further suggested extrapolating the equations up to the intersection point to predict the '*j*' and '*f*' factors in the transition region ($1000 < Re_{Dh} < 2000$). The proposed correlations are expressed as follows:

For $Re_{Dh} \leq 1000$

$$j = 0.483\left(\frac{l}{D_h}\right)^{-0.162} \alpha^{-0.184} Re_{Dh}^{-0.536} \quad (2.3)$$

$$f = 7.661\left(\frac{x}{D_h}\right)^{-0.384} \alpha^{-0.092} Re_{Dh}^{-0.712} \quad (2.4)$$

And for $Re_{Dh} \geq 2000$

$$j = 0.242\left(\frac{l}{D_h}\right)^{-0.322} \left(\frac{t}{D_h}\right)^{0.089} Re_{D_h}^{-0.368} \quad (2.5)$$

$$f = 1.136\left(\frac{l}{D_h}\right)^{-0.781} \left(\frac{t}{D_h}\right)^{0.534} Re_{D_h}^{-0.198} \quad (2.6)$$

where, *l* represents the fin length in flow direction and $\alpha$ is the *s/h* ratio

The above correlations were determined using the best possible fit in the weighted least squares method. He carried out experiments and derived correlations from experimental data using air as a working fluid. Hence, he has mentioned that the applicability of the correlations to fluids other than the gas, may lead to error, due to the varying range of Prandtl number. He indicated that the correlations are useful only for air or gas as fluid medium and further should be extrapolated only for the limited range of parameters. The effect of fin length, height, thickness, spacing and hydraulic diameter on the performance could be assessed and analyzed using the correlations.

Sparrow et al. (1977) carried out numerical analysis to compute the local heat transfer and pressure drops results in channels whose wall are periodically interrupted along the fluid flow passage. They mentioned that these high-performance channels were employed in compact heat exchangers. The Prandtl number considered in their analysis was 0.7. They plotted the Colburn factor '*j*' and the friction *'f'* factor on log-log plot for the overall heat transfer and pressure drop results as a function of a hydraulic diameter and Reynolds number. Their analytical results were represented by the Colburn factor '*j*' and the friction *'f'* factor, as given in the following expressions:

$$j = 3.92(Re_{Dh})^{-0.792} \quad (2.7)$$

$$f = 9.60(Re_{Dh})^{-0.792} \quad (2.8)$$

Joshi and Webb (1987) reported the analytical models for the prediction of heat transfer coefficients and the friction factor of the offset strip-fin surface geometry of the heat exchanger. They developed the empirical correlations to calculate the heat transfer coefficient and friction factor. Their correlations were the modified version of Wieting (1975) with the inclusion of fin ends area. Their correlations achieved within ± 15 % for the overall 82 % of the '*f*' data and 91 % of the '*j*' data. The authors developed analytical models, that were considered for the prediction of '*j*' and '*f'* characteristics. Further, to predict the behaviour in the transition region, the authors also described the transition point Reynolds number represented by *Re**. Thus, they identified the different regions of fluid flow in terms of laminar, turbulent, and transition regions. Based on their experimental findings, they have developed the correlations for '*j*' and '*f'* for the defined laminar and turbulent flow region as $Re \leq Re^*$ and $Re \geq (Re^* + 1000)$, respectively for the 21 geometries. The correlations of '*j*' and '*f'* are given below:

For $Re \leq Re^*$

$$j = 0.53(Re_{Dh})^{-0.50}\left(\frac{l}{D_h}\right)^{-0.15}\alpha^{-0.14} \tag{2.9}$$

$$f = 8.12(Re_{Dh})^{-0.74}\left(\frac{l}{D_h}\right)^{-0.41}\alpha^{-0.02} \tag{2.10}$$

And for $Re \geq (Re^*+1000)$

$$j = 0.21(Re_{Dh})^{-0.40}\left(\frac{l}{D_h}\right)^{-0.24}\left(\frac{t}{D_h}\right)^{0.02} \tag{2.11}$$

$$f = 1.12(Re_{Dh})^{-0.36}\left(\frac{l}{D_h}\right)^{-0.65}\left(\frac{t}{D_h}\right)^{0.17} \tag{2.12}$$

here,

$\alpha$ represents aspect ratio *s/h*.

$$D_h = 2(s-t)h/[(s+h)+th/l] \tag{2.13}$$

$$Re^* = 257\left(\frac{l}{s}\right)^{1.23}\left(\frac{t}{l}\right)^{0.58}D_h\left[t + 1.328\left(\frac{Re}{lD_h}\right)^{-0.5}\right]^{-1} \tag{2.14}$$

Mochizuki et al. (1987) carried out the experimental study on the scale-up model of interrupted fin surfaces in compact heat exchangers. They developed 18 test cores with different fin geometries for the experiments. They considered three types of interrupted surfaces for

experiments namely plain straight fins, offset fins and slotted fins. They reported that in offset strip fin cores, both *'j'* and *'f'* factors are enhanced in the fin length for a given Reynolds number. They further presented their comparison made on the three types of interrupted surfaces. They found that the offset fins have yielded the best performance, when compared to other two fin types. The correlations given by them are as follows:

For $Re < 2000$

$$j = 1.37\left(\frac{l}{D_h}\right)^{-0.25} B^{-0.184} Re^{-0.67} \tag{2.15}$$

$$f = 5.55\left(\frac{l}{D_h}\right)^{-0.32} B^{-0.092} Re^{-0.67} \tag{2.16}$$

And for $Re \geq 2000$

$$j = 1.17\left(\frac{l}{D_h} + 3.75\right)^{-1}\left(\frac{t}{D_h}\right)^{0.089} Re^{-0.36} \tag{2.17}$$

$$f = 0.83\left(\frac{l}{D_h} + 0.33\right)^{-0.5}\left(\frac{t}{D_h}\right)^{0.534} Re^{-0.20} \tag{2.18}$$

here,

$$B = (a - t)/s \text{ and a is the traverse pitch of fins} \tag{2.19}$$

$$D_h = 2sh/(s + h) \tag{2.20}$$

Manglik and Bergles (1995) analysed the heat transfer and friction factor data for 18 offset strip fin surfaces. The effect of fin geometrical parameters ($\alpha$, $\delta$ and $\gamma$) along with Reynolds number were also presented in their study. They developed correlations that describe the asymptotic behaviour of the data in the deep laminar and fully turbulent regions. These asymptotes have been combined to form single predictive correlations for Colburn factor '$j$' and friction '$f$' factor, which are given by following expressions:

$$j = 0.6522Re^{-0.5403}\alpha^{-0.1541}\delta^{0.1499}\gamma^{-0.0678} \times [1 + 7.669 \times 10^{-5}Re^{1.340}\alpha^{0.504}\delta^{-0.456}\gamma^{-1.055}] \tag{2.21}$$

$$f = 9.624Re^{-0.7422}\alpha^{-0.185}\delta^{0.3053}\gamma^{-0.2659} \times [1 + 7.669 \times 10^{-8}Re^{4.429}\alpha^{0.920}\delta^{3.767}\gamma^{0.236}] \tag{2.22}$$

here, $\alpha$, $\delta$ and $\gamma$ are given by aspect ratio *s/h, t/l and t/s,* respectively.

Their derived equations for '*j*' and '*f*' factors correlate the experimental data of the 18 test cores within ± 20 %. These equations rightly predict the heat transfer and pressure loss behaviour of offset strip fins in laminar, transition and turbulent flow regimes. However, they further mentioned that, particularly for liquids, more data should be included to extend the limit and validity of these correlations.

Ranganayakulu and Seetharamu (1999) presented the finite element analysis on a compact tube fin heat exchanger. Their studies involved the combined effects of one-dimensional longitudinal heat conduction through the heat exchanger wall, non-uniform inlet fluid flow and temperature distributions on both hot and cold fluid sides. The authors generated fluid flow / temperature distribution models to calculate the heat exchanger effectiveness for the operating conditions of the heat exchanger. The range of parameters considered by them for the investigation were: $1 \leq NTU \geq 50$, $C_{min}/C_{max} = 1$, 0.6 and 0.2. The heat conduction parameters considered by them were 0.05, 0.1 and 0.2. They analysed and reported in their studies the combined effects of longitudinal heat conduction, fluid temperature and flow non-uniformity in cross tube fin heat exchanger.

Maiti (2002) carried out an extensive numerical investigation on the heat transfer and flow friction characteristics in plate fin compact heat exchanger surfaces with plain, wavy and offset strip fins. The numerical data obtained for plain and offset strip fins were correlated successfully by the best possible curve fitting using pure power law expressions. The indices of the dimensionless geometrical factors in wavy fin geometry were expressed as the simple polynomials of Reynolds number. They presented in their study the dependency on Colburn '*j*' factor and fanning friction '*f*' factor with varying Reynolds number and dimensionless fin geometrical parameters. They have developed different sets of heat transfer and pressure drop correlations for plain, wavy and offset strip fins surfaces and proposed for use in the design and development of heat exchanger.

Hwang et al. (2006) performed experimental study on measurements of local heat / mass transfer coefficient using naphthalene sublimation technique in wavy ducts having a rectangular cross section used in compact heat exchangers. They studied the effects of the flow velocity on the local heat / mass transfer inside wavy ducts. They performed the numerical analysis using the Fluent software to predict the pattern of flow inside wavy ducts. They reported that for the lower Reynolds number range lesser than or equal to 1000, the secondary vortices were generated due to flow instability created by curvature in the duct which is

perpendicular to the stream wise direction. However, at the higher Reynolds number greater than or equal to 1000, the influences of these secondary vortices were not observed, which is due to the transitions of flow from laminar to turbulent.

Kim et al. (2006) conducted experimental investigation using fluid medium as water and refrigerant R113 in offset strip fins. They considered the effects of fin geometry in their studies. Also, they found that Colburn '*j*' factor was about 25 % lower than the findings of Manglik and Bergles (1995) for the Reynolds number lesser than 1000. For the Reynolds number greater than 1000, they found that the variation in their results decreases with Reynolds number when compared with the findings of Manglik and Bergles (1995). They developed a correlation for '*j*' factor and found that 92 % of their experimental data match within ± 12 %.

Sheik Ismail et al. (2009) performed a numerical analysis to predict the flow pattern study on compact plate-fin heat exchangers using CFD Fluent software. They investigated three types of compact plate-fin heat exchangers for the quantification of flow maldistribution effects with ideal and real cases. Type I heat exchanger considered was a cross flow arrangement with one pass for the cold air and two passes for the hot air. Type II heat exchanger considered by them was also a cross flow arrangement with single pass for both hot and cold air sides. Type III was also a simple cross flow heat exchanger, with single pass for both hot fuel and cold air sides. In their investigation, they observed that the pressure drop of Type I heat exchanger has the real case pressure drop of 16 % higher when compared to the ideal case, which has a sharp bend at the heat exchanger inlet pipe. For the Type II heat exchanger, the cold air side has the real case pressure drop of 6 % higher when compared to the ideal case, which is also due to the sharp bend at the heat exchanger inlet pipe. Further, they reported that Type II heat exchanger has more or less uniform velocity distribution as that of Type I heat exchanger, which is due to the header design of Type II heat exchanger, that has a very smooth curvature. They further analyzed the Type III heat exchanger with and without baffle plate. The reported that, cold air in real case has a pressure drop of 34 % higher when compared to the baffle plate case. The authors also generated design data in terms of '*j*' and '*f*' for three types of offset strip fins and 16 types of wavy fins and results are presented in their investigation.

Chennu and Paturu (2011) presented the heat transfer and pressure drop correlations using air medium for offset strip fins, that are widely used in the aerospace industry. They performed numerical studies and proposed correlations in terms of Colburn '*j*' factor for heat transfer coefficient and friction factor '*f*' for the pressure drop. They investigated and presented the

correlations for wide ranges of Reynolds number, that included both laminar and turbulent regions. Their proposed correlations for offset strip fins were obtained after taking into account all the geometrical fin parameters. They further reported the effects of various geometrical parameters of offset strip fins given by fin spacing (*s)*, fin thickness (*t*) and strip length (*l*). Their proposed correlations for Colburn '*j*' factor and friction factor '*f*' for the laminar and turbulent flow ranges are given below:

For laminar range ($300 \leq Re \leq 800$)

$$j = 0.661(Re)^{-0.651}\left(\frac{s}{h}\right)^{-0.343}\left(\frac{t}{s}\right)^{-0.538}\left(\frac{t}{l}\right)^{0.305} \quad (2.23)$$

$$f = 10.882(Re)^{-0.79}\left(\frac{s}{h}\right)^{-0.359}\left(\frac{t}{s}\right)^{-0.187}\left(\frac{t}{l}\right)^{0.284} \quad (2.24)$$

And for turbulent range ($1000 \leq Re \leq 15000$)

$$j = 0.185(Re)^{-0.396}\left(\frac{s}{h}\right)^{-0.178}\left(\frac{t}{s}\right)^{-0.403}\left(\frac{t}{l}\right)^{0.29} \quad (2.25)$$

$$f = 2.237(Re)^{-0.236}\left(\frac{s}{h}\right)^{-0.347}\left(\frac{t}{s}\right)^{-0.151}\left(\frac{t}{l}\right)^{0.639} \quad (2.26)$$

Fernández-Seara et al. (2013) presented the experimental analysis of a titanium brazed plate fin heat exchanger with offset fins using liquid to liquid heat transfer mechanism. They performed the experiments employing water to water as working fluids and also using aqueous solution with 10 - 30 wt% ethylene glycol. They have determined the heat transfer and pressure drop characteristics in brazed plate fin heat exchanger with offset fins. They derived an empirical correlation as a function of Reynolds number using their experimental data, to estimate the single-phase heat transfer coefficient. The Reynolds number range considered by them are ranging from 129 to 1575 for water to water experiments and from 63 to 770 for aqueous solution with 10 to 30 wt% ethylene glycol. During the experiments, the heat transfer rates between the cold and hot fluids were maintained within an error band of ± 5 %. They found that the overall heat transfer coefficient with aqueous solution of 10 - 30 wt% ethylene glycol was lower than water. The general correlation developed for heat transfer coefficient in terms of Colburn factor '*j*' is given as follows:

$$j = 0.357(Re)^{-0.436} \quad (2.27)$$

Ramana Murthy et al. (2015) analyzed the heat transfer and the pressure drop correlations for serrated fins in water media using CFD fluent software. The correlations in terms of Colburn factor '*j*' and friction factor '*f*' allow the computation for all the values of Reynolds number, including the laminar and turbulent regions. In their analysis, the expressions for laminar and fully turbulent regions considered were in the Reynolds number range of $300 \leq Re \leq 1000$ and $1000 \leq Re \leq 15000$, respectively. The correlations developed for Colburn factor '*j*' and friction factor '*f*' are shown below:

For laminar range ($300 \leq Re \leq 1000$)

$$j = 0.426(Re)^{-0.308}\left(\frac{s}{h}\right)^{-0.585}\left(\frac{t}{s}\right)^{-0.929}\left(\frac{t}{l}\right)^{0.943} \tag{2.28}$$

$$f = 3.152(Re)^{-0.481}\left(\frac{s}{h}\right)^{-0.272}\left(\frac{t}{s}\right)^{-1.237}\left(\frac{t}{l}\right)^{0.984} \tag{2.29}$$

For Turbulent range ($1000 \leq Re \leq 15000$)

$$j = 0.097(Re)^{-0.151}\left(\frac{s}{h}\right)^{-0.526}\left(\frac{t}{s}\right)^{-1.238}\left(\frac{t}{l}\right)^{1.033} \tag{2.30}$$

$$f = 0.421(Re)^{-0.205}\left(\frac{s}{h}\right)^{-0.135}\left(\frac{t}{s}\right)^{-1.673}\left(\frac{t}{l}\right)^{1.194} \tag{2.31}$$

From the literature survey, it can be observed that there has been a lot of numerical and experimental investigations to predict the heat transfer and pressure drop, in terms of Colburn factor *'j'* and fanning friction *'f'* factor, respectively in plate fin compact heat exchangers. Some of the findings mentioned above are focused on plate fin compact heat exchangers for various fin configurations and fluid medium.

## 2.3 Phase change heat transfer and pressure drop

Boiling and condensation exhibit convective heat transfer mechanism that involve phase change from liquid to vapour and vapour to liquid, respectively. Typically, heat transfer coefficients ($h_r$) associated with the boiling or condensation are much higher than those with single-phase heat transfer mechanism. The available design data on phase change heat transfer is limited in the literature compared to the single-phase heat transfer mechanism. In the recent times, the applications of compact heat exchanger in phase change heat transfer are also witnessed which leads to the development of compact evaporators and condenser. It is also

observed that a wide scope of phase change application exists in the aerospace and automobile industries, where the phase change is preferred over a single-phase heat transfer.

Apart from heat transfer device in phase change applications, refrigerants also play a significant role in thermal fluid systems of industries. Decades ago, chlorofluorocarbons (CFCs) refrigerants like R12 and later, hydrochlorofluorocarbons (HCFCs) like R22 have been preferred by many users. Subsequently, these are replaced by hydrofluorocarbons (HFCs) refrigerants like R134a, which have been widely used in many sectors for decades. However, due to their high global warming potential (GWP), HFCs are further replaced by low GWP HFO refrigerants like R1234yf and many other natural refrigerants like ammonia and hydrocarbons. These refrigerants play a significant role in meeting the global energy demand and covering wide scope of many thermal fluid systems.

There have been studies on phase change heat transfer by many investigators using various refrigerants and heat transfer devices. In the literature, extensive experimental data and empirical correlations are available for heat transfer coefficient and frictional pressure drop of ozone-friendly refrigerant R134a and other HFC refrigerants inside tubes, helicoidal pipes, channels and plate heat exchangers. It is also found that there are few studies reported on condensation heat transfer when compared to the studies on boiling. The first theoretical study undertaken on laminar condensation over cooled metal surfaces is the work of Nusselt (1916). Further, many authors extended the study by, including the effect of heat capacity (Bromley, 1952), accounting for non-linear temperature distribution within the condensate film (Rohsenow, 1956) and adding the effect of shear stress by including a non-zero negative velocity gradient at the liquid–vapour interface (Chen, 1961). However, the correlation proposed by them is only limited to gravity-controlled laminar film condensation and cannot be employed for the wavy or turbulent condensation regions. Many other studies on condensation heat transfer coefficient ($h_r$) and frictional pressure drop ($\Delta P_f$) of refrigerants like R134a, R410, R404 and R22 inside pipes, tubes, plate heat exchangers, mini-channels are reported in literature, which are described in following paragraphs.

Shah (1979) proposed a general correlation for heat transfer during film condensation inside pipes. The author compared his correlations with the wide variety of experimental data using water, R11, R12, R22, R113, methanol, ethanol, benzene, toluene and trichloroethylene condensing in horizontal, vertical, and inclined pipes. He reported that his investigation covered wide range of mass flux, heat flux, pressures and vapour velocities. The author carried

out 21 experimental studies having 473 data points to derived a correlation for heat transfer, which was predicted with a mean deviation of 15 %. The proposed correlation for heat transfer during condensation inside pipes is given below:

$$h_{tp} = h_l \left[ (1-x)^{0.8} + \frac{3.8x^{0.76}(1-x)^{0.04}}{P_{rp}{}^{0.38}} \right] \tag{2.32}$$

where, $h_{tp}$ represents two phase boiling or condensing heat transfer coefficient, $h_l$ is the heat transfer coefficient assuming all masses to be flowing as liquid, $x$ is the vapour quality and $P_{rp}$ is the reduced pressure.

Yan et al. (1999) studied experimentally the heat transfer coefficient and frictional pressure drop during condensation of refrigerant R134a in a plate heat exchanger. The authors analysed the influences of refrigerant mass flux, heat flux, vapor quality and system pressure on the measured data. They found that condensation heat transfer coefficient and pressure drop increase with the mass flux and also mentioned that at a given mass flux, variation in the pressure drop than heat transfer coefficient with vapour quality was observed to be more effective (much larger). The heat transfer coefficient and frictional pressure drop were higher for higher mean vapour quality. Their study on system pressure (saturated temperature) showed that condensation heat transfer coefficient decreased with increase in pressure. They also reported that the effects of system pressure on frictional pressure drops are less. They derived correlations for heat transfer coefficient and pressure drops in terms of Nusselt number (*Nu*) and two phase friction factor ($f_{tp}$) respectively, which are given as follows:

$$Nu = \frac{h_r \times D_h}{\lambda_l} = 4.118 \times \ Re_{eq}^{0.4} \ Pr_l{}^{1/3} \tag{2.33}$$

$$f_{tp} \times Re^{0.4} \times Bo^{-0.5} \left(\frac{P_m}{P_c}\right)^{-0.8} = 94.75 \times Re_{eq}^{-0.0467} \tag{2.34}$$

where, $Bo$ represents boiling number, $\lambda_l$ and $Pr_l$ are the thermal conductivity and Prandtl number, respectively of refrigerant R134a in liquid phase. $P_c$ and $P_m$ are the critical pressure and average pressure between inlet and outlet, respectively.

Kang et al. (2000) performed experimental study to obtain condensation heat transfer of refrigerant R134a in a 12.7 mm helicoidal pipe. The inner diameter of the outer tube considered by them was 21.2 mm and passage formed by these inner and outer tubes was for water flow. The passage for refrigerant was made to pass through the inner helicoidal tube. The authors

reported the heat transfer coefficient variations for R134a with the coolant flow rate. The authors found that the average heat flux of the refrigerant flow increased with the increase in water flow rate. They reported a special heat transfer phenomenon where they found that the heat transfer coefficients on the refrigerant side decreased with the increase in coolant water flow Reynolds number. They explained that when the coolant water flow rate was increased, the cooling rate was increased, which leads to the higher cooling of refrigerant liquid, resulting in a large amount of increased single-phase liquid inside the tube, which further decrease the heat transfer coefficient on the refrigerant side. Further they expressed the heat transfer characteristics for the flow of R134a in a helicoidal pipe with the following relation:

$$\frac{Nu}{Pr^{0.4}} = 2.3 \times (Re^*)^{-0.94} \tag{2.35}$$

$$Re^* = \frac{G \times d_{in,2}}{\mu_l \sqrt{\rho_l/\rho_v}} \tag{2.36}$$

where, $1100 < Re^* < 2500$, $G$ represents mass flux, $d_{in,2}$ is the internal tube diameter, $\mu_l$ is the viscosity for liquid phase, $\rho_l$ and $\rho_v$ are the densities for liquid and vapour phase, respectively.

Han et al. (2003) conducted condensation experiments to measure the heat transfer coefficient and pressure drop in brazed plate heat exchangers (BPHE) using refrigerants R410A and R22. The BPHE used had chevron angles of 45°, 35°, and 20°. In this study the authors analysed the effects of mass flux, vapour quality, condensation temperature and chevron angle. They reported that both the condensation heat transfer coefficient and the pressure drop increased with the increase in mass flux and vapour quality, however they observed decreased in heat transfer and pressure drops with increase in saturation temperature and chevron angle. The authors further compared the findings of R410A and R22 and observed that heat transfer coefficient of refrigerant R410A was higher by 0 - 10 % and pressure drop was lower by 2 - 21 % than R22. They also derived correlations, wherein they included the effects of the plate geometry. They developed correlations for Nusselts number (*Nu*) and friction factor (*f*) and found that the tested data are within ± 20 % and ± 15 %, respectively. The correlations are given as follows for *Nu* and *f*:

$$Nu = Ge_1 Re_{eq}^{Ge_2} Pr^{1/3} \tag{2.37}$$

where,

$$Ge_1 = 11.22 \left(\frac{b}{D_h}\right)^{-2.83} \left(\frac{\pi}{2} - \beta\right)^{-4.5} \tag{2.38}$$

$$Ge_2 = 0.35\left(\frac{b}{D_h}\right)^{0.23}\left(\frac{\pi}{2}-\beta\right)^{1.48} \quad (2.39)$$

$$f = Ge_3 Re_{eq}^{\,Ge_4} \quad (2.40)$$

$$Ge_3 = 3521.1\left(\frac{b}{D_h}\right)^{4.17}\left(\frac{\pi}{2}-\beta\right)^{-7.75} \quad (2.41)$$

$$Ge_4 = -1.024\left(\frac{b}{D_h}\right)^{0.0925}\left(\frac{\pi}{2}-\beta\right)^{-1.3} \quad (2.42)$$

Here, $Ge_1$, $Ge_2$, $Ge_3$ and $Ge_4$ are non-dimensional geometrical parameters defined in terms of corrugation pitch ($b$), equivalent diameter ($D_h$) and chevron angle ($\beta$).

Longo (2008) carried out experiments on a small brazed plate heat exchanger (BPHE) using HFC refrigerant R134a to estimate condensation heat transfer and pressure drop. Longo (2009) also performed investigation to measure the heat transfer coefficient and frictional pressure drop during condensation of R410A. The author studied the effects of mass flux, saturation temperature vapour super heating during condensation experiments using R134a and R410A. He reported that the heat transfer coefficients are not dependent on lower range of mass flux (< 20 kg/m$^2$s), as the condensation was gravity controlled. He further explained that for higher mass flux, the heat transfer coefficients are significant, as forced convection condensation occurs and dominates. The author also found that at the given mass flux, the super-heated vapour heat transfer coefficients are 8 - 10 % higher than those of saturated vapour. This is due to the reduced condensate film thickness in case of super-heated vapour, compared to saturated vapour. He derived the average heat transfer coefficient of refrigerant in plate heat exchanger using the following global heat transfer coefficient ($U$) and heat transfer coefficient ($h_w$) of water, given below, assuming no fouling resistance:

$$h_{r,avg} = \phi h_{Nu} = \phi \times 0.943\left[\frac{\lambda_l^3 \rho_l^2 g \Delta H}{\mu_l \Delta T L}\right]^{1/4} \quad (2.43)$$

$$h_w = 0.277\left(\frac{\lambda_w}{d_h}\right) Re_w^{\,0.766} Pr_w^{\,0.333} \quad (2.44)$$

where, $\lambda_p$, $\lambda_l$ and $\lambda_w$ are the thermal conductivities (W/mK) of plate, refrigerant liquid and water, respectively, $g$ is gravity acceleration (m$^2$/s), $\mu_l$ is the liquid dynamic viscosity, $\Delta T$ is the temperature difference between saturation and wall, $L$ is the length of vertical surface, $\Delta H$ is

change in enthalpy and ϕ is enlargement factor which is considered as 1.24. Further, the author derived the frictional pressure drop equations in terms of kinetic energy (*KE*) per unit volume (*V*) of the refrigerant flow, which are given as follows for R410A and R134a refrigerants in Eqs. (2.45) and (2.46), respectively. The kinetic energy per unit volume is dependent on mass flux and the average two-phase density at the test section inlet and outlet. Longo (2008) defined the kinetic energy per unit volume ranging from 0.18 to 11 J/m3 and its dependency on frictional pressure drop of refrigerant.

$$\Delta P_f = 2.05 \frac{KE}{V} \tag{2.45}$$

$$\Delta P_f = 1.835 \frac{KE}{V} \tag{2.46}$$

Bohdal et al. (2011) performed experimental investigations of heat transfer and pressure drop during the condensation of the R134a and R404A in mini-channels having internal diameters of 0.31 - 3.30 mm. They reported that the local heat transfer coefficients and pressure drop in the mini-channels. They conducted the comparative analysis of the condensation results. The authors proposed an empirical correlation for the local heat transfer coefficient for refrigerants R134a and R404A and the predicted values from the proposed correlations match were within ± 25 % of the experimental data. The derived correlations proposed by them for the local heat transfer coefficient is given below:

$$Nu = 25.084\, Re_l^{0.285} P_r^{-0.288} \left(\frac{x}{1-x}\right)^{0.266} \tag{2.47}$$

where, *x* is vapour quality of the refrigerant.

Mancin et al. (2012) studied the condensation of superheated vapour of R410A and R407C inside two brazed plate heat exchangers having different geometries, aspect ratios and plate design. The authors have investigated the heat transfer coefficient at the given inlet saturation temperature of 41.8 ºC and 36.5 ºC for refrigerants R407C and R410A, respectively. The mass flux considered for their investigation were varied from 15 to 40 kg/m$^2$s and vapour quality was maintained in between 0.01 and 0.58. From their experimental results, it was found that for both heat exchanger, the condensation heat transfer coefficient increases with vapour quality and decreases with saturation ($t_s$) to wall temperature ($t_{wall}$) difference. They have developed a heat transfer correlation, which is shown below:

$$h = (h_A^2 + h_{nu}^2)^{1/2}[1.074(t_s - t_{wall})^{-0.386}] \quad (2.48)$$

$$h_A = h_{lo}\left[1 + 1.128x^{0.817}\left(\frac{\rho_l}{\rho_g}\right)^{0.3685}\left(\frac{\mu_l}{\mu_g}\right)^{0.2363}\left(1 - \frac{\mu_l}{\mu_g}\right)^{2.144} Pr^{-0.1}\right] \quad (2.49)$$

here $h_{nu}$ and $h_A$ represent the mean heat transfer coefficient for gravity dominated and shear dominated condensation, respectively inside tubes. $h_{lo}$ is the heat transfer coefficient of liquid with total flow rate, $x$ represents vapor quality, $\rho_l$ and $\rho_g$ are the density of the fluid in liquid and gas phase, respectively. $\mu_l$ and $\mu_g$ are the dynamic viscosity in the liquid and gas phase, respectively of fluid.

Ramana Murthy et al. (2017) experimentally investigated the heat transfer coefficient and frictional pressure drop during saturated vapour condensation of refrigerant R134a inside a small brazed compact plate fin heat exchanger with serrated fin surfaces. They have investigated the effects of saturation temperature and mass flux on heat transfer coefficient and frictional pressure drops of refrigerant R134a. They carried out the condensation experiments using refrigerant R134a at five different saturated temperatures (34 ºC, 38 ºC, 40 ºC, 42 ºC and 44 ºC). They reported that the influence on condensation heat transfer coefficient with saturation temperature (pressure) was less, however they observed great sensitivity to refrigerant mass flux and fluid properties. The authors also presented the frictional pressure drops with kinetic energy per unit volume of the refrigerant flow, which have linear dependence to each other. The proposed correlations derived by them for refrigerant heat transfer coefficients and frictional pressure drops, are given below.

For $600 \leq Re \leq 1800$

$$h = 6.909 \times 10^{-28}\left(\frac{\lambda_l}{D_h}\right)^{12.174}\left(Re_{eq}\right)^{1.594}(Pr_l)^{8.024} \quad (2.50)$$

And frictional pressure drops related to kinetic energy per unit volume (KE/V) of refrigerant flow is given as follows:

$$\Delta P_f = 2.389 \times \left(\frac{KE}{V}\right)^{0.283} \quad (2.51)$$

where, $\lambda_l$ represents the thermal conductivity of fluid in liquid phase, $Re_{eq}$ and $Pr_l$ are the equivalent Reynolds number and Prandtl number of the fluid, respectively.

Some of the investigations mentioned in the previous paragraphs on condensation heat transfer and pressure drop, carried out by many investigators were employed using tubes, helicoidal pipes, channels and plate heat exchangers as test sections and some of the important phase change correlations are summarised. Based on the various investigations available in the literature, it is observed that the correlations on condensation heat transfer coefficient and frictional pressure drop of refrigerants are dependent mostly on parameters such as mass flux and vapour quality. The effect of saturation temperature on condensation heat transfer coefficient and frictional pressure drop of refrigerant are found to be comparatively less significant than mass flux and vapour quality. Further, these two parameters mass flux and vapour quality influence the rate of condensation heat transfer and pressure drop and hence their optimum values need to be considered for better results. Higher mass flux of refrigerant and high vapour quality result in higher heat transfer, however at the same time, results in higher pressure drop. Thus, optimum values of these parameters are required to be considered while designing a condenser. The condensation of R1234yf reported for various heat transfer surfaces are discussed in following paragraphs.

### 2.3.1 Condensation of refrigerant R1234yf

Many researchers have conducted condensation experiments using various refrigerants to predict the condensation heat transfer and pressure drop characteristics. Decade ago, ozone-friendly HFC refrigerant R134a was used by many investigators to predict condensation inside tubes, herringbone fins, helicoidal pipe and plate heat exchangers. Further, due to the higher global warming potential (GWP) associated with HFC refrigerant R134a, many investigators have switch over to environmentally friendly HFO refrigerant like R1234yf, which has a lower GWP value. Some of the studies available in the literature on condensation and pressure drop characteristics of R1234yf in various heat transfer equipment are described in subsequent paragraphs.

Del Col et al. (2010) carried out an experimental investigation to estimate the local heat transfer coefficients of R1234yf during condensation within a circular mini-channel having diameter of 0.96 mm. The authors compared their findings on R1234yf with R134a. They reported that for a given mass flux of 200 kg/($m^2$s) and 0.4 vapour quality, the heat transfer coefficient of R1234yf was lower by 15 % than R134a. They also found that, for a given mass flux of 800 kg/$m^2$s and 0.7 vapour quality, refrigerant R1234yf heat transfer coefficient was 30 % lower.

Wang et al. (2012) performed condensation experiments using R1234yf, R134a and R32 in a horizontal tube having inner diameter of 4 mm in the mass flux range of 100 to 400 kg/m$^2$s and saturation temperatures of 40 ℃, 45 ℃ and 50 ℃. They investigated the significances of mass flux and vapour quality on the heat transfer coefficient. The authors found that R32 has the highest heat transfer coefficient, however heat transfer coefficient of R1234yf was 23.8 % lower than R134a at a given mass flux of 100 kg/m$^2$s. The authors also reported the effects of thermophysical properties on the heat transfer coefficient at different saturations temperature.

Navarro-Esbri et al. (2013) and Mota-Babiloni et al. (2014) performed tests using refrigerant R1234yf as a substitute for R134a in a vapor compression system test facility. Navarro-Esbri et al. (2013) observed that the volumetric efficiency and cooling capacity of refrigerant R1234yf were 5 % and 9 % lower, respectively than R134a, when R1234yf was used as replacement in a R134a test facility. The coefficient of performance (COP) values obtained using R1234yf were 5 to 30 % lesser than R134a. Mota-Babiloni et al. (2014) also demonstrated the comparison of cooling capacity, volumetric efficiency and COP values obtained using R1234yf as a substitute in a R134a test facility. They observed that cooling capacity, volumetric efficiency and COP values obtained using R1234yf were 9 %, 3 - 5 % and 3 - 11 %, respectively lesser than R134a. Many researchers have also performed condensation experiments using refrigerant R1234yf inside tubes, microchannels, plate heat exchangers and few of them are described in subsequent sections.

Longo and Zilio (2013) investigated the condensation of the low GWP refrigerant R1234yf inside a brazed plate heat exchanger. The authors investigated the effects of mass flux ($G_r$), saturation temperature ($T_s$) and vapour super-heating on condensation heat transfer coefficient and frictional pressure drop during condensation of R1234yf inside a brazed plate heat exchanger (PHE). They compared their results of R1234yf to R134a and found that the condensation heat transfer coefficient of R1234yf was lower by 10 - 12 % and frictional pressure drop was lower by 10 - 20 % than R134a under the same operating condition. They further proposed a best fit linear equation for the computation of frictional pressure drop from the experimental data based on the kinetic energy per unit volume of the refrigerant flow.

Illan-Gomez et al. (2015) presented an experimental two phase condensation heat transfer coefficient ($h_r$) and frictional pressure drops ($\Delta P_f$) inside a mini-channels with an inner hydraulic diameter of 1.16 mm using R1234yf and R134a. The authors performed the test in the mass flux range of 350 to 940 kg/m$^2$s and saturation temperatures of 30 ℃, 35 ℃, 40 ℃

45 ℃, 50 ℃ and 55 ℃ using R1234yf and R134a as working fluids. They observed the lower values of condensation heat transfer coefficient and frictional pressure drops of refrigerants R1234yf than R134a, operating at same condition.

Yang and Nalbandian (2018) carried out experiments on condensation heat transfer coefficient ($h_r$) and frictional pressure drops ($\Delta P_f$) of R1234yf and R134a in a small circular tube. At higher vapour qualities, they found that the condensation $h_r$ of R1234yf was lower than R134a but similar at lower vapour qualities. Bashar et al. (2020) experimentally studied the condensation heat transfer coefficient and frictional pressure drop of R1234yf inside a smooth and micro-fin tube with a 2.5 mm outer diameter. They developed condensation heat transfer correlation for a smooth tube using their experimental data and from data available in literature. Nalbandian et al. (2020) demonstrated the experimental studies on condensation of R134a and R1234yf in a rectangular microchannel tube. They indicated that, as the R134a liquid thermal conductivity was 27 % higher than R1234yf, the heat transfer coefficient of R134a was higher by 15 - 23 % for different vapor qualities and mass velocities.

Pham and Oh (2021) conducted the experiments on condensation heat transfer coefficient of R1234yf inside two multiport mini-channel tubes having hydraulic diameters of 0.83 mm and 0.97 mm. They presented the significance of different vapour qualities and refrigerant mass flux in the range of 50 to 500 kg/m$^2$s. They further studied the dependency of heat flux on condensation heat transfer coefficient and found increased with heat flux. Mattiuzzo et al. (2022) conducted experimental investigations on condensation heat transfer and pressure drop of R1234yf / HFC mixtures inside small diameter channels. The authors have proposed refrigerants mixtures of HFO/ HFC, such as R234yf / HFC mixtures as an alternative to R134a. The authors have investigated condensation experiments using refrigerants R513A (56 / 44 % by mass mixture of R1234yf / R134a) and R516A (77.5 / 14 / 8.5 % by mass mixture of R1234yf / R152a / R134a) inside a channel having diameters of 0.96 mm and 3.38 mm. They carried out the condensation heat transfer investigations in 0.96 mm channel and observed that heat transfer coefficients of R513A and R516A were about 20 % lower than R134a and about 10 % higher than that of R1234yf. The authors also reported that heat transfer coefficient of R516A was about 4 % higher than R513A, operating at same conditions, as, R516A has lower vapour density and higher vapour velocity. Also, they found that the pressure gradient of refrigerant R516A was slightly higher than R513A.

## 2.4 Literature closure

Based on the literature survey, the following conclusions are made:

- The literature review on heat transfer enhancements in compact heat exchangers shows that adequate data were reported on single-phase heat transfer characteristics. Many researchers have developed correlations based on the Colburn '*j*' factor and friction factor '*f*' data for single-phase heat transfer and pressure drop, respectively which can be directly employed for most of the new development of compact heat exchangers.
- Many researchers have conducted numerical and experimental studies on single-phase heat transfer in compact heat exchangers. The numerical data is most preferred from the user perspective in many cases, as it is both time and cost effective. In general, it is expensive and time consuming to conduct experiments, compared to numerical analysis. If the problem definition of the user meets the requirement based on the numerical correlations available, it could be preferred over experiments. However, experimental investigation remains the best choice to account the critical areas and to employ in various critical applications. Compact heat exchangers are widely preferred in automobile, aerospace, cryogenic and many other refrigeration industries.
- Further, the literature survey indicates that experimental data on phase change heat transfer and pressure drop characteristics are limited compared to single-phase flow. But there exists an extensive scope in many industries where phase change heat transfer can be employed, as it has better performance compared to single-phase heat transfer. In recent times, many researchers have investigated phase change problems and their applications in many fields.
- There have been several works reported in the literature on two phase heat transfer in helicoidal pipes, mini-channels, in-tubes, and plate heat exchanger using refrigerant R134a. It was observed that the studies on phase change condensation heat transfer are limited compared to boiling in brazed plate fin compact heat exchangers.
- In addition, there is a lack of condensation studies on low GWP refrigerant R1234yf in compact heat exchangers. The investigation on condensation heat transfer of refrigerant R1234yf, available in the literature are mostly employed in tubes, channels and micro-fins. Several authors have proposed empirical correlations for condensation heat transfer coefficient and frictional pressure drop. However, these condensation and pressure drop correlations are very specific to a particular geometry and cannot be used

for other complicated geometries. Further, literature survey also indicated that there is no work available on condensation heat transfer of refrigerant R1234yf inside brazed plate fin compact heat exchangers with serrated or wavy fin surfaces.

Considering research gap from the literature, the objectives of the present thesis works are defined. The primary aim of the thesis work is to generate design parameters in terms of condensation heat transfer coefficients and frictional pressure drops for serrated and wavy fin geometries. These heat transfer and pressure drop parameters are the important factors needed for the design and development of compact condenser. Hence, the proposed research work is to investigate the condensation heat transfer coefficient of low GWP refrigerant R1234yf in brazed plate fin compact heat exchanger with serrated and wavy fin surfaces. The detailed objectives of the present work are as follows:

- To obtain single-phase heat transfer coefficient ($h_w$) of water for serrated and wavy fin surfaces using CFD analysis, which is further used for the estimation of refrigerant heat transfer coefficient ($h_r$).
- To estimate the single-phase heat transfer coefficient ($h_w$) of water for both serrated and wavy fins using modified Wilson plot technique and to compare the experimental and numerical results.
- Establishment of vapour cycle system test facility to conduct condensation experiments inside brazed plate fin compact heat exchangers.
- To carry out the condensation experiments using refrigerant R134a and low GWP refrigerant R1234yf and to compare their results under the same operating conditions.
- To study the effects of mass flux ($G_r$) and saturation temperature ($T_s$) on condensation heat transfer coefficient ($h_r$) of R1234yf and also to study the effect of mass flux ($G_r$), saturation temperature ($T_s$) and kinetic energy per unit volume (KE/V, J/m$^3$) of refrigerant on frictional pressure drop ($\Delta P_f$) inside brazed plate fin compact heat exchanger with serrated fin and wavy fin surfaces.
- To derive the suitable correlations for condensation heat transfer coefficient ($h_r$) and frictional pressure drop ($\Delta P_f$) of R1234yf using the experimental data for brazed plate fin compact heat exchanger with serrated and wavy fins surfaces.
- To study the effect of serrated fin geometrical parameters of brazed plate fin compact heat exchanger on condensation heat transfer coefficient ($h_r$) and frictional pressure drop ($\Delta P_f$) of refrigerant R1234yf.

## 2.5 Summary

In this chapter, the detailed literature survey has been carried out on single-phase heat transfer and pressure drop investigations available on compact heat exchangers. This chapter also presents the published works on phase change heat transfer and frictional pressure drop characteristics of various refrigerants in tubes, mini-channels, micro-fins and compact heat exchangers. This chapter further presents the proposed research work based on the various investigations reported in the literature on heat transfer enhancement techniques and usage of friendly refrigerant like HFO R1234yf in compact heat exchanger. The objectives of the PhD thesis work are then discussed and presented in sequence.

# Chapter 3

# Single-Phase Investigation of Colburn '*j*' and Friction '*f*' Factors

## 3.1 Preface

In the present investigation, the primary objective is to estimate condensation heat transfer coefficients and frictional pressure drops during condensation of refrigerants R134a and R1234yf on serrated and wavy fin surfaces of compact heat exchangers. The expression of overall heat transfer coefficient for heat exchangers is used to determine the refrigerant heat transfer coefficient. In this expression, the unknown parameter along with refrigerant heat transfer coefficient is the single-phase heat transfer coefficient of water. In the present study, the test section considered is a compact test condenser, which has a refrigerant circulation in one of the circuit and water flow circulation in other circuit. Thus, the determination of single-phase heat transfer coefficient of water is the prerequisite for estimation of two phase refrigerant heat transfer coefficient. Therefore, in the present chapter, the numerical and experimental estimation of single-phase heat transfer coefficients of water are discussed and presented. The numerical analysis was performed using ANSYS Fluent CFD tool to estimate the single-phase heat transfer coefficient of water ($h_w$) for both serrated and wavy fin surfaces. Based on the CFD data, the suitable equation for heat transfer coefficient of water ($h_w$) was derived for both serrated and wavy fin surfaces. Further, the single-phase water-to-water experiments were also performed to estimate the single-phase heat transfer coefficient of water ($h_w$) in test condensers, with serrated and wavy fin surfaces. This chapter further discusses the three types of test condensers, having two numbers of serrated fins and one number of wavy fins surfaces. These test sections were employed in the present single-phase water to water and

condensation experiments. The numerical and experimental investigations on single-phase heat transfer are presented in subsequent sections.

## 3.2 Numerical investigation on single-phase heat transfer

The numerical analysis was carried out using ANSYS fluent CFD tool to predict the fluid flow and heat transfer characteristics on serrated and wavy fin surfaces of compact heat exchangers. The CFD tool in common practice associated with three processes, which are pre-processing, solver and post-processing. In the present study, as a pre-processing method, the modelling of geometry was performed and the generation of optimum mesh for the defined geometry was also carried out. Another process is the solver method that solves the set of equations using the boundary conditions chosen by the user to compute the flow field. In the post-processing method, it presents the results of the analysis like contours plot, vector plot, flow fields etc. In this section, a numerical approach is presented on the estimation of single-phase the heat transfer coefficient of water for both serrated and wavy fin surfaces.

Typically, the heat transfer is described in terms of Colburn *'j'* factor and pressure drop is described in terms of friction factor *'f'*. Both *'j'* and *'f'* factors are defined for varying range of Reynolds number. In the present numerical analysis, a single layer of brazed plate fin compact heat exchanger as described by Chennu and Paturu (2011) was modelled using CATIA and the mesh of the model was generated using hypermesh software. This fin model was generated for both serrated and wavy fin surfaces. In order to account the entrance effect, periodic fully developed flow phenomena was employed for the flow analysis, as suggested by Patankar et al. (1977). The pressure drop for the unit length was multiplied by the actual length to get the total pressure drop for the corresponding fin, which was the basis for the estimation of friction factor *'f'* as described by Kays and London (1964). The similar approach is applied for all range of Reynolds number to determine the friction factor *'f'*.

In the present analysis, the fin walls are considered as the constant wall temperature. The temperatures and pressures at the inlet and outlet of the fin model are analysed using mass weighted average. The pressure, temperature and velocity profiles are studied and analysed at any sections of the fin models, for the corresponding value of Reynolds number. The temperature difference obtained between inlet and outlet of the fin model was considered for computing the Colburn '*j'* factor, as described by Kays and London (1964). The methodology was applied for all range of Reynolds number, considered in the present investigation. The

Reynolds number range from 100 to 1000 were treated as laminar flow and 1000 to 15,000 were treated as turbulent flow region as reported by Amaranatha Raju et al. (2015). The methodology is followed for all sets of serrated and wavy fins parameters to obtain the Colburn *'j'* factor and friction factor *'f'*. Further, in this chapter, suitable equations were derived for '*j*' and '*f*' factors as a function of Reynolds number and fin geometrical parameters for both serrated and wavy fin surfaces of compact heat exchangers.

### 3.2.1 Numerical approach and governing equations

The finite volume method is employed in ANSYS Fluent to solve the mass, momentum and energy conservation equations. Semi-implicit SIMPLER method as described by Versteeg and Malalasekera (1995) is employed to estimate the turbulent flow in the velocity and pressure conjugated problem and further a second order upwind differential scheme is employed for the approximation of the convection terms. The pressure-based solver and one of the most popular turbulence models, a standard *k*-epsilon model with enhanced wall treatment is considered to analyse the turbulent flow in the heat exchanger with serrated or wavy fin geometry as described by Versteeg and Malalasekera (1995).

The standard *k*-epsilon turbulence model is a two-equation model. This model also solves the two transport equations that accounts for convection and diffusion of turbulent energy, in addition to solving the conservation equations. One of the two transported variables is turbulence kinetic energy (*k*), that accounts for the energy in turbulence and the other one that accounts for the dissipation rate of turbulent kinetic energy is turbulent dissipation rate ($\varepsilon$). This model is widely used and preferred in many industrial fluid flow problems due to the capability of solving wide range of turbulent flows with considerable accuracy. In this analysis, the molecular viscous effects is considered negligible and only the effects of turbulence is considered and hence the standard *k*-epsilon model has been chosen to solve the present numerical problems. The convergent criterion considered for the present numerical analysis is specified to absolute residuals ($\leq 1.0 \times 10^{-6}$). The Reynolds transport equation as defined by Anderson (1995) and Patankar (1980) is expressed as follows:

$$div\ (\rho u \Phi) = div\ (\Gamma\ grad\ \Phi) + S_\Phi \tag{3.1}$$

where $\Phi$ is the generalized transport variable, $\Gamma$ represents the effective diffusivity and $S_\Phi$ is the source term for the respective dependent variable. The description of variables $\Phi$, $\Gamma$ and $S_\Phi$ in the equations of continuity, momentum and energy are listed in Table 3.1.

Table 3.1. Description of variables $\Phi$, $\Gamma$ and $S_\Phi$

| Conservation equations | | $\Phi$ | $\Gamma$ | $S_\Phi$ |
|---|---|---|---|---|
| Continuity equation | | 1 | 0 | 0 |
| Momentum Equation in | *X*-direction | $u$ | $\mu$ | $-\frac{\partial \psi}{\partial x} + \rho g_x + \text{fluid friction} + S_u$ |
| | *Y*-direction | $v$ | $\mu$ | $-\frac{\partial \psi}{\partial y} + \rho g_y + \text{fluid friction} + S_v$ |
| | *Z*-direction | $w$ | $\mu$ | $-\frac{\partial \psi}{\partial z} + \rho g_z + \text{fluid friction} + S_w$ |
| Energy equation | | $\theta$ | $\frac{k}{c_p}$ | $-\frac{D\psi}{D\lambda} + \text{Viscous dissipatio} + \text{Other heat Sources}$ |

The variables $\Phi$, $\Gamma$ and $S_\Phi$ as defined in Table 3.1 are substituted in Eq. (3.1). The following governing Eqs. (3.2), (3.5) and (3.6) are obtained:

i) Continuity equation

$$\frac{D\rho}{D\lambda} = -\rho(\nabla . v) \tag{3.2}$$

where,

$$\frac{D}{D\lambda} = \frac{\partial}{\partial \lambda} + u\frac{\partial}{\partial x} + v\frac{\partial}{\partial y} + w\frac{\partial}{\partial z} \tag{3.3}$$

$$\nabla . v = \frac{\partial u}{\partial x} + \frac{\partial v}{\partial y} + \frac{\partial w}{\partial z} \tag{3.4}$$

ii) Momentum equation

$$\rho\frac{Du}{D\lambda} = -\nabla\rho - [\nabla . \tau] + \rho g \tag{3.5}$$

iii) Energy equation

$$\rho\frac{DU}{D\lambda} = -(\nabla . q) - \psi(\nabla . v) - (\tau . \nabla v) \tag{3.6}$$

### 3.2.2 Assumptions

In this section, the assumptions made for the numerical analysis of serrated and wavy fins surfaces are presented. The assumptions considered are as follows:

1. Fluid flow is considered as steady and incompressible.
2. No slip boundary condition is considered on the fin wall.
3. Fluid flow meets the Boussinesq assumption.
4. Effect of heat conduction is considered through the fin and plate material.
5. Fluid flow is periodically developed, both hydro-dynamically and thermally.

### 3.2.3 Boundary conditions

The following boundary conditions are considered for the present numerical analysis to compute the heat transfer and pressure drop in serrated and wavy fin surface model. The boundary conditions applied on the serrated fin and wavy fin surfaces are also shown in the Figs. 3.1 (a) and (b), respectively.

1. No-slip boundary condition on the fin wall is considered.
2. Isothermal condition is considered during the estimation of pressure drop across the heat exchanger fin surfaces.
3. Periodic boundary condition is considered while estimating pressure drop as described by Patankar et al. (1977). The compact heat exchangers with serrated or wavy fin surfaces have a flow passage of repeating nature at regular intervals along the fluid flow path.
4. Total fluid flow is provided at the inlet of the fin model, computed based on the Reynolds number.
5. Total temperature of fluid is considered at the inlet of the fin model.
6. Symmetry or adiabatic boundary condition is considered on the outlined heat exchanger fin channel, where the expected pattern of the flow / thermal solution is adiabatic, as employed by Chennu and Paturu (2011), Sheik Ismail et al. (2009) and Amaranatha Raju et al. (2015). Similarly, in the present analysis, symmetry or adiabatic boundary condition is employed and, in such regions, no heat flow occur across the specified boundary.
7. Constant wall temperature boundary condition is applied on the top and bottom wall.

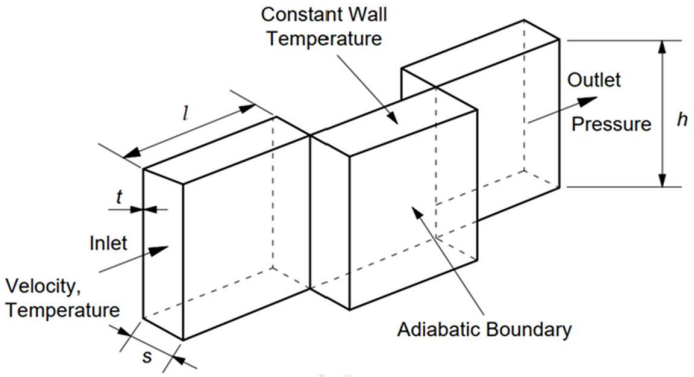


(a)

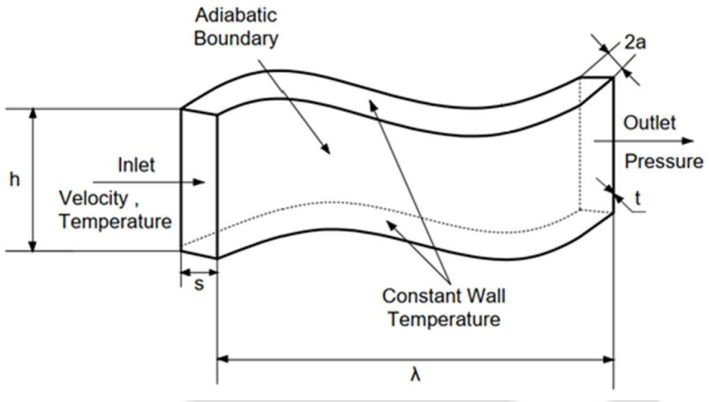


(b)

Fig. 3.1. Boundary condition for (a) serrated fin (Chennu and Paturu, 2011), and (b) wavy fin (Amaranatha Raju et al., 2015)

### 3.2.4 Computation of Colburn factor '*j*' and friction '*f*' factor

The heat transfer and pressure drop in compact heat exchangers for both serrated and wavy fins are defined by Colburn factor *'j'* and fanning friction '*f'* factor, respectively. The friction '*f'* factor includes the effect of both viscous shear and form drag. In the present study, the heat transfer and pressure drop characteristics (*'j'* and '*f'* factors) are computed as a function of Reynolds number and fin geometrical parameters. The Colburn factor *'j'* and the friction '*f'* factor for both serrated and wavy fin surfaces are estimated for water medium. Based on these CFD data, a suitable correlation for single-phase heat transfer coefficient of water is derived, which is further used in the estimation of refrigerant heat transfer coefficient, as described in the subsequent chapters. The correlations of '*j'* and *'f'* factors are computed based on the parameters obtained for different serrated and wavy fin geometries and different range of Reynolds number are considered.

The Colburn factor *'j'* is defined as follows:

$$j = \frac{h_w}{G C_p} Pr^{\frac{2}{3}} \tag{3.7}$$

here, *G* represents the mass flux (kg/m$^2$s).

Logarithmic mean temperature difference (LMTD) is employed to determine the Colburn factor '*j*', which is the average temperature difference between the hot and cold fluids passing through the heat exchanger. The relation for *'j'* as shown in Eq. (3.7) can also be expressed as follows in terms of estimated variables from numerical analysis.

$$j = \frac{D_h}{4L} \ln \left[\frac{T_{wall} - T_m(0)}{T_{wall} - T_m(L)}\right] Pr^{\frac{2}{3}} \tag{3.8}$$

here, $T_{wall}$ is the wall temperature.

The friction '*f*' factor is determined from the area averaged mean pressure drop ($\Delta P$) over the periodic length '*L*' as given below:

$$\Delta P = \frac{4f\, L\, \dot{G}^2}{2\rho D_h} \tag{3.9}$$

$$f = \frac{\Delta P\, D_h}{2 v_m{}^2 \rho L} \tag{3.10}$$

here, *L* represents the length (mm) of the passage. For the serrated fin surface, *L* is given by serration length '*l'* and for wavy fin surface, *L* is given by wave length '$\lambda$'. The area averaged mean velocity at any cross section is given by $v_m$ and the hydraulic diameter is given by $D_h$.

### 3.2.5 Problem description

The numerical analysis is performed for both serrated and wavy fin surfaces of compact heat exchanger. The geometrical fin parameters of the serrated fin are defined by the fin height (*h*), fin spacing (*s*), fin thickness (*t*) and serration length (*l*). The geometrical parameters of the wavy fin are defined by the fin height (*h*), fin spacing (*s*), fin thickness (*t*), wave amplitude (*a*) and wave length ($\lambda$). These fin geometrical parameters are further given by dimensionless representations of flow cross-section aspect ratio namely *s/h*, *t/s* and *t/l* for serrated fins and *s/h*, *a/s* & $\lambda/a$ for wavy fins. These fin geometrical parameters play a significant role, that

accounts in the behaviour of heat transfer and pressure drop characteristics as reported by London and Shah (1968).

### 3.2.6 Serrated fin surface

The serrated fins in common practice are widely preferred in brazed plate fin compact heat exchanger due to higher effectiveness. This type of fin has periodical interruptions in the fluid flow path that leads to breakage of boundary layers and creation of fresh ones, which enhance the heat transfer. This periodic fluid flow interruption in serrated fin also leads to higher pressure drop. Thus, the usage of this type of fin configuration depends on the optimal requirement of heat transfer and pressure drop. The serrated fin surface and pictorial representation of serrated fin illustrated by Sheik Ismail et al. (2009) are shown in Figs. 3.2 (a) and (b), respectively.

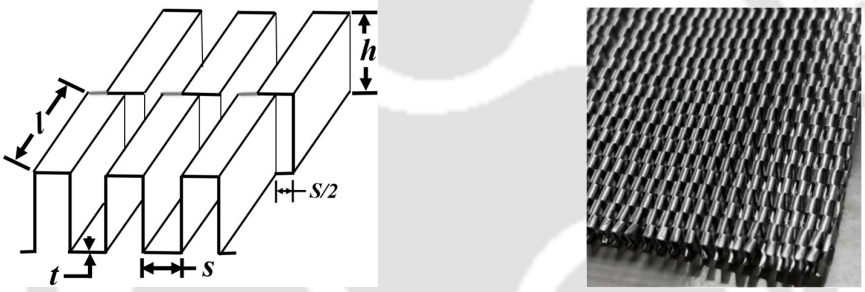


(a) (b)

Fig. 3.2. (a) Serrated fin surface, and (b) Serrated fin

#### 3.2.6.1 Numerical model

The geometrical parameters of the serrated fin are described by fin height ($h$), fin spacing ($s$), fin thickness ($t$), and serration length ($l$). In the present numerical analysis, the computational domain of serrated fin is modelled using CATIA software, as illustrated in Fig. 3.3. Further, the grid is generated on this model using the hypermesh software, as shown in Fig. 3.4. The grid of the fin model is created based on the generation of 2D domain using quad elements and 3D domain using hexa elements. As the quality of grid size influences the solution of the analysis, precaution is taken in choosing the features of grid size like orthogonality, control of spacing and skewness. In this study, the low aspect ratios of grid cells and highly stretched grids are avoided to obtain better results. The computational domain of serrated fin considered for the analysis has a fin spacing ($s$) in the x-direction, serration length ($l$) in the y-direction and fin height ($h$) in the z-direction.

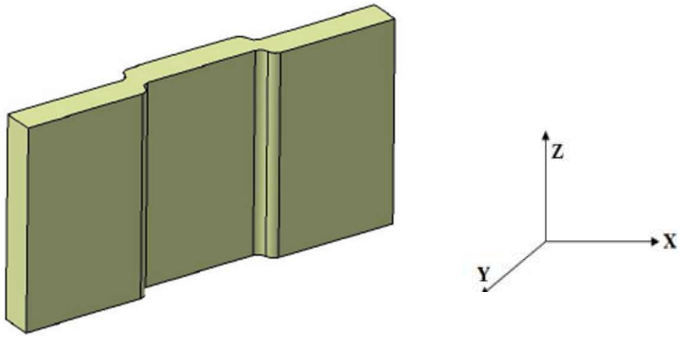


Fig. 3.3. Serrated fin computational model

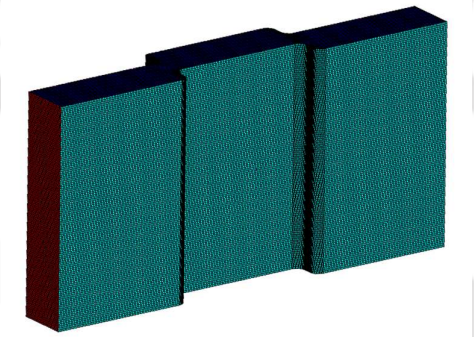

Fig. 3.4. Serrated fin mesh model

### 3.2.6.2 Dimensionless parameters

The geometrical fin parameters, such as height ($h$), spacing ($s$), thickness ($t$) and serration length ($l$) are represented by the dimensionless cross-sectional aspect ratios, $s/h$, $t/s$ and $t/l$ for serrated fins. The parametric study of the serrated fin surfaces is carried out to compute the Colburn factor '$j$' and friction '$f$' factor for the varying range of Reynolds number ranging from 100 to 15000 and for dimensionless fin parameters. The parametric studies in terms of Colburn factor '$j$' and friction '$f$' factor are presented for both laminar and turbulent regions. The varying range of the Reynolds numbers defined the laminar and turbulent regions of the fluid flow in the present analysis. The range of the dimensionless cross-sectional aspect ratios considered in the present analysis are as follows:

$$0.0806 \leq s/h \leq 0.8117 \tag{3.11}$$

$$0.0431 \leq t/s \leq 0.1959 \tag{3.12}$$

$$0.022 \leq t/l \leq 0.0598 \tag{3.13}$$

The Reynolds number range considered are given below:

$$100 \leq Re \leq 1000 \text{ for laminar region} \quad (3.14)$$

$$1000 \leq Re \leq 15000 \text{ for turbulent region} \quad (3.15)$$

### 3.2.6.3 Grid independency

Grid independency check is performed to evaluate the optimal mesh sizes to verify the mesh correctness, as the quality of mesh influences the solution results. The various mesh sizes from coarse to fine mesh are selected and analysed for the same boundary conditions. As mentioned by Chennu and Paturu (2011), Sheik Ismail et al. (2009) and Amaranatha Raju et al. (2015), the grid independency check was performed for each fin surface before every analysis at a particular Reynolds number to finalize the number of elements as the grid sensitivity depends on fin surface. In this study, pressure drop is chosen as the grid independency parameter and its dependency is plotted against the number of elements. Further, the same computational model that predicts the pressure drop in the first phase of simulation is used to analysed the heat transfer by switching on the energy equation, thus the separate independency check for the heat transfer was not carried out as reported by Chennu and Paturu (2011). Fig. 3.5 shows that after certain numbers of elements, significance change in the pressure drop is not observed. Based on the plotted result, the mesh size is finalised in terms of numbers of elements.

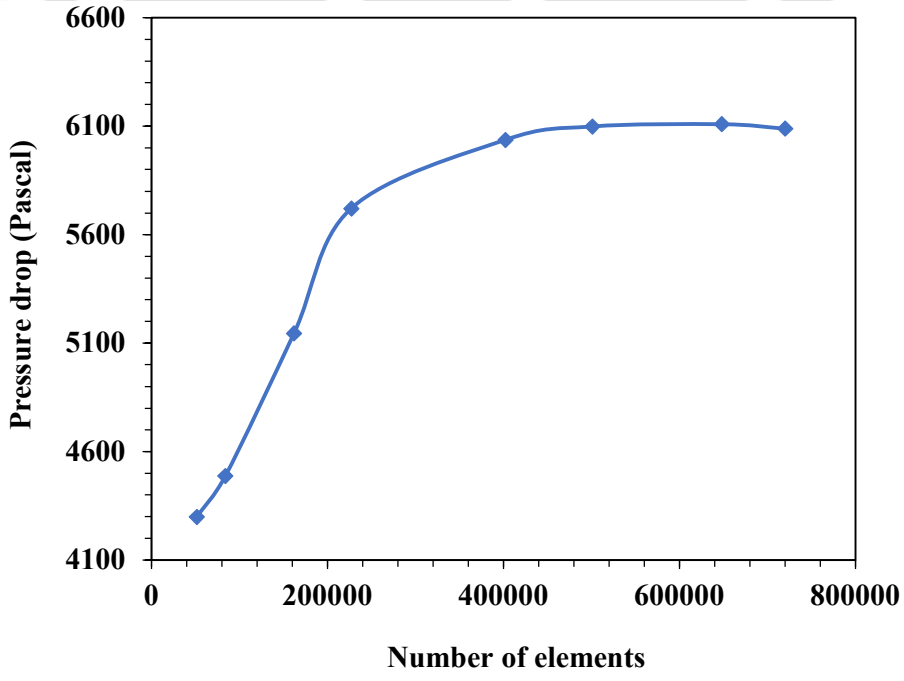


Fig. 3.5. Grid independency

### 3.2.6.4 Simulation approach

The numerical analysis is carried out on serrated fin surfaces to compute the Colburn factor '*j*' and fanning friction '*f*' factor for laminar region ($100 \leq Re \leq 1000$) and turbulent region ($1000 \leq Re \leq 15000$). Initially, the CFD analysis is performed for air medium by choosing the serrated fin geometry, considered by Kays and London (1964) and Sheik Ismail et al. (2009). The serrated fin geometries are modelled and suitable mesh are generated for these fin geometries. Further, the CFD analysis is performed on these serrated fins using ANSYS Fluent software. The CFD results are analysed and compared with the results of Kays and London (1964) and Sheik Ismail et al. (2009), as shown in Fig. 3.6. The comparison is found to be in good agreement and variations observed are found to be less than 12 % for both Colburn factor '*j*' and friction '*f*' factor results.

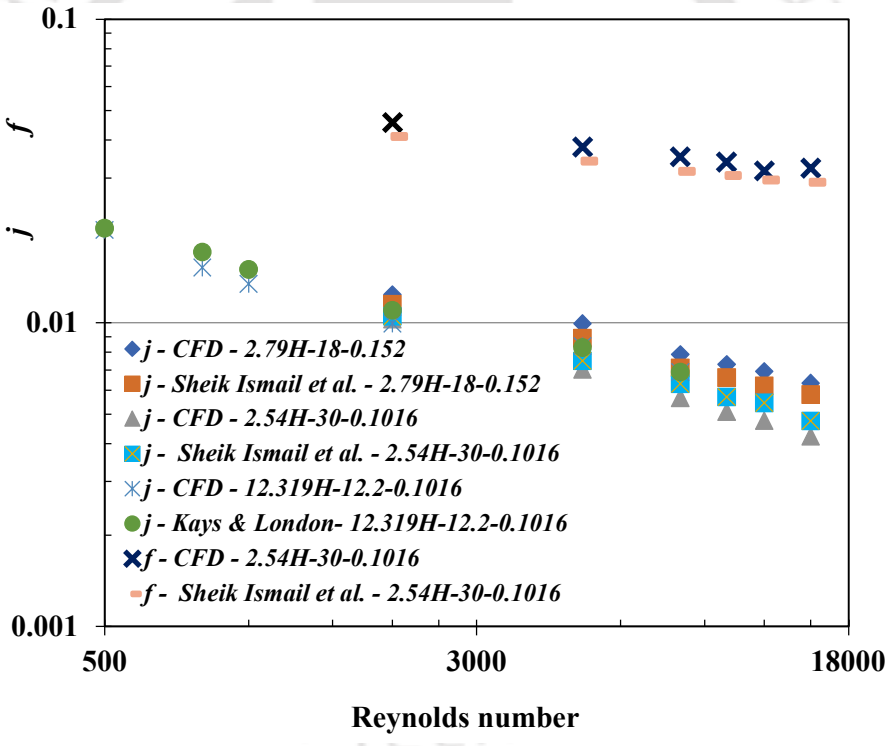


Fig. 3.6. Comparison of '*j*' & '*f*' factors with Reynolds number

### 3.2.6.5 Simulation results and discussion

In this section, the simulation results of serrated fin surfaces are discussed and presented. The present analysis is performed using water medium on the smooth serrated fin surfaces for various fin geometrical parameters and Reynolds number ranging from 100 to 15000. The

behaviour of velocity, pressure and temperature fields for these range of Reynolds number are established and analysed. The effects of the dimensionless fin geometrical parameters on the performance of serrated fin are presented in the subsequent section. The contours of pressure, velocity and temperature profiles for the Reynolds number ($Re$ = 800) are shown in Figs. 3.7 to 3.9. In the pressure contour shown in Fig. 3.7, the highest pressure is observed at the leading edge of the fin. It is evident that the pressure decreases at the first interruptions after the recirculation zone and then recovers slightly and then further drops again in the following recirculation zone interruptions. In the velocity contour as shown in Fig. 3.8, it is evident that the flow is separating from the diverging side of the fin and flows towards the converging side that creates the recirculation zone in the flow, which enhances the heat transfer rates. It is also evident that the velocity reaches its maximum point at the interruptions, where the highest values of pressure drop occur. In the static temperature profiles shown in Fig. 3.9, it is observed that the temperature is higher near the wall than the core region. The Reynolds number has a significant influence on the pressure, velocity and the static temperature profiles.

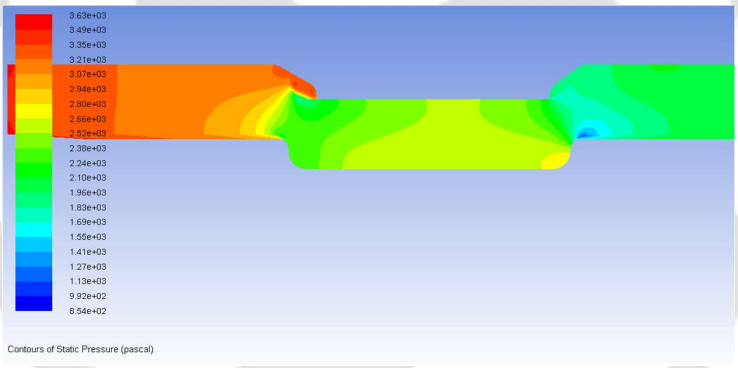


Fig. 3.7. Static pressure profile at Re = 800

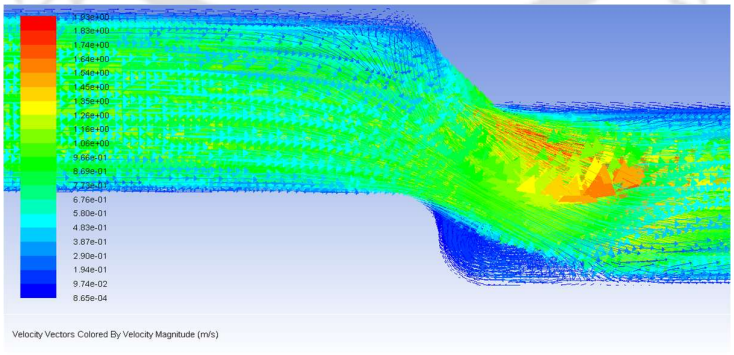


Fig. 3.8. Velocity profile at $Re$ = 800

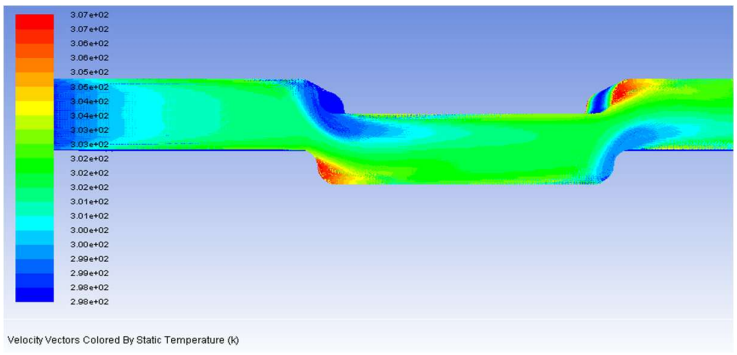


Fig. 3.9. Static temperature profile at *Re* = 800

### 3.2.6.6 Effect of fin geometrical parameter and Reynolds number

The numerical analysis on the serrated fin surfaces is carried out using water for analysing the effect of Reynolds number and variations of dimensionless fin geometrical parameters (*s/h, t/s* and *t/l*) on both Colburn '*j*' factor and friction '*f*' factor. These effects of geometrical fin parameters are carried out to predict the heat transfer and flow friction characteristics of the serrated fin surfaces.

**a) Effect of *s/h* ratio on '*j*' *and* '*f*' factors for serrated fin**

In this section, the effects of dimensionless parameter, fin spacing to height (*s/h*) ratio on Colburn '*j*' factor are studied and plotted in Fig. 3.10 for varying range of Reynolds number.

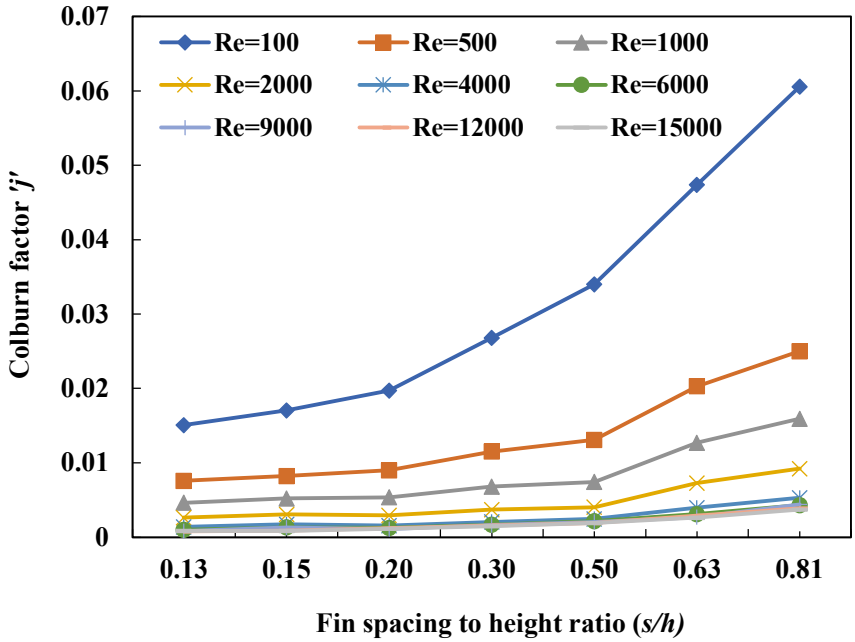


Fig. 3.10. Effect of fin spacing to height ratio on Colburn factor '*j*'

Fig. 3.10 shows that with the increase in Reynolds number, the value of *'j'* factor decreases, which indicates the higher heat transfer rates in this analysis, as *'j'* factor is proportional to the ratio of heat transfer coefficient and Reynolds number. It can be seen that the rate of decrease in *'j'* value is found higher for lower Reynolds number, predominantly for $Re < 1000$ and it is found lower for higher Reynolds number ($Re > 1000$). The effect of fin spacing to height (*s/h)* ratio on '*j'* is same for both laminar and turbulent flows. It is observed that for lower values of *s/h* ratio up to 0.20, values of Colburn *'j'* factors are lower or even close to constant values for a given Reynolds number. The significance of higher *s/h* ratio is also observed in the plot. At lower Reynolds number ($Re < 1000$), the values of Colburn '*j'* factor are increased with the increase in *s/h* ratio from 0.15 to 0.81. It is true for other Reynolds number also ($Re > 1000$), but the rate of increase in '*j'* factor is comparatively lower.

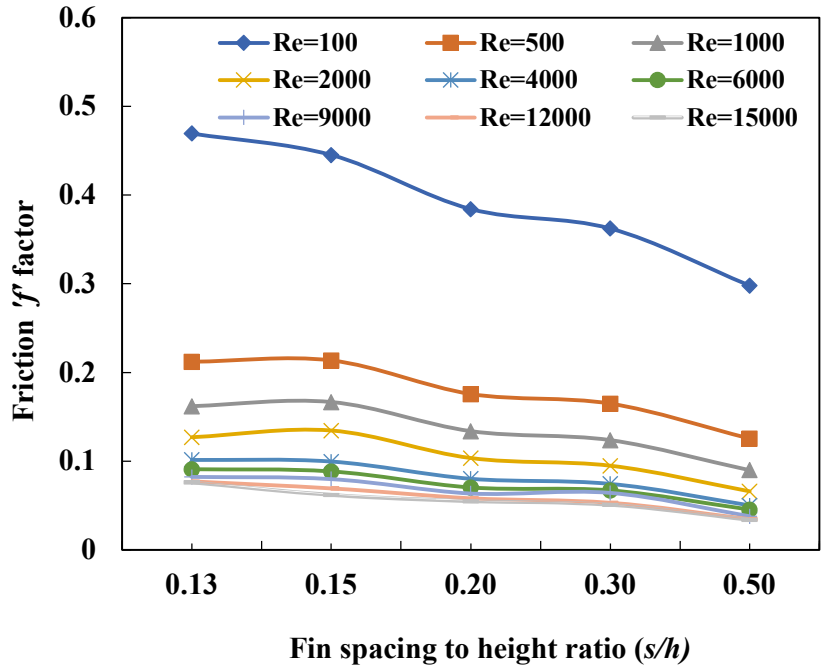


Fig. 3.11. Effect of fin spacing to height ratio on friction '*f'* factor

Fig. 3.11 shows the friction factor *'f'* plotted against fin spacing to height (*s*/*h*) ratio for varying Reynolds number. It is observed that the friction factor *'f'* decreases as expected, with Reynolds number. The rate of decrease in *'f'* factor is also found to be higher for lower Reynolds number and lower for higher range of Reynolds number. Further, it is observed that '*j*' factors are increased and '*f*' factors are decreased with increase in (*s*/*h*) ratio. This is because with the increase in spacing (*s*), (*s*/*h*) ratio is increased and hence the free flow area is increased in the fluid flow direction, which in turns decrease the friction factor '*f*'. Further, '*j*' factors are

increased (heat transfer is deceased in this case) with the increase in spacing (*s*), because the surface area available per unit length is lower, when spacing is higher and also the boundary layer will be thicker when spacing is increased.

**b) Effect of *t/s* ratio on *'j'* and *'f'* factors for serrated fin**

The Colburn '*j*' factors are plotted against the fin thickness to spacing (*t*/*s*) ratio for varying Reynolds number as shown in Fig. 3.12. As discussed in the previous section, it is observed that as the Reynolds number increases, *'j'* factor decreases. Fig. 3.12 shows that *'j'* factor decreases with increase in *t/s* ratio for a given value of Reynolds number. This is because, the fin thickness primarily increases with *t/s* ratio which introduces the resistances in the flow and eventually influences the heat transfer. Further, for a given value of Reynolds number, as *'j'* factor decreases with increase in fin thickness (*t*), heat transfer coefficient will also decrease in this case. This is because, heat transfer coefficient ($h_w$) is proportional to '*j*' factor, when the fin thickness (*t*) is increased and other fin parameters are kept constant.

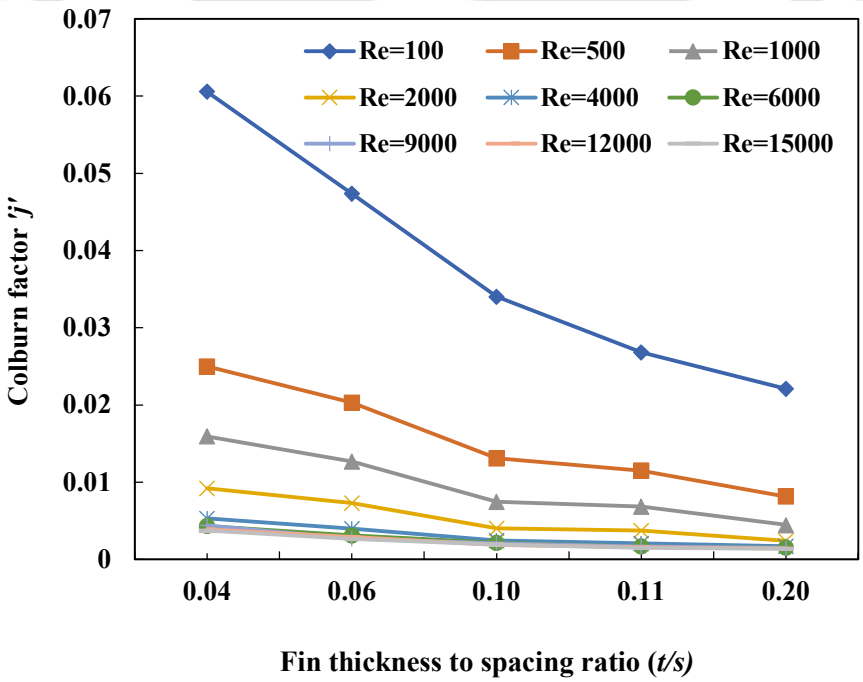


Fig. 3.12. Effect of fin thickness to spacing ratio on Colburn factor '*j*'

Fig. 3.13 shows the friction factor '*f*' plotted against the fin thickness to fin spacing (*t*/*s*) ratio for varying Reynolds number from 100 to 15000. It is observed that friction factor '*f*' decreases with Reynolds number and the rates of decrease is higher for lower Reynolds number and lower for higher range of Reynolds number. It is also found that the friction factor '*f*' decreases with

*t/s* ratio ranging from 0.04 to 0.20 for a given value of Reynolds number. In this study, effect of *t/s* ratio on '*j*' and '*f*' factors for serrated fin were carried out by varying fin thickness '*t*' and keeping the other fin parameters (*s*, *h* and *l*) constant. Friction '*f*' factor was plotted varying only the thickness '*t*' and it was observed that the '*f*' factor was increased when *t/s* ratio was increased as the increased fin thickness creates more resistances in the fluid flow path.

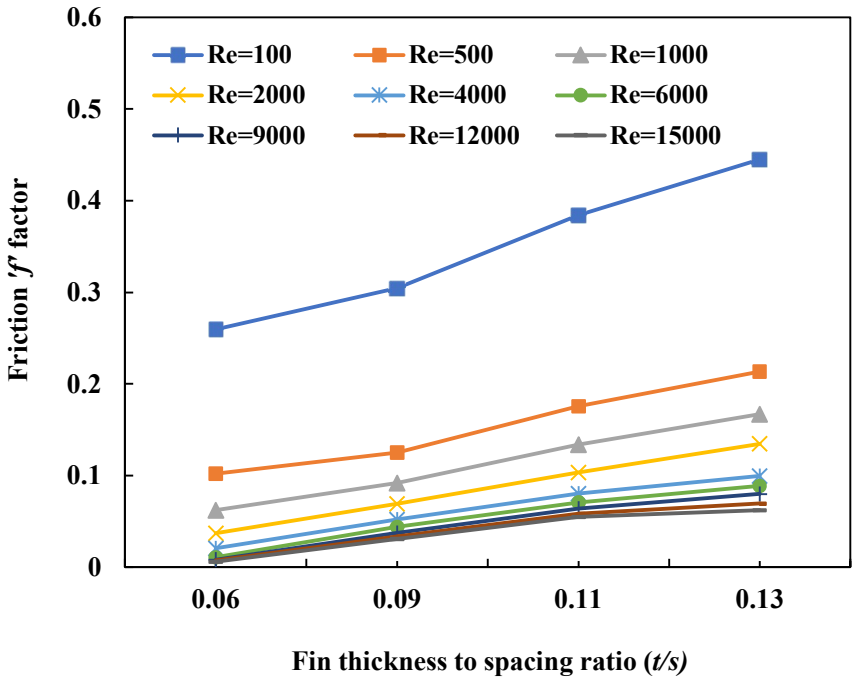


Fig. 3.13. Effect of fin thickness to spacing ratio on friction '*f*' factor

**c) Effect of *t/l* ratio on *'j'* and *'f'* factors for serrated fin**

The Colburn '*j*' factor is also presented against the fin thickness to length (*t*/*l*) ratio as shown in Fig. 3.14 for varying Reynolds number from 100 to 15000. It is observed that as Reynolds number increases, '*j*' is found to decrease and also the rate of decrease is higher for lower Reynolds number and lower for higher Reynolds number. Further, as *'j'* factor decreases at a given value of Reynolds number with the increase in fin thickness (*t*), heat transfer coefficient will also decrease in this case. This is because, heat transfer coefficient ($h_w$) is proportional to '*j*' factor when the fin thickness (*t*) is increased and other fin parameters are kept constant.

Fig. 3.15 shows the friction factor *'f'* plotted against the fin thickness to length (*t*/*l*) ratio for varying Reynolds number ranging from 100 to 15000. As expected, similar to other cases, it is also observed that as Reynolds number increases, *'f'* factor is found to decrease. The rate of decrease in this case also noticed to be higher for lower Reynolds number and lower for higher

Reynolds number. The fin thickness to length (*t*/*l*) ratio of serrated fin surfaces considered in this analysis is in the range of 0.02 to 0.06.

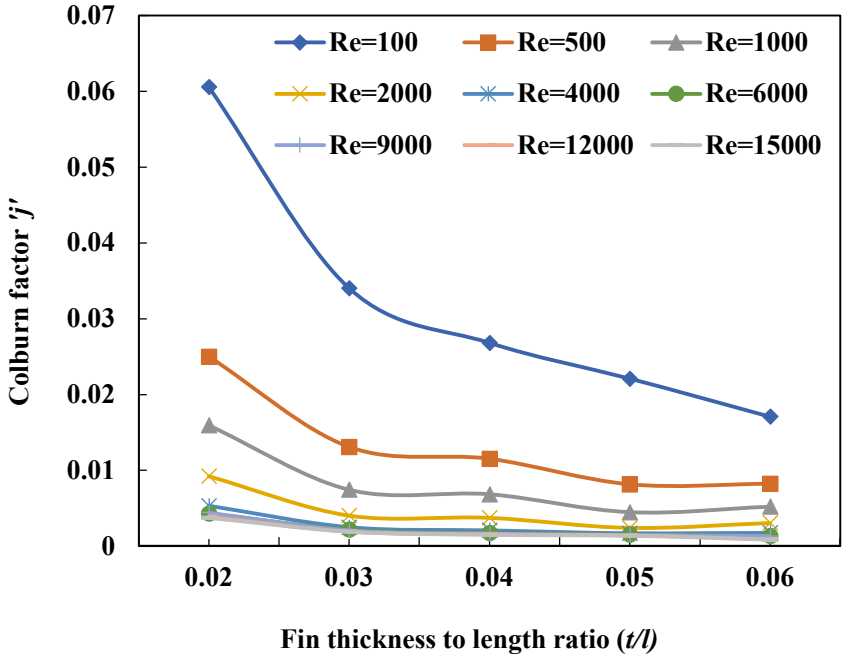


Fig. 3.14. Effect of fin thickness to length ratio on Colburn factor '*j*'

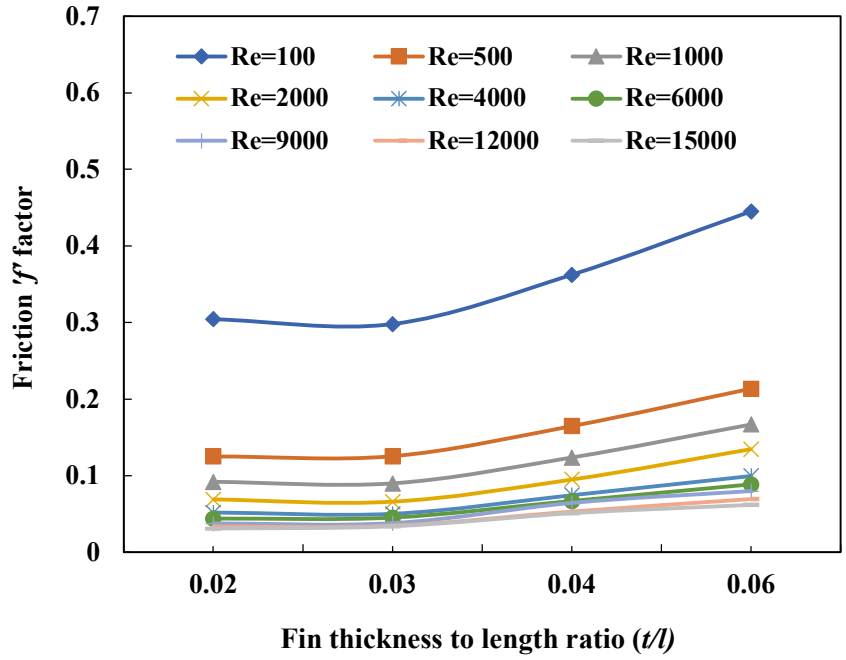


Fig. 3.15. Effect of fin thickness to length ratio on friction '*f*' factor

It is observed that the friction '*f*' factor increases while *t/l* ratio increases. This is because when thickness '*t*' is increased, *t/l* ratio is increased, keeping the other fin parameters constant. This thicker fin creates more resistances in the fluid flow path and thereby increase the factor '*f*'.

#### 3.2.6.7 Heat transfer and flow friction correlations for serrated fin surfaces

The numerical investigation is performed on the serrated fin surfaces of a brazed plate fin compact heat exchanger to estimate the heat transfer and pressure drop characteristics. As described in the previous sections, it is evident that there is a significant non-linearity in values of '*j*' and '*f*' factors. In the present study, 36 numbers of serrated fin surfaces are modelled for deriving suitable correlations of '*j*' and '*f*' factors. Based on the CFD data, these '*j*' and '*f*' correlations are derived in terms of non-dimensional fin geometrical parameters for both laminar and turbulent regions. Using the power law expressions, the correlations for Colburn '*j*' factor and friction '*f*' factor are derived as the function of Reynolds number, *s/h, t/s* and *t/l* ratios for serrated fin surfaces as indicated by Chennu and Paturu (2011), Sheik Ismail et al. (2009), which is expressed as follows:

$$j \text{ or } f = C(Re)^{a_0}\left(\frac{s}{h}\right)^{a_1}\left(\frac{t}{s}\right)^{a_2}\left(\frac{t}{l}\right)^{a_3} \tag{3.16}$$

where *C,* $a_0$, $a_1$, $a_2$ and $a_3$ are constants depend on the fin surfaces.

The correlations derived for Colburn factor '*j*' and friction '*f*' factor are shown in Eqs. (3.17) to (3.20) as the function of Reynolds number and dimensionless fin geometrical parameters (*s/h, t/s* and *t/l*) for water medium. These equations are derived for two range of Reynolds number, as shown in the following expressions:

For $100 \leq Re \leq 1000$

$$j = 1.007 * Re^{-0.42}\left(\frac{s}{h}\right)^{0.59}\left(\frac{t}{s}\right)^{-0.92}\left(\frac{t}{l}\right)^{0.94} \tag{3.17}$$

$$f = 4.014\, Re^{-0.47}\left(\frac{s}{h}\right)^{-0.17}\left(\frac{t}{s}\right)^{-1.11}\left(\frac{t}{l}\right)^{0.92} \tag{3.18}$$

For $1000 \leq Re \leq 15000$

$$j = 0.12\, Re^{-0.13}\left(\frac{s}{h}\right)^{0.57}\left(\frac{t}{s}\right)^{-1.09}\left(\frac{t}{l}\right)^{1.002} \tag{3.19}$$

$$f = 2.61\, Re^{-0.34}\left(\frac{s}{h}\right)^{-0.2}\left(\frac{t}{s}\right)^{-1.58}\left(\frac{t}{l}\right)^{1.4} \tag{3.20}$$

The correlations in Eqs. (3.17) to (3.20) correctly predict the present *'j'* and *'f'* numerical data, which is found to be more than 90 % accurate for most of the numerical data for both laminar and turbulent regions. Further, these present numerical results for serrated fin surfaces are also fitted in the correlations of Ramana Murthy et al. (2015) for '*j*' and '*f'* factors and found to be to be in fair agreement as shown in the Figs. 3.16 and 3.17, respectively.

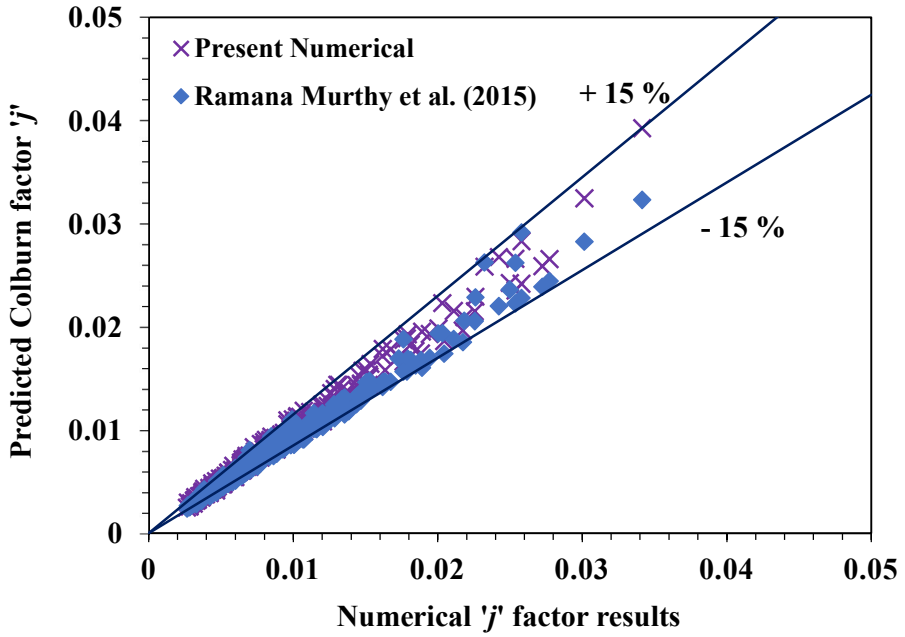


Fig. 3.16. Comparison of '*j*' results for serrated fin surfaces

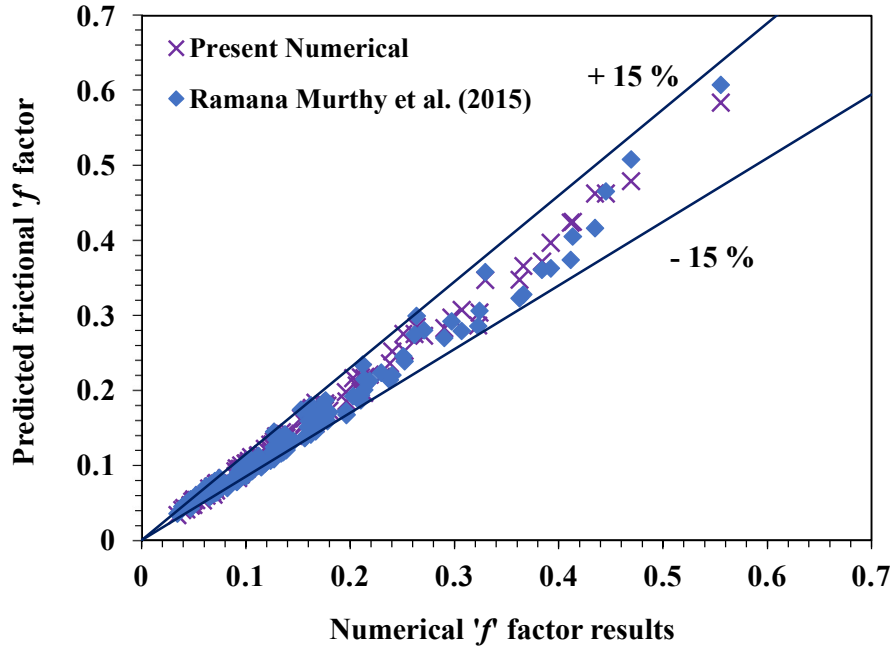


Fig. 3.17. Comparison of '*f*' results for serrated fin surfaces

### 3.2.7 Wavy fin surface

Wavy fins are mostly preferred in brazed plate fin compact heat exchanger, where the pressure drops are critical. However, wavy fins have lower heat transfer rate when compared to serrated fins. They have a lower flow interruption than serrated fin which results in lower pressure drop. The wavy fin is defined by fin thickness ($t$), wave amplitude ($a$), wave length ($\lambda$), fin height ($h$) and fin spacing ($s$). The wavy fin surface and pictorial representation of wavy fin illustrated by Amaranatha Raju et al. (2015) are shown in Figs. 3.18 (a) and (b), respectively.

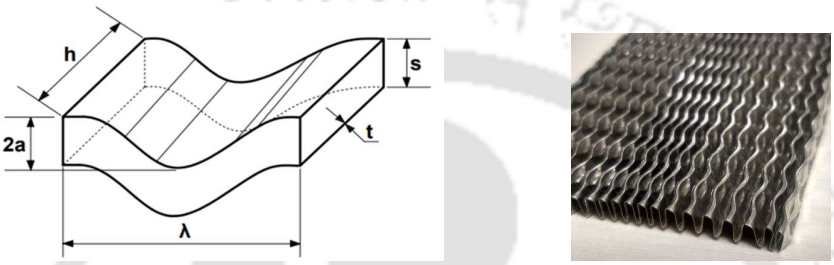


(a) (b)

Fig. 3.18. (a) Wavy fin surface, and (b) Wavy fin

#### 3.2.7.1 Numerical model

The numerical analysis has been performed in wavy fin surface using water medium for various fin geometrical parameters to predict the heat transfer and pressure drop characteristics in terms of Colburn factor '$j$' and friction '$f$' factor, respectively. In the present study, wavy fin model is created using CATIA software and then grid model is generated using hypermesh software. Initially, 2D mesh elements are generated using quad elements and then the 3D domain is generated using hexa elements. Figs. 3.19 (a) and (b) show the computational wavy fin domain and generated mesh model, respectively for the present heat transfer and fluid flow analysis. The wavy fin model constitutes fin spacing ($s$) in the $x$-direction, wave length ($\lambda$) in the $y$-direction and fin height ($h$) in the $z$-direction.

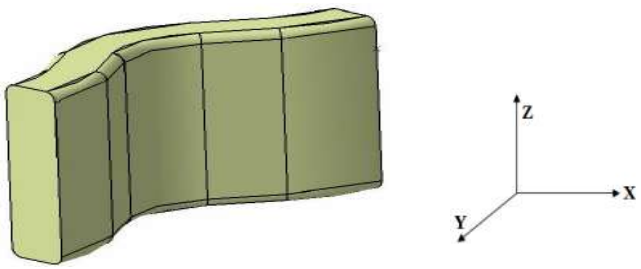


(a)

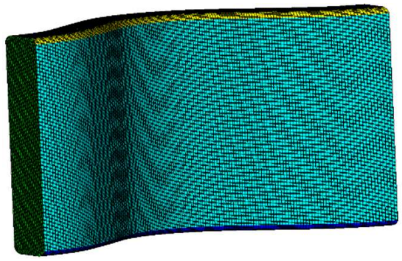

(b)

Fig. 3.19. (a) Wavy fin computational model, and (b) Wavy fin mesh model

#### 3.2.7.2 Dimensionless parameters

The wavy fin geometrical parameters are expressed in terms of dimensionless fin parameters, given by the flow cross-sectional aspect ratios, $s/h$, $a/s$ and $\lambda/a$. The correlations for Colburn factor '$j$' and friction '$f$' factor are expressed in terms of these dimensionless parameters and Reynolds number. The effect of fin thickness is neglected in this analysis. A total number of 41 wavy fin surfaces are considered for the numerical analysis. The range of dimensionless cross-sectional aspect ratios considered for the analysis are as follows:

$$0.0817 \leq s/h \leq 0.7967 \tag{3.21}$$

$$1.2126 \leq a/s \leq 2.4427 \tag{3.22}$$

$$\lambda/a = 4.8387 \tag{3.23}$$

The wave length ($\lambda$) and wave amplitude ($a$) of wavy fin surfaces considered for the present analysis are 9.53 mm and 1.97 mm, respectively. The Reynolds number range considered for both laminar and turbulent region are given below:

$$100 \leq Re \leq 1000 \text{ for laminar region} \tag{3.24}$$

$$1000 \leq Re \leq 15000 \text{ for turbulent region} \tag{3.25}$$

#### 3.2.7.3 Grid independency

In the present study, as mentioned in previous section for serrated fin surfaces, the grid independency check was performed for each fin surface before every analysis at a particular Reynolds number to finalize the number of elements as reported by Chennu and Paturu (2011), Sheik Ismail et al. (2009) and Amaranatha Raju et al. (2015). The pressure drop is taken as the

criteria in this analysis to verify the independency of the mesh in terms of numbers of elements, as shown in Fig. 3.20. It can be observed that after certain numbers of elements, there is no significant change in the pressure drop. Accordingly, the mesh size is finalised based on the numbers of elements after which the pressure drop value does not change.

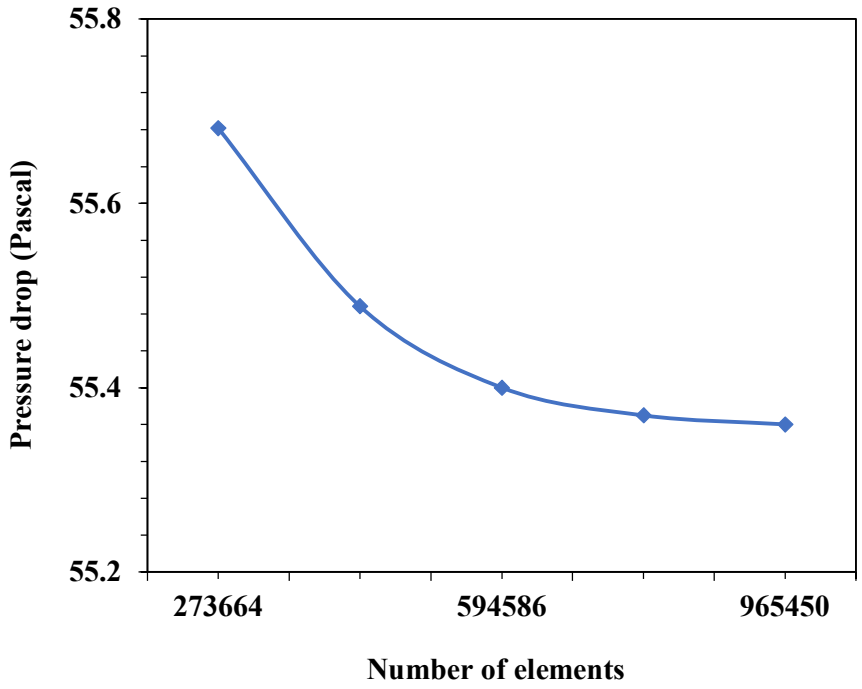


Fig. 3.20. Grid independency

### 3.2.7.4 Simulation results and discussion

The numerical studies are carried out on the smooth wavy fin surfaces of brazed plate fin compact heat exchanger to estimate the heat transfer and flow friction characteristics. The contours of pressure, velocity and temperature profiles for the Reynolds number ($Re$ = 800) are plotted as shown in Figs. 3.21 to 3.23. In the static pressure profiles shown in Fig. 3.21, it is observed that the highest pressure occurs at the leading edge of the fin. It is evident that the pressure is higher on the diverging side, when compared to the converging side of the fin. In the velocity profile shown in Fig. 3.22, it is evident that the flow is separating from the diverging side of the fin and flows towards the converging side, which creates the flow recirculation. Further, in the static temperature profiles shown in Fig. 3.23, it is observed that the temperature is higher near the wall than the core region. In the recirculation region, more heat transfer is visible on the temperature contour. The Reynolds number has a significant impact on the pressure, velocity and temperature profiles.

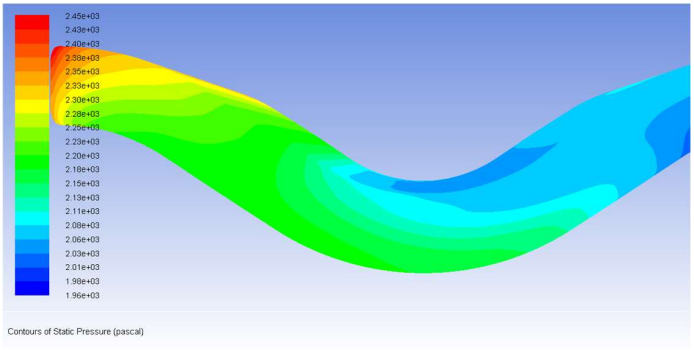


Fig. 3.21. Pressure profile at *Re* = 800

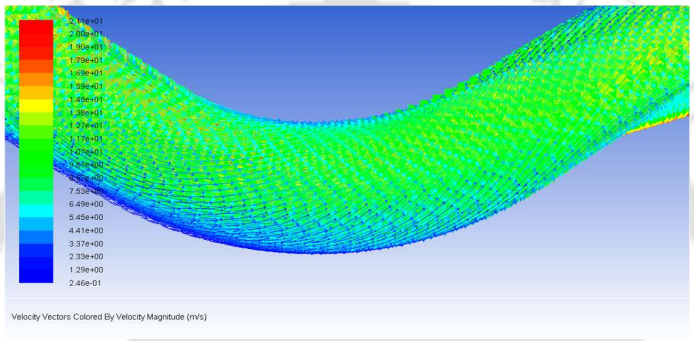


Fig. 3.22. Velocity profile at *Re* = 800

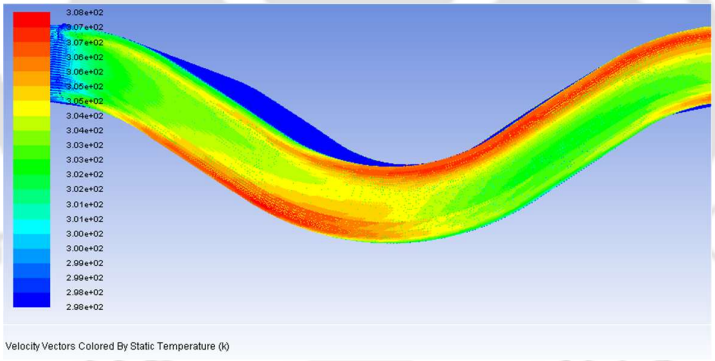


Fig. 3.23. Temperature profile at *Re* = 800

### 3.2.7.5 Effect of fin geometrical parameters and Reynolds number

The numerical analysis on wavy fin surfaces is performed to analyse the effect of Reynolds number and dimensionless fin parameters (*s/h* and *a/s*) on Colburn '*j*' factor and friction factor *'f'* using water medium. The effect of Reynolds number for the range of 100 to 15000 and fin dimensionless parameters are explained in the subsequent sections.

**a) Effect of *s/h* ratio on *'j'* and *'f'* factors for wavy fin**

The Colburn '*j*' factor and friction factor '*f*' are plotted as shown in Figs. 3.24 and 3.25, respectively against the fin spacing to height (*s/h*) ratio for varying Reynolds number ranging from 100 to 15000.

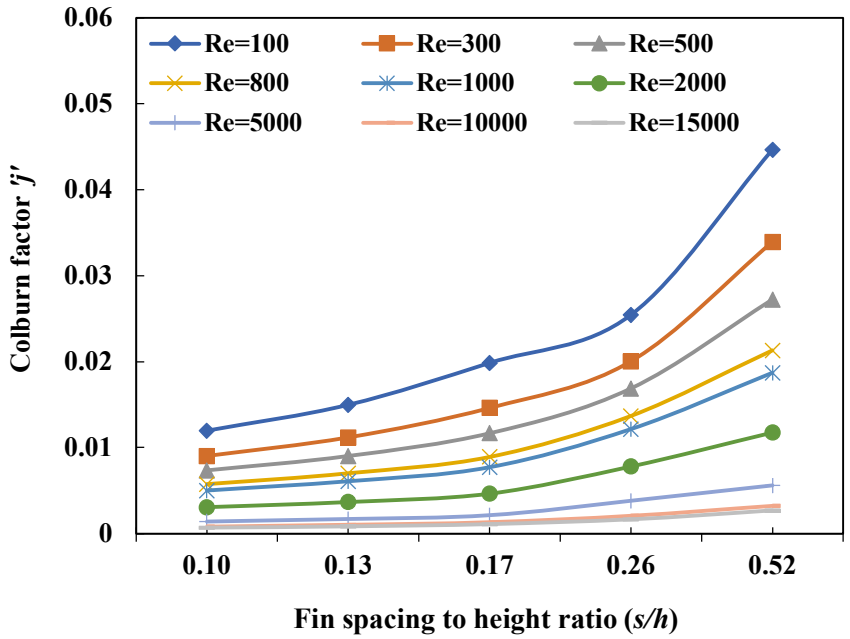


Fig. 3.24. Effect of fin spacing to height (*s/h*) ratio on Colburn factor *'j'*

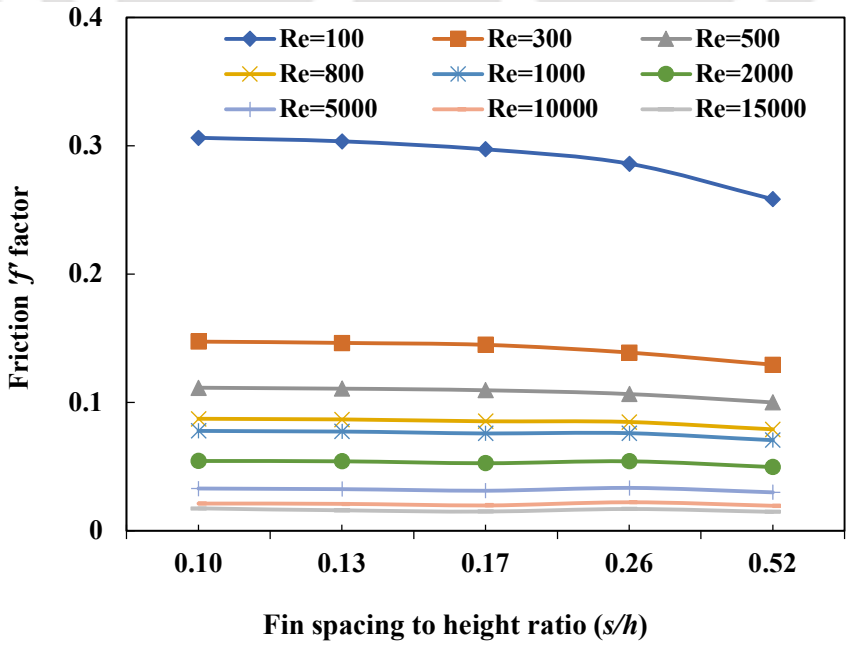


Fig. 3.25. Effect of fin spacing to height (*s/h*) ratio on friction *'f'* factor

Figs. 3.24 and 3.25 shows that both '*j*' and '*f*' factors decrease with the increase in Reynolds number as expected. The rate of decrease in '*j*' & '*f*' factors are found to be higher for lower Reynolds number and lower for higher Reynolds number, as observed for serrated fins. It is evident that the increase in *s/h* ratio is predominant for lower Reynolds number range (*Re* < 1000) and it is not that significant for higher Reynolds number (*Re* > 1000). The effect of *s/h* ratio is clearly evident and the effect is same for both laminar and turbulent flow regions. For lower values of *s/h* ratio up to 0.17, the values of '*j*' and '*f*' factors are found to be lower or even become close to constant values for a given Reynolds number. Fig. 3.24 shows that the Colburn '*j*' factor values are less effective for lower value of *s/h* ratio up to 0.172. The friction '*f*' factor values are also less effective for lower value of *s/h* ratio up to 0.3 as illustrated in the Fig. 3.25. In both cases, it can be observed that '*j*' and '*f*' factors are more effective for lower range of Reynolds number.

**b) Effect of *a/s* ratio on '*j*' and '*f*' factors for wavy fin**

The Colburn '*j*' factor and friction factor '*f*' are plotted against wave amplitude to spacing (*a/s*) ratio for varying Reynolds number ranging from 100 to 15000, as shown in Figs. 3.26 and 3.27, respectively.

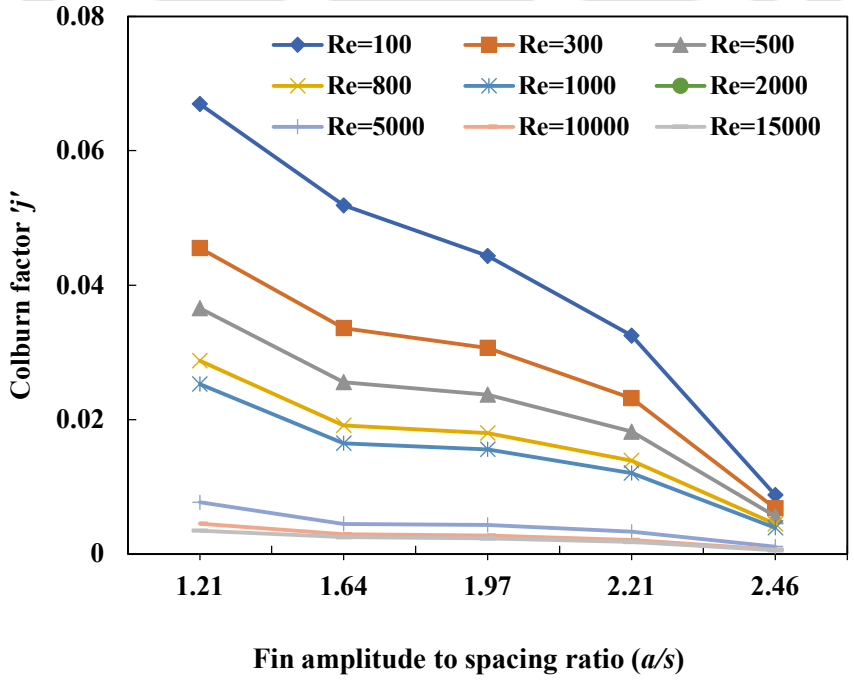


Fig. 3.26. Effect of fin amplitude to spacing (*a/s*) ratio on Colburn factor '*j*'

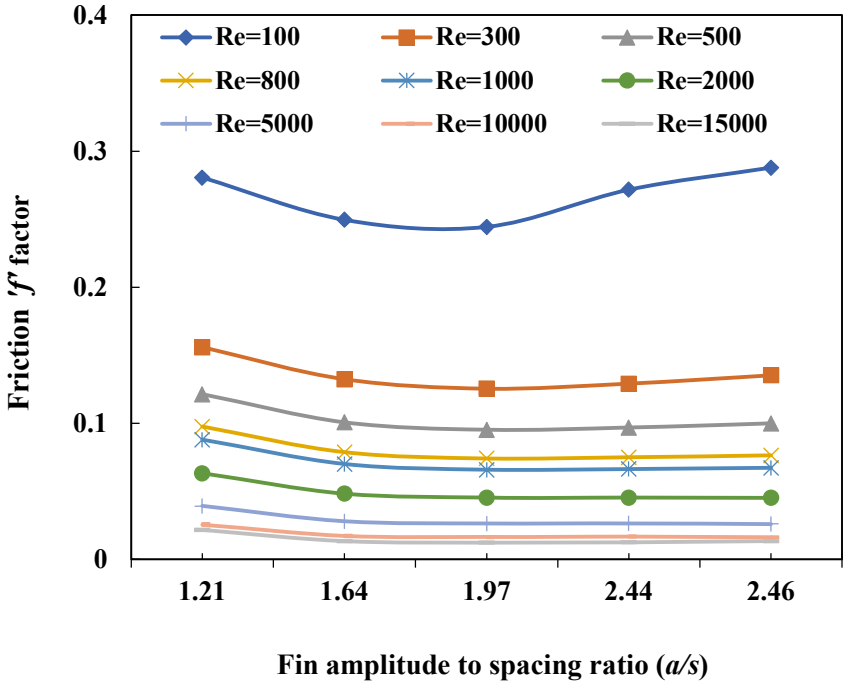


Fig. 3.27. Effect of fin amplitude to spacing (*a/s*) ratio on friction '*f*' factor

Figs. 3.26 and 3.27 show that both values of '*j*' and '*f*' factors decrease with the increase in Reynolds number as expected. The '*j*' factor decreases with *a/s* ratio as shown in Fig. 3.26. This is because an increase in the wave amplitude leads to the flow recirculation in the wavy flow passages and results in higher heat transfer. Fig. 3.27 shows that the friction factor '*f*' decreases with *a/s* ratio up to 2, for a given Reynolds number and beyond this value of *a/s* ratio, '*f*' factor becomes almost constant or tends to increase at higher Reynolds number. This ratio is found to be critical after which the slope becomes constant or tend to increase for a particular Reynolds number. This is because higher value of wave amplitude introduces the form drag causing increase in friction factor and pressure drop.

### 3.2.7.6 Heat transfer and flow friction correlations for wavy fin surfaces

An extensive numerical study has been carried out on heat transfer and pressure drop phenomena on wavy fin surfaces. From the previous sections, it can be understood that there is a significant non-linearity in values of '*j*' and '*f*' factors with varying Reynolds number and fin geometrical parameters. In this section, the correlations derived for Colburn factor '*j*' and friction factor '*f*' are discussed, which are developed considering the CFD data of 41 numbers of wavy fin surfaces, Reynolds number ranging from 100 to 15000 and dimensionless fin

parameters. Two separate equations for '*f*' and '*j*' factors are expressed for both low and high Reynolds number regions. Using power law expressions, the suitable correlations for Colburn factor '*j*' and friction factor '*f*' are derived as a function of Reynolds number and dimensionless fin parameters (s/*h* and *a/s*). The derived correlations can be represented in general form as follows as indicated by Amaranatha Raju et al. (2015):

$$j \text{ or } f = C(Re)^{a_0}\left(\frac{s}{h}\right)^{a_1}\left(\frac{a}{s}\right)^{a_2} \tag{3.26}$$

where $C$, $a_0$, $a_1$ and $a_2$ are constants depends on the fin surfaces and geometry. The two separate equations have been proposed for both laminar and turbulent regions based on the range of Reynolds number, given as follows:

For $100 \leq Re \leq 1000$

$$j = 2.55\, Re^{-0.69}\left(\frac{s}{h}\right)^{1.02}\left(\frac{a}{s}\right)^{0.22} \tag{3.27}$$

$$f = 4.042\, Re^{-0.55}\left(\frac{s}{h}\right)^{-0.093}\left(\frac{a}{s}\right)^{-0.604} \tag{3.28}$$

For $1000 \leq Re \leq 15000$

$$j = 3.82\, Re^{-0.76}\left(\frac{s}{h}\right)^{1.003}\left(\frac{a}{s}\right)^{0.3} \tag{3.29}$$

$$f = 6.42\, Re^{-0.59}\left(\frac{s}{h}\right)^{-0.08}\left(\frac{a}{s}\right)^{-0.92} \tag{3.30}$$

The above correlations in Eqs. (3.27) to (3.30) accurately predict the numerical data of *'j'* and *'f'* factors, which is found to be more than 90 % accurate for most of the numerical data for both laminar and turbulent regions. These correlations for *'j'* and *'f'* factors predict the heat transfer and pressure drop characteristics of wavy fins surfaces for water medium. These heat transfer correlations are further used in the present study in estimating the refrigerant heat transfer coefficient. Furthermore, these present numerical results for wavy fin surfaces are also fitted in the corelations of Amaranatha Raju et al. (2015) for Colburn '*j*' and friction '*f*' factors and the numerical results are found to be in fair agreement, as shown below in the Figs. 3.28 and 3.29, respectively.

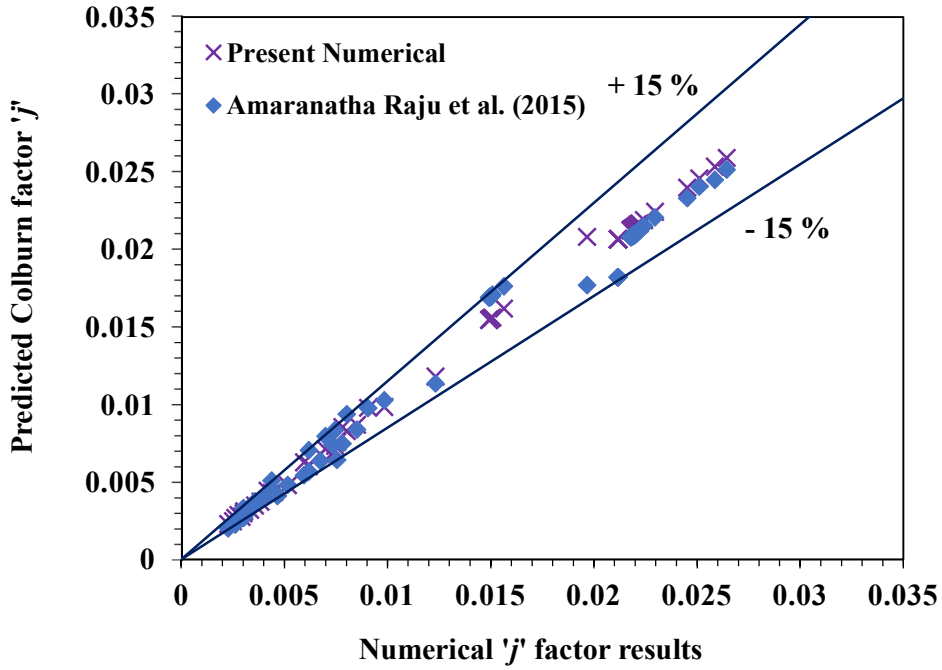


Fig. 3.28. Comparison of '*j*' results for wavy fin surfaces

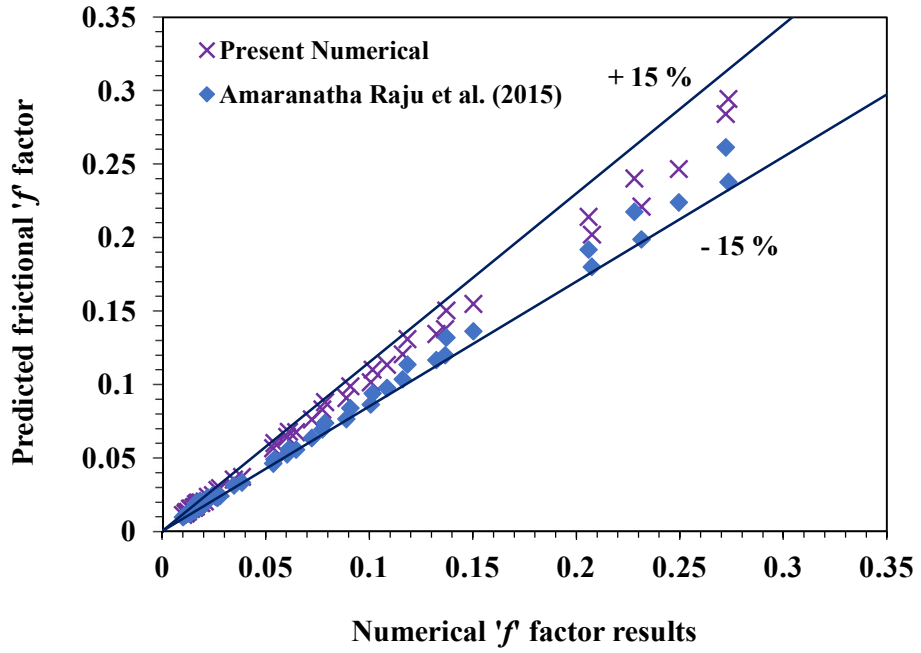


Fig. 3.29. Comparison of '*f*' results for wavy fin surfaces

### 3.3 Experimental investigation on single-phase heat transfer

The primary objective of the present investigation is to estimate the condensation heat transfer coefficient of refrigerants R134a and R1234yf in test condenser. There are two flow circuits in the test condenser, one for the refrigerant flow and other circuit is for the demineralised (DM)

water flow. Thus, the single-phase experimental investigation was carried out to estimate the heat transfer coefficient of DM water in serrated and wavy fin test condensers. Further, it was used in the expression of overall heat transfer coefficient of heat exchanger to estimate the refrigerant heat transfer coefficient. In this section, the comparison of experimental single-phase heat transfer coefficient of water with the numerical results estimated in the previous sections is presented. In this chapter, the test condensers (brazed plate fin compact heat exchangers) considered for the present experiments are discussed and presented in the subsequent sections. The three types of test condensers considered in the present investigation are with two numbers of serrated fin surfaces and one number of wavy fin surfaces. These test sections are employed in the present investigation for both water-to-water single-phase test and also for the condensation experiments.

### 3.3.1 Brazed plate fin test condenser

The test condensers considered are the brazed plate fin compact heat exchanger with serrated and wavy fin surfaces. These test condensers (TC) are made of aluminium alloy that is widely preferred in the manufacturing of compact heat exchangers, due to its lower density, higher thermal conductivity and higher strength as compared to other materials. The present test condenser is made up of aluminium alloy AA3003 and insulated with aerospace grade insulation material of 10 mm thick polyamide foam coated with hypalon. The size of the test condenser is 150 mm x 150 mm. This test condenser has a cross flow arrangement and it has a single passage for refrigerant, through the inner channel of the test section and two outer passages are for DM water circulation. These test condensers either have a serrated or wavy fin surfaces arrangement, for both refrigerant and water passages.

The selection of fin geometry plays a significant role in the design and development of a brazed plate fin compact heat exchanger. The heat transfer and pressure drop characteristics in common practice highly depend on the fin geometry used in the heat exchanger. The heat transfer in the heat exchanger is usually higher with fins having larger fin densities and higher compactness and the pressure drop associated in this case is also higher. There are various types of fins that are mostly used in the brazed plate fin compact heat exchanger namely serrated fins, wavy fins, plain fins, perforated and louvered fins. The performance of serrated fins in terms of heat transfer is higher and also results in higher pressure drops, compared to other types of fins. This is due to the offset nature of fins, as it leads to the frequent interruptions and breakage of boundary layers in the fluid flow path. In the present investigation, based on the

availability of fins and their usage in wide areas, two types of serrated fin surfaces and one type of wavy fin surfaces are selected. The test condensers employed in the present experiments are developed based on the varying geometrical parameters of serrated and wavy fin surfaces. The schematic representation of test condenser core model is shown in Fig. 3.30. The geometrical parameters of serrated and wavy fin test condensers are given in Table 3.2, which are named as TC1, TC2 and TC3.

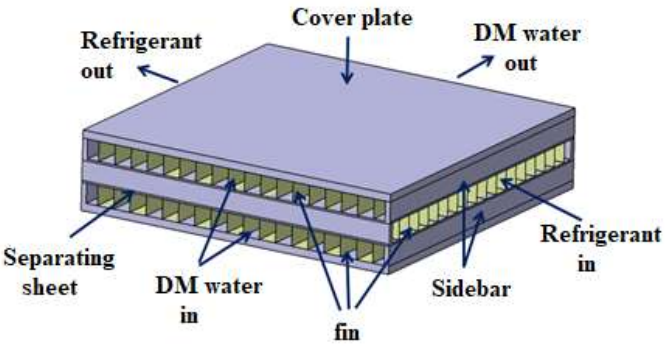


Fig. 3.30. Test condenser core model

Table 3.2. Geometrical parameters of serrated and wavy fins test condensers

| Test unit | Flow circuit | Fin density (FPI) | Fin height (mm) | No. of fins layers | Fin thickness (mm) | Fin size (mm) | | Fin type |
|---|---|---|---|---|---|---|---|---|
| | | | | | | Flow length | Width | |
| TC1 | Refrigerant | 18 | 3.8 | 1 | 0.254 | 150 | 142 | Serrated |
| | DM water | 28 | 5 | 2 | 0.127 | 150 | 142 | |
| TC2 | Refrigerant | 28 | 3 | 1 | 0.127 | 150 | 142 | |
| | DM water | 28 | 5 | 2 | 0.127 | 150 | 142 | |
| TC3 | Refrigerant | 16 | 4.1 | 1 | 0.0762 | 150 | 142 | Wavy |
| | DM water | 18 | 10.2 | 2 | 0.152 | 150 | 142 | |

The present test condensers (TC1, TC2 and TC3) are manufactured by the vacuum brazing process, which is a very popular technique in the development of compact heat exchangers having interrupted and uninterrupted fins. In this process, the corrugated fins, sidebars, separating sheets, top and bottom cover plates are held together in a fixture with predefined

load. It is then placed in a vacuum brazing furnace having a pre-defined brazing cycle, to obtained a brazed heat exchanger core as illustrated in Fig. 3.31. This core has a stack of three fin layers, the middle section of fin layer is for refrigerant flow and the outer two layers of fins are for DM water flow. After the brazing process, the pneumatic leak test is performed and once it is passed, the headers, connectors manifolds and ports are then welded to the brazed test core to obtain an assembled test condenser. The overall size of test condenser after the insulation is about 400 mm x 400 mm and the height of the test condenser is dependent on the fin height used. The final assembled test condenser with insulation is shown in Fig. 3.32.

Fig. 3.31. Brazed test core

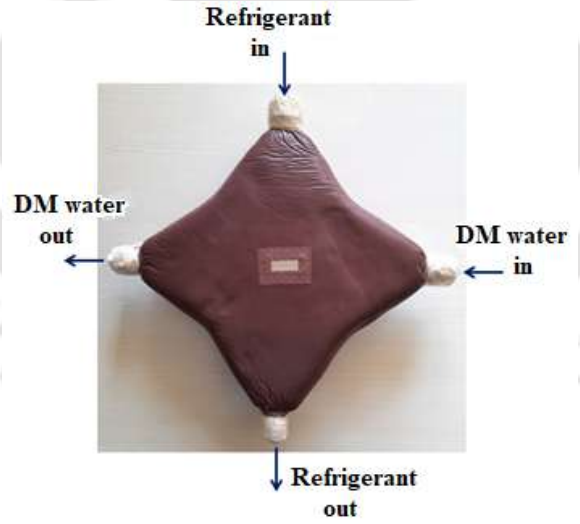


Fig. 3.32. Assembled test condenser with insulation

### 3.3.2 Single-phase water-to-water investigation

In this section, a single-phase experimental investigation performed on serrated and wavy fins test condensers are discussed and presented. The water-to-water test are carried out to estimate

the single-phase heat transfer coefficient of DM water using Modified Wilson plot technique as described by Muley and Manglik (1999), Longo and Gasparella (2007) and Kwon et al. (2019). The single-phase test set up was established and experiments were performed on serrated and wavy fins test condensers (TC1 and TC3), respectively which are described in the previous sections. These two test condensers were also considered for the present condensation experiments.

### 3.3.2.1 Single-phase test setup

The experimental set up was established to carry out the single-phase test to estimate the heat transfer coefficient of DM water. The layout of the single-phase test facility is illustrated in Fig. 3.33, which consists of chillers, test heat exchanger and a data acquisition system to record the measured data in the form of digital output. The test heat exchangers used is this analysis are the test condensers (TC1 and TC3) having serrated and wavy fins, respectively. The de-mineralized (DM) water circulations as a hot and cold streams are used in the circuits of test condenser during the experiments. These two circuits of the test condensers are integrated to the chillers as shown in Fig. 3.33, which are capable of supplying DM water at the varying temperatures ranging from 5 °C to 60 °C. The required water flow rates up to 60 lpm during the test are controlled and maintained by the flow regulating valves for the two separate streams of hot and cold water. Each test condition was obtained at the inlet of the test condenser by controlling the flows and temperatures circulating from the chillers. The temperatures of hot and cold streams water in the respective chillers are also maintained separately. The photograph of experimental set up is shown in Fig. 3.34.

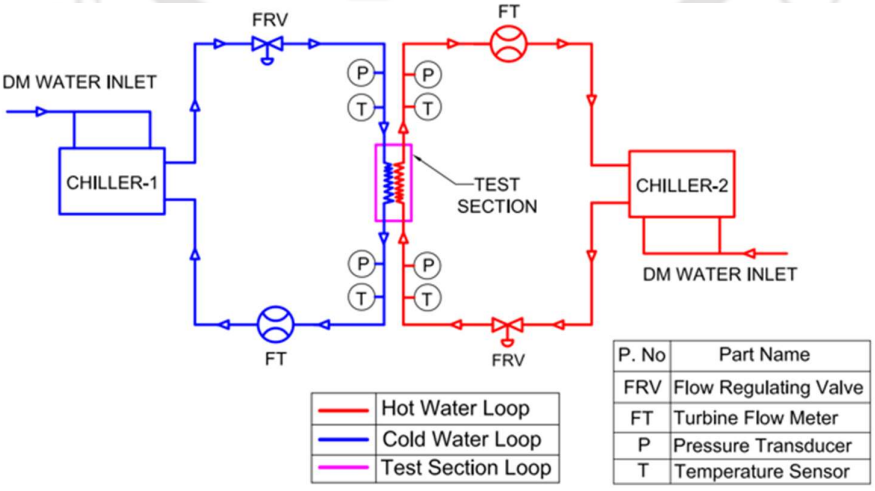


Fig. 3.33. Single-phase test facility layout

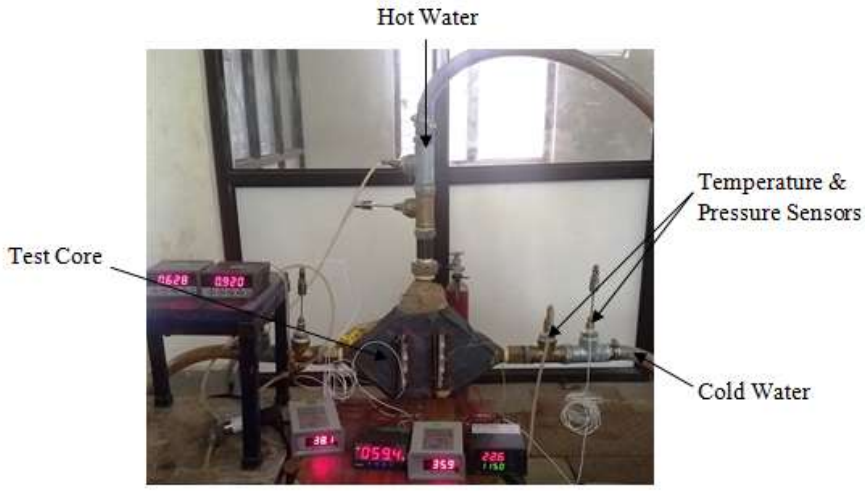


Fig. 3.34. Single-phase test setup

The temperatures of DM water at the inlet and outlet of the test condenser were measured by using resistance thermometer (RTD). The pressure at the inlets of test section on both circuits were measured by strain gage pressure transducer and the mass flow rate of DM water was measured by turbine flow meter installed in both the circuits. The data acquisition system connected to the industrial PC was employed to record the measured pressures, temperatures, differential pressures and water flow rates at different test points. The accuracy range of the measuring devices are listed in Table 3.3.

Table 3.3. Accuracy range of measuring devices

| Device | Type | Accuracy |
|---|---|---|
| Resistance thermometer | RTD | ± 0.2 °C |
| Pressure transducer | Strain gage | ± 0.25 % FS |
| Differential pressure transducer | Strain gage | ± 0.25 % FS |
| Flow meter | Turbine | ± 0.25 % |

### 3.3.2.2 Data reduction of single-phase heat transfer

The data reduction was performed and discussed in this section to estimate the single-phase heat transfer coefficient of DM water. The amount of heat transfer rate from hot to the cold stream of DM water can be determined from the principle of energy conservation. During the experiments, the energy balance estimated for both hot side ($\dot{Q}_h$) and cold side ($\dot{Q}_c$) water

streams was in close match within ± 5 % for all the tests. The analysis on single-phase energy balance is discussed in later section in this chapter. The average of $\dot{Q}_h$ and $\dot{Q}_c$ was considered as the total heat load ($\dot{Q}_{avg}$) for the analysis. The heat transfer rate from hot to the cold water can be calculated as follows:

$$\dot{Q}_c = \dot{m}_c C_{p,c}\left(T_{o,c} - T_{i,c}\right) \tag{3.31}$$

$$\dot{Q}_h = \dot{m}_h C_{p,h}\left(T_{i,h} - T_{o,h}\right) \tag{3.32}$$

$$\dot{Q}_{avg} = \frac{1}{2}\left(\dot{Q}_c + \dot{Q}_h\right) \tag{3.33}$$

Here, $T_{i,h}$ and $T_{o,h}$ are the temperatures of hot side water at the inlet and outlet of the test condenser, respectively. $T_{i,c}$ and $T_{o,c}$ represent the temperatures of cold water at the inlet and outlet, respectively. The mass flow rate and heat capacity of both hot and cold-water streams are given by $\dot{m}$ and $C_p$, respectively.

Based on Newton's law of cooling, the overall heat transfer coefficient ($U$) of heat exchanger is determined by the following expression:

$$\dot{Q}_{avg} = UA_c\Delta T_{ln} \tag{3.34}$$

where, $A_c$ is cold side area of the test section and $\Delta T_{ln}$ is the logarithm mean temperature difference (LMTD), defined as follows:

$$\Delta T_{ln} = \frac{\left(T_{i,h}-T_{o,c}\right)-\left(T_{o,h}-T_{i,c}\right)}{ln\frac{\left(T_{i,h}-T_{o,c}\right)}{\left(T_{o,h}-T_{i,c}\right)}} \tag{3.35}$$

The heat transfer coefficient ($h_c$) on cold side of the test condenser is derived considering the cold side area ($A_c$) of the test section and using the expression of following overall heat transfer coefficient ($U$), assuming no fouling resistance.

$$\frac{1}{U} = \frac{1}{\eta_{o,h}h_h\frac{A_h}{A_c}} + \frac{t_p}{\lambda\frac{Ap}{A_c}} + \frac{1}{\eta_{o,c}h_c} \tag{3.36}$$

where, $t_p$ is the plate thickness of test condenser, $A_p$ is the area of the plate, $\lambda$ is the plate thermal conductivity, $A_h$ is area of the hot stream water side and $\eta_o$ is the overall fin surface efficiency of heat exchanger, which is given by:

$$\eta_o = 1 - a(1 - \eta_f) \tag{3.37}$$

where, '$a$' is the ratio of the fin area to the total area and fin efficiency ($\eta_f$) is defined as:

$$\eta_f = \frac{\tanh(ml)}{ml} \tag{3.38}$$

$$\text{here, } m = \sqrt{\frac{2h\left(1+\frac{t}{l}\right)}{\lambda * t}} \tag{3.39}$$

$$l = \frac{h}{2}, \text{ here } h \text{ is height} \tag{3.40}$$

In the present study, water-to-water experiments are performed in the serrated and wavy fin test condensers (TC1 and TC3) separately, to determine the heat transfer coefficient of DM water. This study is performed using modified Wilson plot technique as described by Muley and Manglik (1999) and Kwon et al. (2019). The modification of the Wilson plot technique (Wilson, 1915) takes into account the influences of varying fluid property. The water-to-water data from the present analysis are plotted in terms of parameters *X* and *Y* as shown in Figs. 3.35 and 3.36 for the serrated and wavy fin, respectively. The expression of *X* and *Y* shown below have linear function to each other and are derived from the expression of overall heat transfer coefficient of water. The exponents on Reynolds number (0.4 for serrated fins and 0.43 for wavy fins) are derived by a best fitting equation, based on the experimental data. The hot (h) and cold (c) suffixes in the equations corresponds to the hot and cold side of the test condenser. The expression of parameters *X* and *Y* for serrated fins test condenser (TC1) are as follows:

$$X = \frac{\eta_h}{\eta_c}\frac{A_h}{A_c}\frac{\left(\frac{\lambda_w}{D_h} Re^{0.4} Pr^{0.33}\right)_{Hot}}{\left(\frac{\lambda_w}{D_h} Re^{0.4} Pr^{0.33}\right)_{Cold}} \tag{3.41}$$

$$Y = \left(\frac{\eta_h}{U}\frac{A_h}{A_c} - \frac{\eta_h\, t\, A_h}{\lambda_p\, A_p}\right)\left(\frac{\lambda_w}{D_h}\, Re^{0.4}\, Pr^{0.33}\right)_{Hot} \tag{3.42}$$

The expression of parameters *X* and *Y* for wavy fins test condenser (TC2) are as follows:

$$X = \frac{\eta_h}{\eta_c}\frac{A_h}{A_c}\frac{\left(\frac{\lambda_w}{D_h} Re^{0.43} Pr^{0.33}\right)_{Hot}}{\left(\frac{\lambda_w}{D_h} Re^{0.43} Pr^{0.33}\right)_{Cold}} \tag{3.43}$$

$$Y = \left(\frac{\eta_h}{U}\frac{A_h}{A_c} - \frac{\eta_h\, t\, A_h}{\lambda_p\, A_p}\right)\left(\frac{\lambda_w}{D_h}\, Re^{0.43}\, Pr^{0.33}\right)_{Hot} \tag{3.44}$$

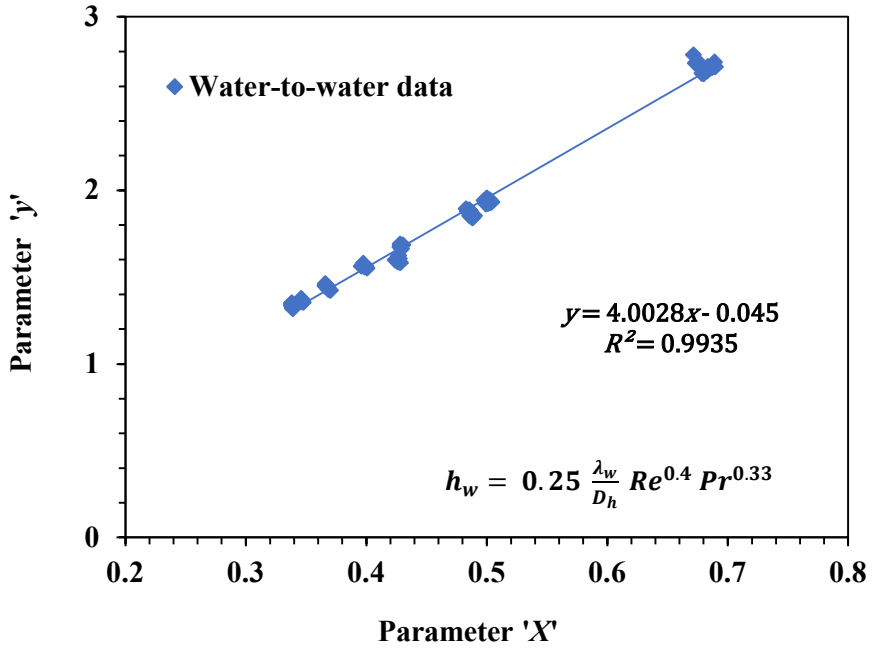


Fig. 3.35. Water-to-water data for serrated fin test condenser

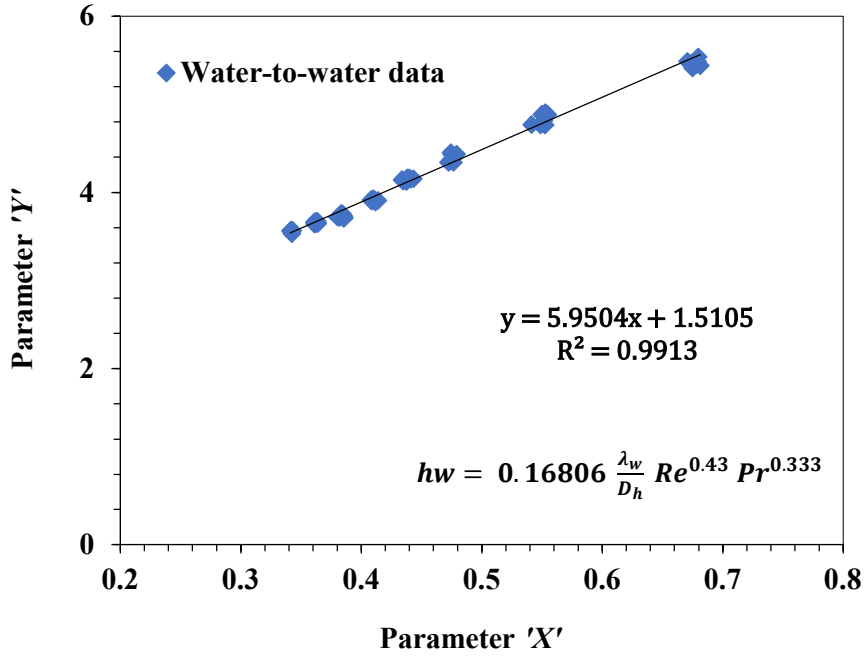


Fig. 3.36. Water-to-water data for wavy fin test condenser

The heat transfer coefficient of DM water ($h_w$) estimated from the experimental data for both serrated and wavy fins are presented in Eqs. (3.45) and (3.46), respectively.

$$h_w = 0.25 \left(\frac{\lambda_w}{D_h}\right) {Re_w}^{0.4} Pr^{0.33} \quad (3.45)$$

$$h_w = 0.168\,(\frac{\lambda_w}{D_h})\,Re_w{}^{0.43}Pr^{0.33} \tag{3.46}$$

Eqs. (3.45) and (3.46) are calibrated for Reynolds number range of 150 to 690 for serrated fin surfaces and 120 to 650 for wavy fin surfaces and these equations are valid only for these limited range of present water-to-water experimental data. The uncertainty in heat transfer coefficient of DM water ($h_w$) was estimated to be within ± 4.3 % and the uncertainty analysis estimation is provided in Appendix B. The subsequent condensation experiments were maintained within this range of water-to-water data to determine the refrigerant heat transfer coefficient and frictional pressure drop.

### 3.4 Comparison of numerical and experimental heat transfer coefficients

In the previous sections, the estimation of numerical and experimental heat transfer coefficient of water ($h_w$) for serrated and wavy fin surfaces are presented. In this section, the present experimental heat transfer coefficients of water are compared with the numerical results as shown in Figs. 3.37 and 3.38 for serrated and wavy fin surfaces, respectively.

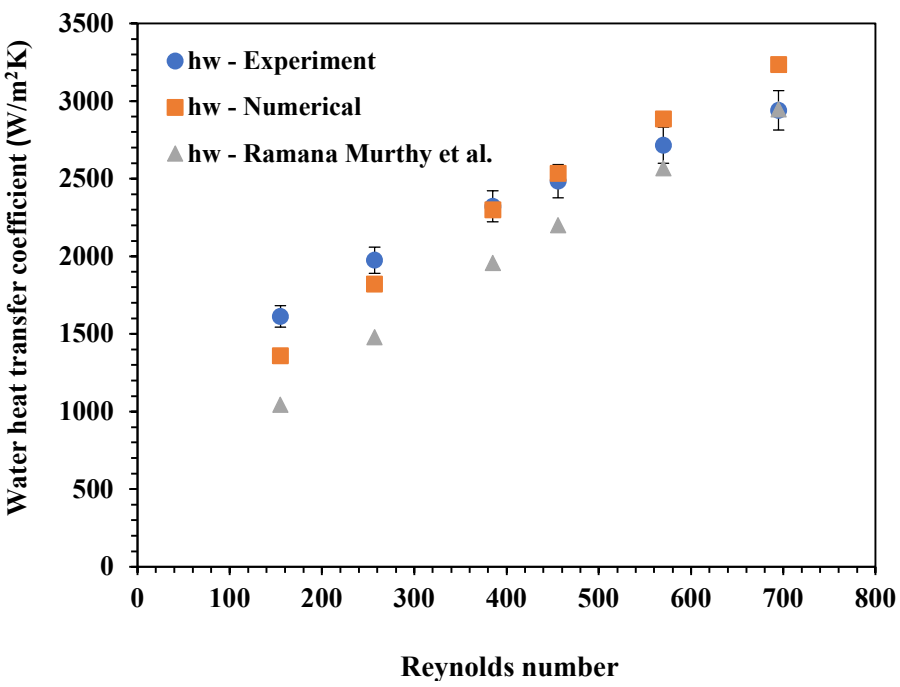


Fig. 3.37. Heat transfer coefficient of water for serrated fins

The comparison of the experimental and numerical results for serrated fin surfaces is shown in Fig. 3.37 along with the findings of Ramana Murthy et al. (2015) and the results are found to

be in fair agreement. It was observed that the experimental and numerical results match within 15 % for the lower Reynolds number range up to 160 and deviations are less than 10 % for the higher Reynolds number. Fig. 3.38 shows the comparison of experimental and numerical results for wavy fin surfaces along with findings of Amaranatha Raju et al. (2015). It was found that the experimental and numerical results match within 11 % for the Reynolds number range of 120 to 650.

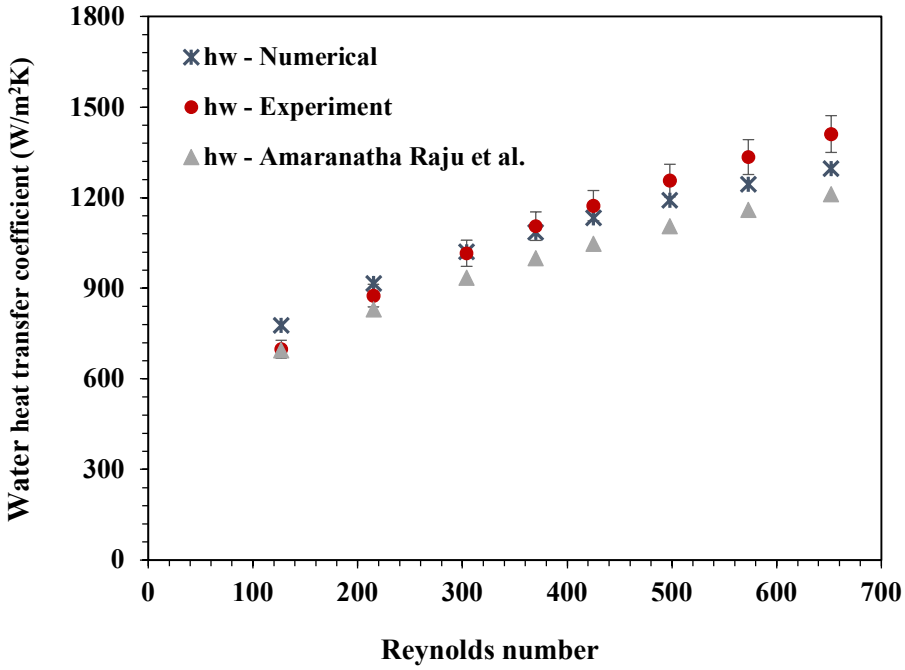


Fig. 3.38. Heat transfer coefficient of water for wavy fins

## 3.5 Single-phase energy balance

In this section, single-phase experimental analysis is discussed, that was conducted prior to the present condensation experiments, discussed in later chapters. In this single-phase analysis, the heat transfer between the superheated refrigerant vapour and the cold DM water in the test condenser was considered. The energy balance between the refrigerant superheated vapour and cold DM water was within ± 5 % during the experiments. This is due to the errors and the accuracies of various sensors and instruments, which are employed in the test facility. Further, in practice small amount of heat transfer from the test section to surrounding ambient is also expected during the analysis, which is discussed in this section. Most of the heat from the refrigerant superheated vapour circulating in one of the circuits of the test condenser is expected to be transferred to the cold DM water circulating in the other circuit of the test

condenser. However, a small portion of the heat dissipation to the surroundings by the external surface of the test condenser jacket is inevitable. These heat losses are reduced in the present investigation because the test condenser considered is well insulated with an aerospace grade insulation material having a thickness of 10 mm, which is a polyamide foam coated with hypalon. In addition, the outer heat transfer surface area of the test condenser is considerably smaller in size (150 mm × 150 mm).

In this single-phase analysis, the surface temperature was measured at the external surface of the test section before conducting the experiment and also during the experiment. The analysis showed that, based on the surface temperature measured prior and during the experiment, the estimated heat loss to the surrounding ambient was observed only up to 0.1 % of the total heat load. This lower value of heat loss was observed because of the high quality aerospace grade insulation material of the test condenser. Thus, in the present analysis, the heat loss to the surroundings is not considered because the estimated heat loss to the surroundings during the single-phase test is very low. These lower values of heat loss are also neglected as these values do not affect the estimation of the present condensation heat transfer characteristics, as indicated by Park et al. (2011) and Vakili-Farahani et al. (2013).

## 3.6 Summary

In the expression of overall heat transfer coefficient for heat exchangers, the unknown parameter in present study along with refrigerant heat transfer coefficient is single-phase heat transfer coefficient of water. Thus, in this chapter, the numerical estimation of single-phase heat transfer coefficient of water was presented for both serrated and wavy fin surfaces. Further, the single-phase water-to-water experiments were also performed to estimate the single-phase heat transfer coefficient of DM water in two types of test sections, one with serrated fins and other with wavy fin surfaces. The numerical and experimental results are then compared and presented in this chapter. Further, this chapter also discusses the three types of test condensers, having two numbers of serrated fin surfaces and one number of wavy fin surfaces. These test sections were employed in the present investigation for both water-to-water single-phase tests and condensation experiments. Single phase energy balance of superheated vapour and cold DM water is also discussed in this chapter.

# Chapter 4
# Experimental Facility for Condensation Investigation

## 4.1 Preface

Investigations on boiling and condensation phenomenon for various heat transfer equipment have been reported by many investigators. Many researchers have designed and developed condensers and evaporators for several industrial applications. Establishing a dedicated test facility is vital for conducting experiments on test sections and generating design parameters and characteristics according to requirements. Many investigators have conducted condensation experiments to estimate the heat transfer coefficient and frictional pressure drop in tubes, helical pipes, mini-channels and plate heat exchangers using R134a and other environmentally friendly refrigerants. In the present investigation, the primary objective is to estimate the condensation heat transfer coefficient and frictional pressure drop of the low GWP refrigerant R1234yf inside a compact test condenser with serrated and wavy fin surfaces. The experimental facility is established for the characterization and generation of the design parameters during the condensation of the refrigerant inside the test condensers. The experimental data generated using the test facility will be useful for designing compact condensers, particularly for aerospace and automobile applications.

In this study, the experiments were initially performed in a test facility using refrigerant R134a and later replaced by the low-GWP refrigerant R1234yf to estimate the condensation characteristics. Based on the data available in the literature, the present test facility was established to perform condensation experiments on the test condensers. The condensing temperatures considered were varied in the range of 30 °C to 42 °C and these ranges of

condensing temperatures are adequate and acceptable for many applications in various thermal fluid industries. Accordingly, the present experimental facility was established to carry out condensation experiments. The work presented in this chapter primarily focuses on the establishment of an experimental facility. This chapter describes the layout of the test facility, different loops, circuits, various equipment employed and their functions in the test facility. This chapter also discusses the instrumentation, measurements, and data-acquisition system of the test facility.

## 4.2 Specification of the test facility

In this section, the specifications of the test facility and various components employed are described. The specifications of the test facility were finalised based on the test section parameters and their requirements suitable for various applications. The test facility was established to analyze the condensation characteristics of refrigerants R134a and R1234yf inside test condensers with serrated and wavy fin surfaces. The test facility has the five major circuits namely a refrigerant loop, a condenser loop, an evaporator loop, a superheater loop and a de-superheater loop. In the refrigerant circuit, the refrigerant flow rate was varied through compressor with a variable frequency drive. There were four parallel semi-hermitically sealed reciprocating compressors with different capacities. In the test facility, the refrigerant was circulated in the refrigerant loop, and in the other loops, de-mineralized (DM) water was circulated at different flow rates and temperatures maintained through a chiller. The test facility was fully equipped to monitor and measure pressure, flow rate, and temperature of both the refrigerant and DM water. All digital instruments were integrated into a data acquisition system of the test facility to log data. Safety measures, such as automated cut-off features, were included to detect refrigerant leakage. In this chapter, the various circuits of the test facility are presented in the subsequent sections and the specification of the experimental facility considered are given below:

### 4.2.1 Refrigerant circuit

- Refrigerant flow rate: 0.005 kg/s to 0.07 kg/s
- Operating pressure range: 0 to 15 bar
- Operating temperature range: 10 ℃ to 70 ℃
- Working fluid: Refrigerants R134a and R1234yf
- Power supply: 440 V, 3 Phase, 50 Hz

### 4.2.2 Condenser / evaporator water side circuit

- DM water Flow rate: 0 to 60 lpm
- Operating pressure range: 0 to 2 bar
- Operating temperature range in condenser circuit: 10 ℃ to 60 ℃
- Operating temperature range in evaporator circuit: 10 ℃ to 40 ℃
- Working fluid: DM Water
- Power supply: 440 V, 3 Phase, 50 Hz

## 4.3 Experimental facility layout

In the test facility, the temperature and pressure sensors were located at the inlet and exit of the test condenser, and differential pressure transducers were fitted across the test condenser. The coriolis and turbine flow meters were installed at the outlet of the test condenser on the refrigerant and DM water sides. Other major components of the test facility were also instrumented to monitor and record the test parameters. Fig. 4.1 shows a schematic layout of the experimental facility.

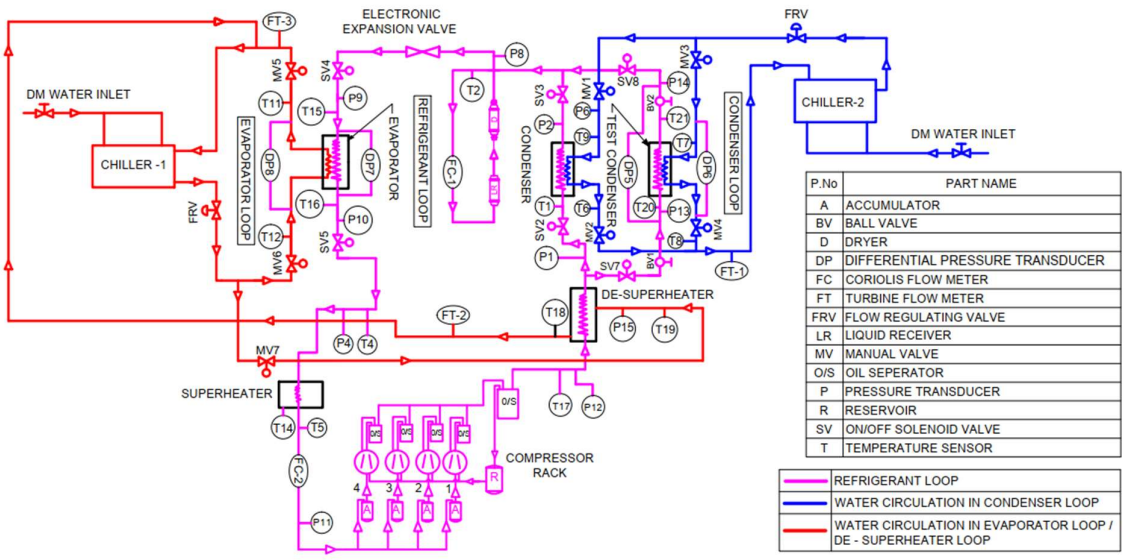


Fig. 4.1. Layout of experimental facility

The refrigerant loop consists of major components, such as compressor, standard condenser (used for the test facility stabilization before the experiments on the test section), test condenser (present test section), electronic expansion valve, evaporator, de-superheater, and superheater. In the test facility, four parallel semi-hermitically sealed reciprocating compressors are

integrated having different flow capacities ranging from 0.005 to 0.07 kg/sec. The compressed refrigerant from the compressor outlet was passed through a de-superheater installed at the upstream of the test condenser. The required test condition of the refrigerant in the test condenser was maintained in the de-superheater loop by controlling the temperature and flow rate of the DM water in the de-superheater. The refrigerant was then condensed in the condenser by using the cooled DM water circulated in the condenser loop. In this loop, the refrigerant was passed through the standard condenser or test condenser as and when required during the experiments. Further, the refrigerant was passed through the electronic expansion valve, where the refrigerant was expanded and circulated to the evaporator. The refrigerant evaporates in the evaporator by taking heat from the hot DM water circulating in the evaporator loop. In this refrigeration loop, a superheater was installed at the downstream of the evaporator to ensure dry compression in the compressor.

In the test facility, a gas charging and evacuation system was employed to charge and discharge the refrigerant gas. The refrigerant circuit has two charging ports that are used to charge the refrigerant gas. The charging of the pure refrigerant was always ensured and maintained. An evacuation system was also employed to evacuate the refrigerant gas as and when required. The components used in the test facility were connected through pipelines made of seamless copper tubes, which were fully insulated to prevent heat loss to the surroundings. The pictorial representations of the experimental facility are illustrated in Figs. 4.2 to 4.4.

Fig. 4.2. Pictorial view of experimental facility

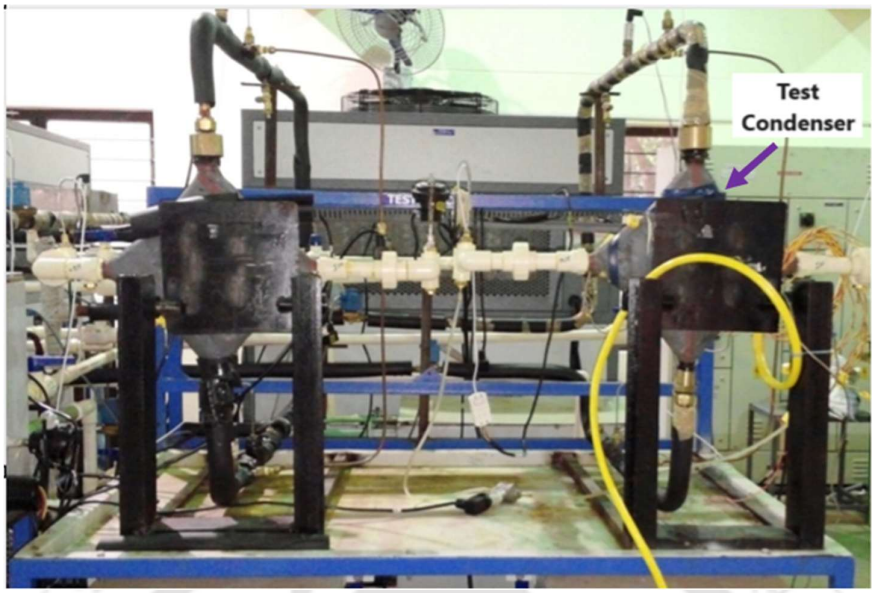


Fig.4.3. Test section installed in the test facility

Fig. 4.4. Data acquisition system of the test facility

In the test facility, the standard condenser was used to stabilise the test facility before the experiments on the test condenser. Once the required test conditions were achieved, the bypass line was connected parallel to the standard condenser was closed and the test condenser was opened. The refrigerant was then circulated through the test condenser, where it exchanged heat with the DM water circulated in the other circuit of the test condenser. Further, the de-superheater is installed at the upstream of the test condenser, where heat exchange between the refrigerant and DM water takes place. Thus, by controlling the DM water temperature and flow rate in the de-superheater, the test conditions at the outlet of the de-superheater (also a test condenser inlet) were maintained. Hence, each condition during the experiment was achieved and maintained according to the requirements. Initially, the flow rate of the refrigerant was controlled using a suitable compressor, and then the required pressure and temperature were controlled by adjusting the DM water flow rates and temperatures. Individual loops and circuits of the test facility are described in the following sections.

### 4.3.1 Refrigerant circuit

The test facility has a refrigerant circuit that consists of reciprocating compressors with different flow capacities, a de-superheater, test condenser (test section which is a brazed plate fin compact plate exchanger with serrated or wavy fins), standard condenser (for initial test facility stabilization), electronic expansion valve, standard evaporator and superheater. The refrigerant circuit is also equipped with temperature sensors and pressure and differential pressure transducers to measure the data during the experiments. The reciprocating compressors in the refrigerant circuit were semi-hermetically sealed and have a variable-frequency drive. Based on the flow requirements of the refrigerant during the experiments, a suitable compressor was operated. The refrigerant circuit has a varying flow capacity of 0.005 to 0.07 kg/s, obtained by controlling the speed of the compressor. The refrigerant circuit also has accumulators, oil separators, a liquid receiver, a filter drier, and a Coriolis flow meter for refrigerant measurement. The compressors are integrated with accumulators and non-return valves to avoid any back flow of the refrigerant. An oil separator is provided downstream of each compressor to isolate the oil from the refrigerant and ensure effective lubrication of its moving parts in the refrigerant circuit. A common oil separator is also installed at the downstream of all the compressors, which also captures the oil that is mixed with the compressed refrigerant and then returns it back to the crankcase of the compressor. These oil separators, by removing oil traces, provide efficient heat transfer surfaces for the condenser and evaporator. In the refrigerant circuit, two sampling ports are located, one at the downstream

of the condenser and the other at the evaporator side, which are used to charge or discharge the refrigerant to the test facility. The layout of the refrigerant loop is illustrated in Fig. 4.5.

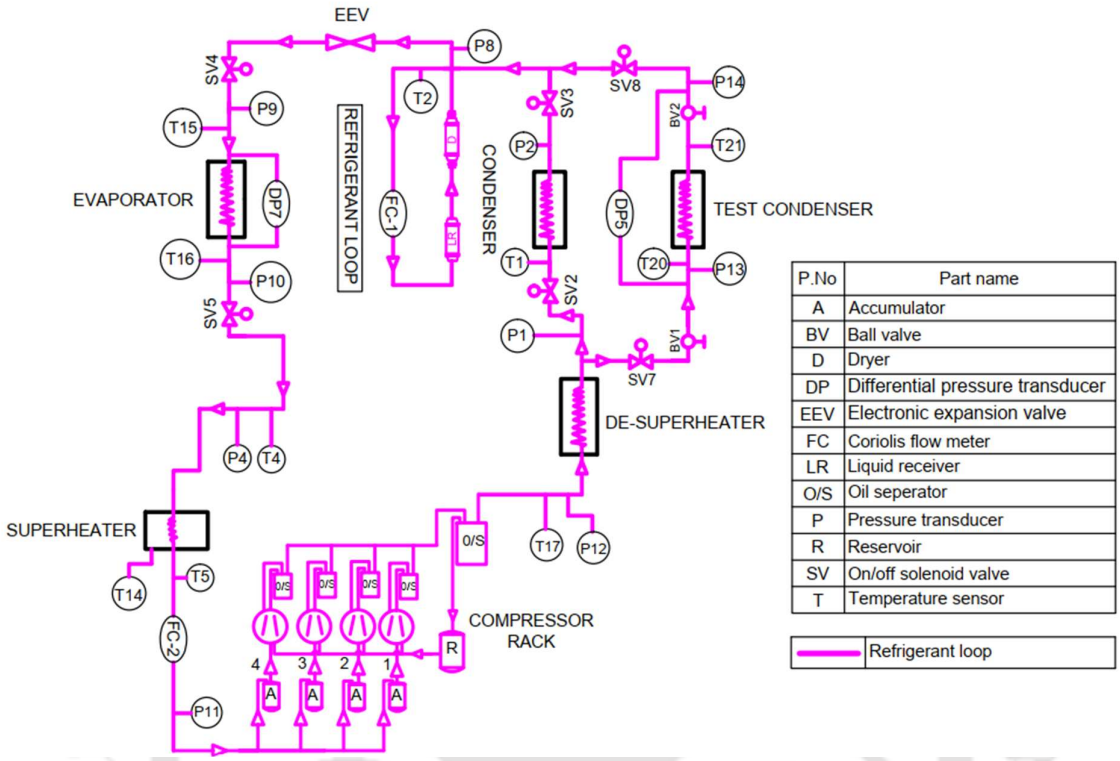


Fig. 4.5. Refrigeration loop layout

The test condenser along with the standard condenser were integrated in the refrigerant circuit. This standard condenser was initially used to stabilize the condition in the refrigerant circuit before conducting the experiments on the test section. Once the conditions of the experiment were met, the bypass line connecting the test condenser was opened for the refrigerant to flow. This bypass line was kept opened or closed using solenoid valves installed before and after the condensers. The refrigerant conditions were also controlled by the DM water circulation in the other side of condenser circuit. In the present investigation, condensation experiments were planned on three test condensers with two types of serrated fin surfaces and one type of wavy fin surface. This test section was provided with easy access for installation or removal from the test facility. Further, the de-superheater was installed at the downstream of the compressor and at the upstream of the condensers. This de-superheater controlled the inlet conditions at the test condenser, which have a separate DM water circulation system. A filter drier and liquid receiver were installed at the downstream of the condenser. Once the refrigerant is condensed, it flows back to the receiver. The filter drier containing silica gel absorbs traces of moisture present in

the refrigerant and stores it in the liquid receiver. This filter drier prevents the moisture content from entering the narrow cross-section of the electronic expansion valve, which can cause choking when it freezes. Thus, the liquid-line filter drier protects the refrigeration circuit system from moisture and solid particles. The electronic expansion valve and evaporator are installed at the upstream of the compressor in the refrigeration circuit, as shown in Fig. 4.5. In the refrigerant circuit, temperature sensors, pressure transducers, and differential pressure transducers across both condensers and evaporator are used to measure the data during the experiments. The refrigerant mass flow rate is measured using a coriolis flow meter installed at the downstream of the condensers and the evaporator in the refrigerant circuit.

### 4.3.2 Condenser circuit

The condenser circuit mainly consists of a test condenser, a standard condenser, and a DM water circulation system using a chiller unit. This test condenser is employed to investigate the heat transfer and pressure drop characteristics during the condensation of refrigerants R134a and R1234yf. The condenser circuit layout of the test facility is illustrated in Fig. 4.6.

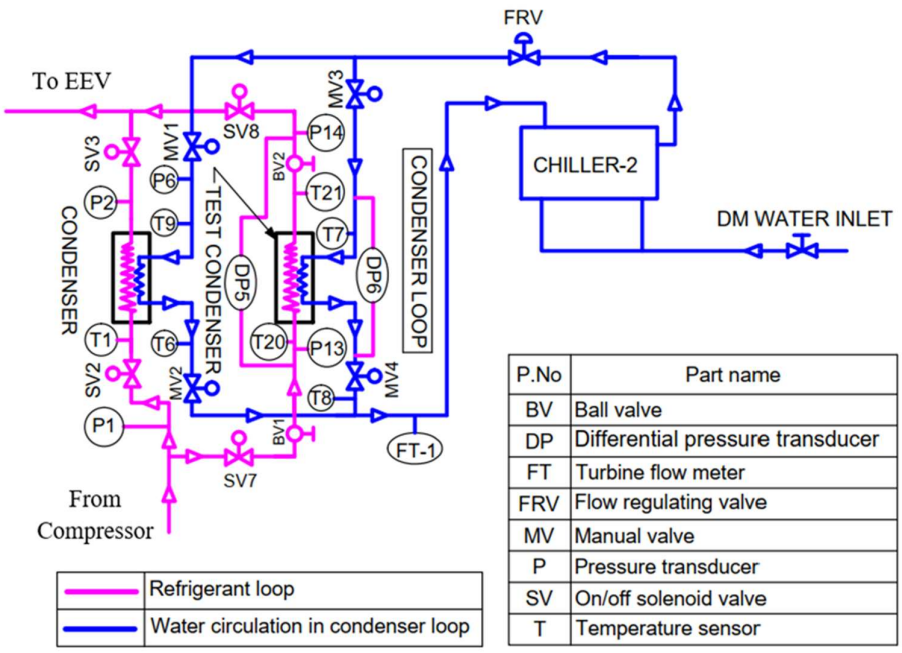


| P.No | Part name |
|---|---|
| BV | Ball valve |
| DP | Differential pressure transducer |
| FT | Turbine flow meter |
| FRV | Flow regulating valve |
| MV | Manual valve |
| P | Pressure transducer |
| SV | On/off solenoid valve |
| T | Temperature sensor |

Fig. 4.6. Condenser loop layout

In this circuit, a standard condenser is used initially for the stabilization of the test conditions before carrying out the condensation experiments on the test condenser. These two condensers are connected to the DM water circulation systems, which have a chiller unit. Once the test

conditions are achieved, the bypass line connecting to the test condenser is opened for the refrigerant to flow, and at the same time, the bypass line connecting to the standard condenser is kept closed. This bypass line is kept open or closed using solenoid valves installed before and after the condensers. The conditions of the refrigerants at the test condenser and standard condenser are controlled by the DM water circulation which have a dedicated chiller unit for cooling or heating the DM water. The chiller unit consists of tanks with hot and cold DM water, pumps, flow control valves, and shut-off valves. These water tanks are connected to pumps and used when required. DM water is circulated in the condenser to condense the refrigerant vapour. The water mass flow rates are available up to 60 lpm, which are measured and monitored by a turbine mass flow meter installed at the downstream of the condenser on the water side. The inlet temperatures of the DM water at the standard condenser and test condenser can be adjusted in the range of 10 ℃ to 60 ℃.

The chiller unit used in the test facility is a refrigeration system consisting of a compressor, condenser, expansion valve, and evaporator. In this system, R407 is used as the refrigerant. In this chiller unit, the temperatures of the cold water tank are maintained up to 10 °C using a chiller evaporator, and the temperature in the hot water tank can be maintained up to 60 °C using a thermostat with a heating system in the hot water circuit. The cold DM water at the desired temperature and flow rates is circulated through the water circuit of the standard condenser or test condenser. The DM water absorbs heat from the refrigerant vapour circulating through the refrigerant circuit of the standard condenser or test condenser. The refrigerant vapour condenses by releasing heat into the cold water in the condenser, and the water is heated by absorbing heat from the refrigerant. Furthermore, the condenser circuit also consists of solenoid valves to bypass the DM water flow towards the standard condenser or test condenser as and when required. Flow control valves and turbine flow meters are also installed in the condenser circuit to control and measure the DM water flow rates.

### 4.3.3 Evaporator circuit

The evaporator circuit consists of mainly an evaporator and a DM water circulation system using a chiller unit. This circuit has the circulation of both refrigerant and the DM water. Once the refrigerant is expanded in the expansion valve, it is then passed through the evaporator, where the liquid refrigerant is evaporated by taking heat from the DM water of evaporator loop. The layout of the evaporator loop is illustrated in Fig. 4.7.

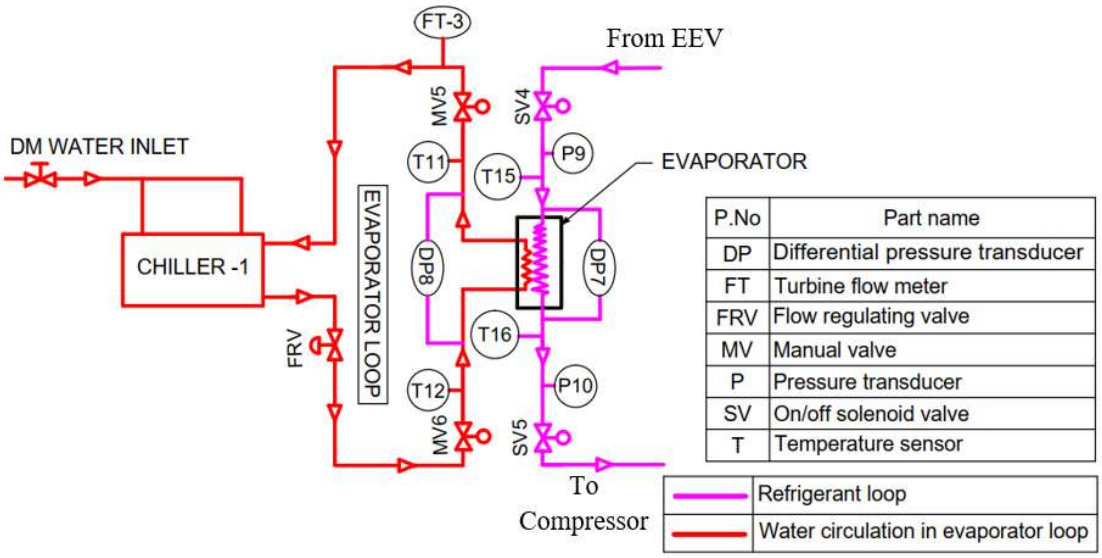


Fig. 4.7. Evaporator loop layout

The chiller unit consists of tanks with hot and cold DM water, a pump, a flow control valve, and shut-off valves. These water tanks were connected to pumps and used when required. The chiller unit that is integrated to evaporator circuit is also a refrigeration system, which consists of compressor, condenser, expansion valve, evaporator and in this system, R407 is employed as a refrigerant. In chiller unit, temperatures in the cold water tank are maintained up to 10 °C using a refrigeration system, and temperatures in the hot water tank are maintained up to 40 °C using a thermostat with a heating system. The water mass flow rates from the chiller unit to the evaporator can be varied up to 60 lpm. Hot DM water at the desired temperature is circulated through the DM water circuit of the evaporator, and the refrigerant circulating through the refrigerant circuit is at a lower temperature, thus after absorbing the heat from the DM water, the liquid refrigerant evaporates into vapour. Flow control valves and a turbine flow meter are provided in the evaporator circuit to control and measure the DM water flows, respectively.

### 4.3.4 De-superheater circuit

The de-superheater circuit consists of a standard heat exchanger, flow regulating valves, turbine flow meter, temperature sensors and pressure transducers. This de-superheater circuit has a passage for refrigerant vapour in superheated conditions coming out of the compressor, and also has a passage for DM water. The superheated vapor condition of the refrigerant to the saturated condition at the condenser inlet is maintained using a de-superheater circuit. The plate heat exchanger is considered as a de-superheater, which is used to exchange heat between the

DM water and refrigerant. This de-superheater heat exchanger is installed at the inlet of the test condenser to provide the required test conditions. The cold DM water tapped from the chiller unit at the desired temperature and flow rate is circulated through the water circuit of this de-superheater heat exchanger. In this process, the DM water of the de-superheater absorbs heat from the refrigerant, thereby lowering the temperature of the superheated refrigerant vapour to required test conditions, which is achieved by regulating the water flow rates and temperatures. The layout of the de-superheater loop is illustrated in Fig. 4.8.

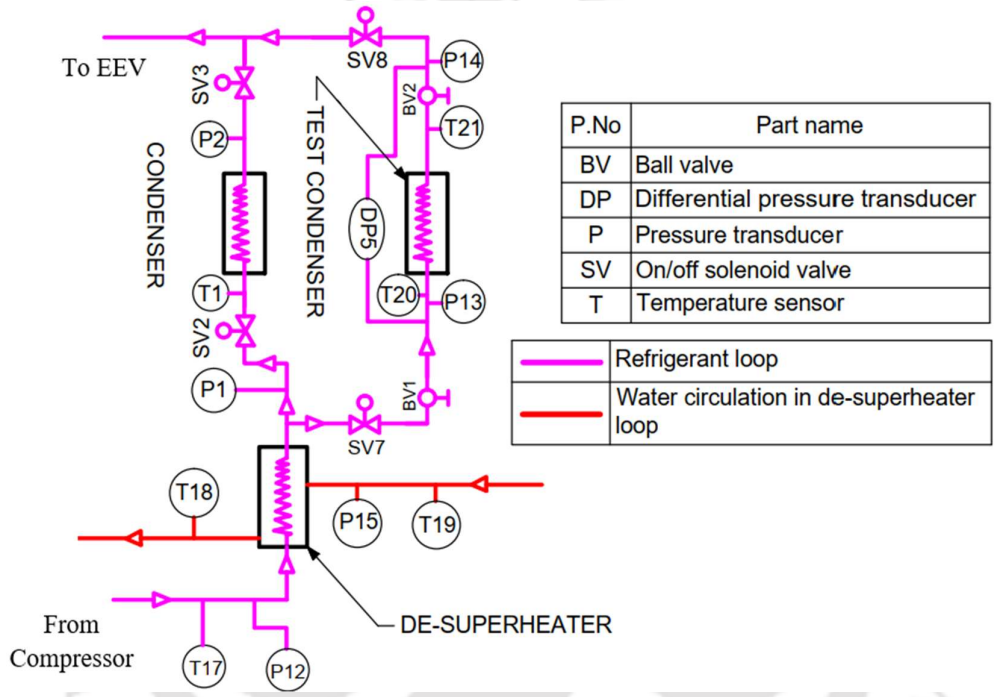


Fig. 4.8. De-superheater loop

### 4.3.5 Superheater circuit

The superheater circuit in the test facility is a 3 kW heating system, which mainly consists of a buffer tank, pump, heat exchanger, shut-off valves, mass flow meter, pressure transducer, and temperature sensors. In this superheater circuit, the DM water is circulated in the superheater tank, which is maintained up to a desired temperature as per the requirement. The refrigerant coming out of the evaporator is then circulated through this superheater tank, which ensures fully vapour form of the refrigerant and provides dry compression in the compressor by providing the required heat. The layout of the superheater circuit integrated in the test facility is shown in Fig. 4.9.

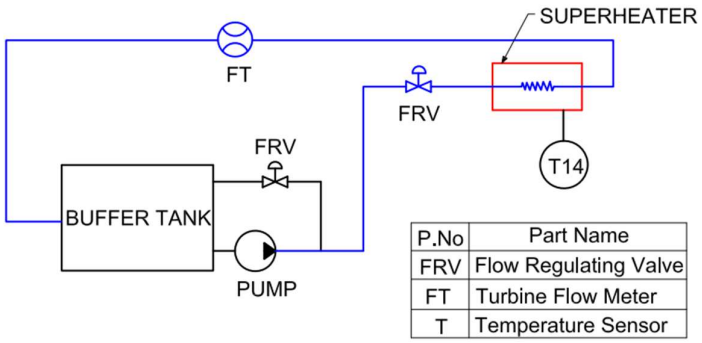


Fig. 4.9. Superheater loop

### 4.3.6 Major components of test facility

The major components employed in the present test facility are the compressors, condenser, electronic expansion valve, evaporator, chiller units, solenoid valves, and flow-control valves. The test facility consists of a data acquisition system and is equipped with temperature sensors, pressure transducers, differential pressure transducers, coriolis flow meters, and turbine flowmeters for measuring and logging the data during the experiments. The major components of the test facility are discussed in the following paragraphs.

#### 4.3.6.1 Compressor

A semi-hermetically sealed reciprocating compressor is employed in the refrigerant circuit of the test facility. There are four semi hermetically sealed reciprocating compressors parallelly installed in the facility with a variable frequency drive. Suitable compressors are operated in the refrigerant circuit based on the refrigerant flow requirements during the experiments. The reciprocating compressor used in the present investigation is shown in Fig. 4.10, and its specifications are listed in Table 4.1.

Fig. 4.10. Reciprocating compressor

Table 4.1. Specification of compressor

| Model no. | Qty. | No. of cylinders | Maximum power consumption (kW) | Weight (kg) |
|---|---|---|---|---|
| 2SB-34.07 | 1 | 2 | 1.9 | 43 |
| 2SB-38.2 | 1 | 2 | 2.4 | 45 |
| 2SB-55.4 | 2 | 2 | 5.6 | 70 |

These compressors are integrated in an assembled rack and the variable flow rates are obtained by controlling the speed of the compressors. Each compressor is integrated with an accumulator and non-return valves to avoid refrigerant backflow. During the operation of the compressor, the refrigerant vapour pressures and temperatures are increased above the condenser pressure and corresponding condensing temperature. The vapour pressure of the refrigerant in this type of reciprocating compressor is increased by reducing its volume. The compressor employed is supplied by Sea-Bird Refrigeration Pvt. Ltd., New Delhi, India.

#### 4.3.6.2 Standard condenser and evaporator

In the present investigation, the standard condenser and evaporator integrated in the test facility are plate heat exchangers. Generally, this type of plate heat exchanger is constructed using corrugated plates that are welded or brazed together, depending on the application. The standard condenser in the refrigerant circuit is employed to maintain the stability of the test facility, prior to the experiments on test condenser. The evaporator of the test facility is used to evaporate the refrigerant liquid by taking heat from the DM water circulation. The pictorial view of the plate heat exchanger is shown in Fig. 4.11 and the technical details of the standard evaporator and condenser are listed in Table 4.2.

Fig. 4.11. Plate heat exchanger

Table 4.2. Specification of standard condenser and evaporator

| Heat exchanger | Model no. | Type | Capacity | Make |
|---|---|---|---|---|
| Condenser | PHE B3-030-70-3.0-HQ | Plate heat exchanger | 30 kW | Danfoss |
| Evaporator | PHE B3-052-60-3.0-HQ | Plate heat exchanger | 30 kW | Danfoss |

There are two condensers in the refrigerant circuit, which are test condenser and standard condenser. These test condenser and standard condenser are installed in parallel in the refrigerant circuit through a bypass line. Once the test parameters are achieved, the refrigerant is passed through the test condenser by opening the bypass valve, and simultaneously, closing the passage through the standard condenser. The standard condenser and evaporator are brazed plate heat exchangers, manufactured and supplied by Danfoss Industries Pvt. Ltd., India.

#### 4.3.6.3 Electronic expansion valve (EEV)

An electronic expansion valve is installed at the downstream of the condenser in the test facility. It is used to control the flow of the refrigerant entering the evaporator and reduce the pressure of the liquid refrigerant coming from the condenser. The electronic expansion valve controls are available in the programmable logic controller rack of the test facility. The electronic expansion valve, shown in Fig. 4.12, is supplied by CAREL India, Mumbai. The specifications of the EEV are presented in Table 4.3.


Fig. 4.12. Electronic expansion valve

Table 4.3. Specification of electronic expansion valve

| | |
|---|---|
| Device | $E^2V$ |
| Make | CAREL Industries |
| Model no. | $E^2V$-24 |
| Maximum operating pressure | 40 bar |
| Operating temperature | - 40 to 65 °C |

#### 4.3.6.4 Oil separator

The primary use of an oil separator is to intercept the oil mixed with the refrigerant and return it to the crankcase of the compressor to avoid entry into the other components of the system. In the present test facility, hermetically sealed oil separators are mounted on the discharge line of each compressor (upstream of the de-superheater and condenser). These oil separators are also integrated with a common oil separator at the downstream of all the four compressors. When the compressed refrigerant vapour from the compressor enters the large chamber of the oil separator, the velocity of the compressed vapor decreases. A portion of the oil transported with the refrigerant vapour is intercepted by the metallic filter of the oil separator. Further, the oil forms droplets and eventually fall down to the bottom of the oil separator. Once the oil level at the oil separator is sufficiently high, a float valve is opened, allowing the high pressure to recover the oil back to the crankcase of the compressor. This ensures efficient lubrication of compressor moving parts and also provides the efficient performance of the condenser and evaporator by removing the oil traces from their heat transfer surfaces. The photograph of oil separator employed in the test facility is shown in Fig. 4.13, which is supplied by Sea-Bird Refrigeration Pvt. Ltd, New Delhi, India.

Fig. 4.13. Oil separator

#### 4.3.6.5 Chiller unit

There are two chiller units employed for the DM water circulation in the test facility. These chiller units circulate the DM water in the condenser and evaporator circuit of the test facility at the temperatures ranging from 10 °C to 60 °C. The photograph of the chiller unit, which is supplied by Werner Finley Pvt. Ltd., India, is shown in Fig. 4.14. The specifications of the chiller unit are listed in Table 4.4.

Fig. 4.14. Chiller unit

Table 4.4. Specification of chiller unit

| | |
|---|---|
| Make | Werner Finley Pvt. Ltd. |
| Model no. | 6TC10WC1X/HS |
| Capacity | 6 TR |
| Temperature range | 10 °C to 60 °C |
| Flow rate | 75 LPM |

The chiller unit consists of water tanks, a thermostat with a heater, pump, flow control valve, and shut-off valves. The two tanks of the chiller unit are connected to water pumps for cold and hot water. Both hot and cold water tanks are interconnected through a pipe line with a solenoid valve between them. Furthermore, these chiller units have two separate circuits, namely cold and hot water circuits. The cold-water circuit consists of a refrigeration system with a compressor, condenser, evaporator, and expansion valve, which uses R407 as the refrigerant. In this cold circuit, water is provided by the pump from the tank and circulated through the evaporator of the chiller unit, where it is cooled and supplied back to the tank. The temperature of the cold water tank is maintained up to 10 ℃. Furthermore, the chiller unit also consists of a hot water circuit that is integrated with a thermostat and heater system. In this system, the water is heated in the tank, and the temperature is maintained up to 60 ℃.

#### 4.3.6.6 Solenoid valve

In the test facility, solenoid valves are used to bypass or cut off the refrigerant and the DM water flows. The solenoid valves are installed in the test facility at the inlet and outlet of the

evaporator, condenser and test condenser. The solenoid valves at this location are in open or closed positions, based on the requirements of the refrigerant or water passage through these components. These solenoid valves are electromechanically operated and controlled by an electric current through the solenoid. These valves are connected to a programmable logic controller and an industrial computer. The photograph of the valve is shown in Fig. 4.15.

Fig. 4.15. Solenoid valve

#### 4.3.6.7 Piping

The present test facility is equipped with the seamless copper tubes. The selection and sizing of the copper pipe tubing are performed based on the ASTM B-88 standard**.** These pipelines are properly insulated to prevent heat loss to the surroundings.

#### 4.3.6.8 Refrigerant charging and evacuation system

A gas charging and evacuation system is employed in the test facility to charge and discharge the refrigerant gas. The photograph of refrigerant evacuation unit is shown in Fig. 4.16.


Fig. 4.16. Refrigerant evacuation unit

The refrigerant circuit of the test facility has two charging ports that are used to charge the refrigerant gas. Before charging a system, all moisture and air must be eliminated from the components using an evacuation system. An evacuation system is also used to evacuate the refrigerant gas as and when required. This movable evacuation unit consists of a vacuum pump

mounted on the wheels. The amount of refrigerant is monitored using a pressure gauge at the discharge line of each compressor. Whenever pressure losses are observed in the pressure gauge, the refrigerant is further charged until the required pressure is maintained.

### 4.3.7 Instrumentation and data acquisition system

In the present investigation, the instrumentation system has been integrated in the test facility, which consists of temperature sensors, pressure transducers, differential pressure transducers, turbine flowmeters, and coriolis flow meters. The test facility also has a data acquisition system which records and stores the data. The test results and analysis of any investigation depend on the accuracies of the instruments used. Specifications of the instruments used in the test facility are given in the following sections.

#### 4.3.7.1 Coriolis flow meter

A coriolis flow meter is used to measure the refrigerant flow rate in the test facility. This flow meter is considered for the refrigerant, as it has a very high accuracy. Two coriolis flow meters are installed in the circuit (i) one at the downstream of the condenser liquid line and (ii) second one at the downstream of the evaporator vapour line. The coriolis flowmeter used in the test facility is shown in Fig. 4.17, and the details are given in Table 4.5.

Fig. 4.17. Coriolis flow meter

Table 4.5. Specification of coriolis flow meter

| | |
|---|---|
| Make | Micro Motion |
| Model no. | CMFS015 |
| Flow rate | 10 to 330 kg/hr |
| Accuracy | ± 0.05 % of rate for liquid and ± 0.35 % of rate for gas |
| Pressure rating | 413 bar |
| Temperature rating | - 240 ℃ to 204 ℃ |

#### 4.3.7.2 Turbine flow meter

A turbine flow meter is installed in the various DM water circuits of the present test facility to measure the DM water flow rates. Four turbine flow meters are considered in the present test facility, and these flow meters are installed at the DM water circulation line of the evaporator circuit, condenser circuit, superheater circuit, and de-superheater circuit of the test facility. The turbine flow meter, supplied by Rockwin Flowmeter India Pvt., Ltd, employed in the test facility is shown in Fig. 4.18 and the specifications are listed in Table 4.6.

Fig. 4.18. Turbine flow meter

Table 4.6. Specification of turbine flow meter

| | |
|---|---|
| Make | Rockwin |
| Model no. | TFM1015/-S |
| Flow rate range | 3 to 66 LPM |
| Maximum temperature | 150 °C |
| Maximum pressure | 250 kg/cm$^2$ |
| Accuracy | ± 0.25 % |

#### 4.3.7.3 Pressure transducer and differential pressure transducer

In the present test facility, the pressure transducers are integrated at the inlet and outlet of all the major equipment. Differential pressure transducers are also installed across some of the major components of the refrigerant and DM water circulation lines. The pictorial view of the pressure transducer and differential pressure transducer employed in the test facility are shown in Figs. 4.19 and 4.20, respectively. The pressures and differential pressures are measured during the experiments using diaphragm-type transducers. The specifications of the pressure transducers and differential pressure transducers integrated into the test facility are listed in Table 4.7 and Table 4.8, respectively.

Fig. 4.19. Pressure transducer

Fig. 4.20. Differential pressure transducer

Table 4.7. Specification of pressure transducer

| | |
|---|---|
| Make | Measurement Specialties |
| Model no. | M5100 |
| Pressure range | 0 to 20 bar |
| Temperature range | - 40 to 125 °C |
| Accuracy | ± 0.25 % FS |

Table 4.8. Specification of differential pressure transducer

| | |
|---|---|
| Make | Sensocon |
| Model no. | 251-01 |
| Pressure range | 0 to 5 PSI |
| Electric supply | 12 to 36 VDC |
| Accuracy | ± 0.25 % FS |

#### 4.3.7.4 Temperature sensors

Platinum resistance RTD-type temperature sensors are integrated in the test facility to measure the temperatures of the refrigerant and DM water at the inlet and outlet of the test condenser,

standard condenser, evaporator, electronic expansion valve, compressors, superheater circuit, and de-superheater circuit. The details of the temperature sensors used in the test facility are provided in Table 4.9.

Table 4.9. Specification of temperature sensor

| Make | Measurement Specialties |
|---|---|
| Model no. | PT100 |
| Temperature range | - 30 to 300 °C |
| Accuracy | ± 0.15 °C |
| Power supply | 230 VAC |

### 4.3.8 Data acquisition system (DAS)

The present test facility has a Supervisory Control and Data Acquisition System (SCADA) which consists of a GE Versamax programmable logic controller (PLC) and an industrial grade computer (PC) for data logging. A block diagram of the data acquisition system of the test facility is illustrated in Fig. 4.21.

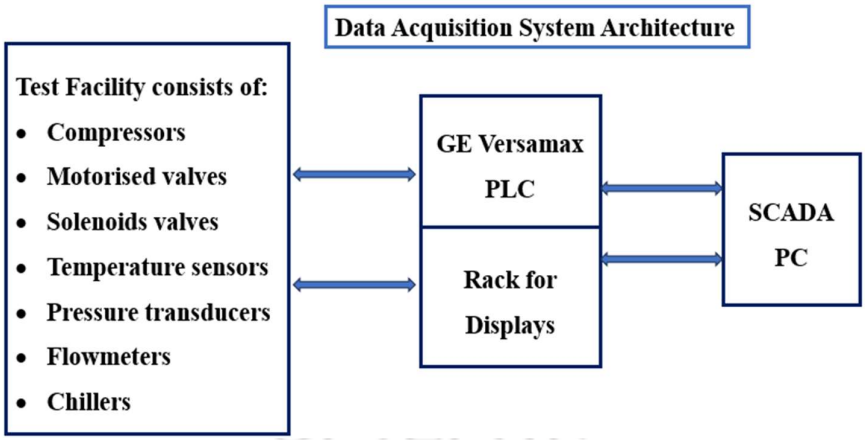


Fig. 4.21. Block diagram of data acquisition system

The programmable logic controller is connected to an industrial computer with GE CIMPLICITY SCADA software through Ethernet communications. Pressure transducers, differential pressure transducers, temperature sensors, and flow meters are connected to an industrial computer through the PLC and SCADA systems for data gathering. The data acquisition system recorded the data at 20 samples / second and logged the data for 30 second

or more. The compressors, motorized valves, solenoid valves, and chillers are all controlled and monitored by the SCADA system through an industrial computer with GE CIMPLICITY software. This data acquisition system consists of GE make input / output modules, connected through a profinet to a GE VERSAMAX PLC. Instruments such as temperature and pressure digital displays and chiller temperature digital displays are all connected to the SCADA system through MODBUS RTU communication protocols. The operations of various sensors / instruments are performed and monitored with the help of the SCADA system, which are programmed to control the different valve positions, operations, and to generate the report.

#### 4.3.8.1 Display details and controls

The display and controls are installed on a rack panel provided in the data acquisition room of the test facility. All the operations, controls, and monitoring of the test facility performance are facilitated in this data acquisition room. The displays and controls available in the test facility are provided below:

**a) Display on main rack panel:**

- 3-phase supply indications lamp
- Pressure display of refrigerant and DM water
- Temperature of refrigerant and DM water
- Flow rates of refrigerant and DM water
- Differential pressure of refrigerant
- Voltmeter with selector switch
- Ammeter with selector switch

**b) Operator control panel**

- Mains ON/OFF with indications
- Emergency push button

**c) Electrical control details**

- MCB for motor, MCCB as incomer
- Double earthing interconnections
- 4 core insulated copper cable for incoming power

**d) Electrical control panel:** The electrical control panel consists of:

- Main power isolator,

- Compressors and pumps ON/OFF switches
- Mains indication and fuse units.
- Digital indication of upstream and downstream pressure, temperature and flow rates of refrigerant and water line.

### 4.3.9 Calibration of measuring instruments

All the temperature sensors, pressure transducers, differential pressure transducers, and flow meters are calibrated according to the applicable standards and integrated in the test facility.

## 4.4 Uncertainty Analysis

An uncertainty analysis was performed in the present study, and the uncertainties obtained for the derived parameters are discussed and presented in this section. Various parameters, such as pressure, temperature, differential pressure, and flow rates of the DM water and refrigerant, were measured during the experiments. Pressure transducers and temperature sensors were installed at the entry and exit of test condenser to measure the pressure and temperature, respectively, of the refrigerant and DM water. A differential pressure transducer was installed across the test condenser to measure the refrigerant and the DM water pressure drops across the test condenser. Coriolis flow meters were fitted at the exit of the standard evaporator and test condenser to measure the refrigerant flow rates, and turbine flow meters were used to measure the flow rates of the DM water. The accuracies of various sensors and measurement instruments are listed in Table 4.10.

Table 4.10. Measuring devices and their accuracies

| Device | Type | Accuracy |
|---|---|---|
| Pressure transducer | Strain gage | ± 0.25 % FS |
| Differential pressure transducer | Strain gage | ± 0.25 % FS |
| Resistance thermometer | RTD | ± 0.15 ℃ |
| Water flow meter | Turbine | ± 0.25 % |
| Refrigerant flow meter | Coriolis | ± 0.05 % |

An uncertainty analysis was performed to determine the uncertainties associated with the derived parameters as per Kline and McClintock (1954) and is presented in this section. The overall uncertainties of the condensation heat transfer coefficient ($h_r$) and frictional pressure

drop ($\Delta P_f$) of the refrigerant were found to be within ± 14.8 % and ± 1.6 %, respectively. The sample calculation of uncertainty analysis is provided in Appendix B. The summary of the uncertainties associated with the derived parameters are provided in Table 4.11.

Table 4.11. Summary of derived uncertainties

| Variables | Uncertainty |
|---|---|
| Heat transfer rate, $\dot{Q}$ (%) | ± 5.5 |
| Overall heat transfer coefficient, $U$ (%) | ± 6.5 |
| Water heat transfer coefficient, $h_w$ (%) | ± 4.3 |
| Refrigerant heat transfer coefficient, $h_r$ (%) | ± 14.8 |
| Frictional pressure drop, $\Delta P_f$ (%) | ± 1.6 |

## 4.5 Summary

In this chapter, the establishment of a dedicated test facility to conduct condensation experiments on test condensers is described. The test facility is used to carry out the experiments and to generate the design parameters of heat transfer and pressure drop during condensation in serrated and wavy fin test condensers. The experimental data generated using this test facility will be useful for designing and developing compact condensers, particularly for aerospace and automobile applications. The present test facility is established to predict the condensation characteristics of refrigerant R134a and low-GWP refrigerant R1234yf inside the test condensers. Various major components employed in the test facility are described and presented, along with the technical specifications. The data acquisition system and the details of the measuring instruments used for data logging are also presented in this chapter.

# Chapter 5
# Experimental Procedure and Data Reduction

## 5.1 Preface

The experimental procedure and data reduction performed in the present study are described in this chapter. Condensation experiments were conducted using refrigerants R134a and R1234yf in serrated and wavy fin test condensers. In this chapter, the data reduction and methodology used are described to estimate the condensation heat transfer coefficient ($h_r$) and frictional pressure drop ($\Delta P_f$) of refrigerants R134a and R1234yf inside a brazed plate fin compact heat exchanger with serrated and wavy fins. All data and parameters considered during the analysis were ensured under steady-state conditions. The parameters obtained were then recorded using a data acquisition system, as described in the previous chapter. The present experiments were performed for saturated vapour conditions of the refrigerant and for varying mass flux and saturation temperatures.

## 5.2 Testing methodology on test condenser

The test condensers (TC1, TC2, and TC3) intended for the present investigation were mounted in the test facility in a vertical direction, as illustrated in Fig. 5.1. It has a single passage for the refrigerant through the inner channel of the test condenser and two outer passages for the DM water circulation. The test condenser has either a serrated or wavy fin surface for both the refrigerant and water passages. This test condenser has a cross-flow arrangement with the refrigerant and DM water passage in the vertical and horizontal directions, respectively. Pressure transducers and temperature sensors were installed at the entry and exit of the test

condenser on both sides of the refrigerant and water. The differential pressure transducer across the test condenser was also fitted to measure the pressure losses. Coriolis flow meters were fitted at the exit of the evaporator and test condenser to measure the refrigerant flow rates. Turbine flow meters were fitted to measure the DM water flow rate. In each test condition, the refrigerant flow rate was initially controlled using a suitable compressor, and the pressure and temperature required were controlled by maintaining the flow rates and temperatures of the DM water in the other circuits of the test facility.

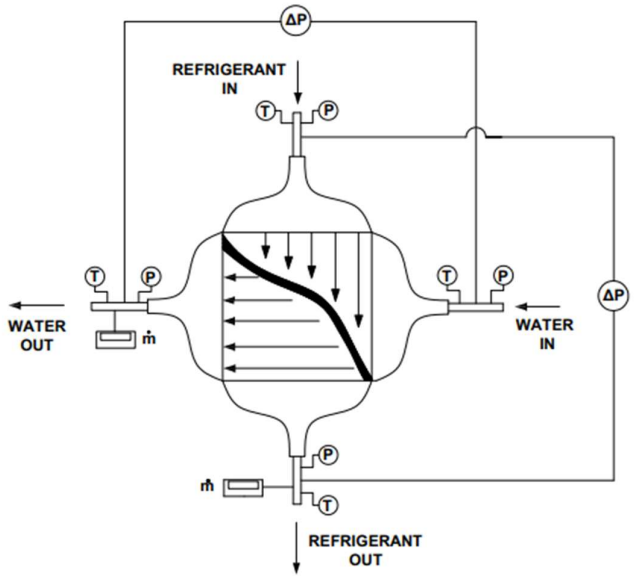


Fig. 5.1. Test condenser installation

## 5.3 Experimental procedure

In this section, the detailed testing procedure employed during the condensation experiments is described. The test facility was automated and all the operations were performed remotely from the data acquisition room. The compressors, electronic expansion valve, and shut-off valves were operated using the SCADA program. All transducers and sensors were connected through a SCADA system to an industrial computer for data gathering. In the test facility, the refrigerant was circulated in the refrigerant loop, and in the other loops, the DM water was circulated in the variable flow rates and temperature range, maintained by the two chillers. The required condition of the refrigerant in the test condenser was obtained by controlling the DM water flow rates and the temperatures of the other loops.

The refrigerant loop consists of four parallelly connected reciprocating compressors with variable flow capacities. The refrigerant was compressed in the compressors and circulated in

the de-superheater loop. The entry condition of the test condenser was maintained by a de-superheater (installed at the upstream of the test condenser) by controlling the DM water circulation. Further, there are two condensers, namely the standard condenser and the test condenser, which are operated as and when required. The refrigerant was circulated in the condenser and then condenses as heat exchange occurs between the DM water and the refrigerant. The refrigerant was then circulated in the electronic expansion valve and then to the evaporator in the refrigeration loop, which was installed at the upstream of the compressor. The refrigerant evaporates in the evaporator by taking heat from the hot DM water. Further, downstream of the evaporator, a superheater loop is available, which ensures dry compression in the compressor. In the refrigerant loop, an experiment was performed on a standard condenser to maintain the stability of the test facility prior to the experiments on the test condenser. The standard and test condensers were installed in parallel in the test facility and connected by a bypass line. Once the test parameters were attained, the refrigerant was passed through the test condenser by opening the bypass valve, and the passage through the standard condenser was closed.

Further, in the de-superheater loop, a heat transfer takes place from refrigerant to DM water. As a result, the test conditions are maintained at the test condenser by varying the DM water temperature and flow rates in the de-superheater. The heat transfer rate between the refrigerant and water in the test condenser was varied by changing the temperature and flow rate of the DM water. Any change in the system variables leads to fluctuations in the temperature and pressure of the flow. It takes approximately 30 minutes or more to reach a steady-state condition during the experiments, after the operation of the test facility for a given test point. The data acquisition system then records the data at 20 samples per second and logged data for 30 second or more. The mean or values closer to each other obtained from the SCADA system were considered to evaluate the refrigerant heat transfer coefficient and frictional pressure drops inside the test condenser. Steady-state conditions were maintained for refrigerant saturated inlet temperatures in the range of 30 to 42 °C during the condensation experiments.

This section discusses the general procedures employed to operate the test facility for carrying out the experiments. First, the power supply was switched on and the test facility was observed for any malfunctioning. Once the power was turned on, the valve positions were checked, and then the valves of the main refrigeration circuit were opened until the pressure levels were stabilized in the test facility. The position of the electronic expansion valve was set as per the

requirement. Furthermore, the valves on the water loop sides were opened, and the chiller was set to obtain the temperature and flow rates of the DM water. Once the conditions were achieved, the selected compressor was switched on based on the flow rate requirement, which was controlled using a variable frequency drive (VFD). The compressed superheated refrigerant from the compressor was then cooled in a de-superheater to ensure the required conditions at the test condenser. Once the refrigerant parameters were set and steady-state conditions were achieved, the data were logged to obtain the required test parameters.

## 5.4 Data reduction

The data reduction was performed and parameters considered to estimate the condensation characteristics inside test condenser are presented in this section.

### 5.4.1 Condensation heat transfer

In this study, the heat transfer between the refrigerant and the DM water in the test condenser was computed using the law of energy conservation. The rate of heat transfer ($\dot{Q}$) is estimated using Eq. (5.1) and the overall heat transfer coefficient ($U$) is estimated by the Newton's law of cooling using the expression, shown in Eq. (5.2):

$$\dot{Q}_w = \dot{m}_w C_{pw}(T_{wo} - T_{wi}) \tag{5.1}$$

$$\dot{Q} = UA_r\Delta T_{ln} \tag{5.2}$$

here logarithm mean temperature difference ($\Delta T_{ln}$) is expressed as follows:

$$\Delta T_{ln} = \frac{T_{wo}-T_{wi}}{ln\frac{T_s-T_{wi}}{T_s-T_{wo}}} \tag{5.3}$$

where, $T_s$ represents the saturation temperature, and $T_{wi}$ and $T_{wo}$ represent the temperatures of DM water at the test condenser entry and exit, respectively. Further, considering no fouling resistance in the expression of overall heat transfer coefficient ($U$), the average refrigerant heat transfer coefficient ($h_r$) in the test condenser is determined from the following relation:

$$\frac{1}{U} = \frac{1}{\eta_{or}h_r} + \frac{t}{\lambda\left(\frac{A_p}{A_r}\right)} + \frac{1}{\eta_{ow}h_w\left(\frac{A_w}{A_r}\right)} \tag{5.4}$$

$$A_p = L_f W_f \tag{5.5}$$

$$A_r = A_w = 2L_f W_f f_n + \left[\left(\frac{h-t}{s+t}\right) * 2W_f L_f f_n\right]\eta_f \tag{5.6}$$

where $A_w$ and $A_r$ are the surface areas in the water and refrigerant side, respectively, $A_p$ represents the plate area and $h_w$ represents the heat transfer coefficient of the DM water and its estimation is described in the later section. $L_f$ and $W_f$ are the flow length and width of the test condenser, respectively. The fin efficiency is given by $\eta_f$ and $f_n$ is the number of fin layers. The following relationship gives the overall fin surface efficiency ($\eta_o$);

$$\eta_o = 1 - a\left(1 - \eta_f\right) \tag{5.7}$$

where fin area to the total area ratio of the heat exchanger is defined by '$a$',

$$a = \frac{(h-t)}{[(h-t)+(s-t)]} \tag{5.8}$$

$$\eta_f = \frac{tanh(ml)}{ml} \tag{5.9}$$

$$\text{here, } m = \sqrt{\frac{2h(1+\frac{t}{l})}{\lambda * t}} \quad \text{and} \quad l = \frac{h}{2} \tag{5.10}$$

The rate of heat transfer ($\dot{Q}_r$) from the saturated vapour refrigerant to the DM water is estimated using the relation shown in Eq. (5.11):

$$\dot{Q}_r = \dot{m}_r \Delta H \tag{5.11}$$

where $\dot{m}_r$ is defined as the refrigerant flow rate, and $\Delta H$ is the refrigerant enthalpy change.

The energy balance between the refrigerant and DM water during the experiments was within ± 5 %. This was obtained due to the errors and the accuracies of various sensors and instruments, employed in the test facility. This also includes the small amount of heat transfer from the test section to surrounding ambient, which is inevitable. The single-phase energy balance is discussed in the previous chapter. In the present analysis, the heat loss to the surroundings was not considered because the estimated heat loss to the surroundings from the external surface of the test condenser during the single-phase test was found to be very low (up to 0.1 % of the total heat), as discussed in the previous chapter. This is obtained as the test condenser was insulated with 10 mm thickness polyamide foam coated with hypalon, a high quality aerospace-grade insulation material. The steady state criteria considered for the analysis

is also an energy balance criterion, as indicated by Ramana Murthy et al. (2017) and Han et al. (2005), which is expressed as follows:

$$\frac{|\dot{Q}_r - \dot{Q}_w|}{\dot{Q}_{avg}} \leq 5\ \% \tag{5.12}$$

Here, the average heat transfer rate ($\dot{Q}_{avg}$) between the DM water and refrigerant is given as:

$$\dot{Q}_{avg} = \frac{1}{2}(\dot{Q}_r + \dot{Q}_w) \tag{5.13}$$

### 5.4.2 Single-phase heat transfer coefficient of water

In common practice, single-phase heat transfer coefficient of water ($h_w$) is expressed in terms of Colburn '*j*' factor, shown as follows:

$$j_w = \frac{h_w}{GC_p} Pr_w^{\frac{2}{3}} \tag{5.14}$$

Reynolds number ($Re_w$) and Prandtl number ($Pr_w$) for water flow are defined as follows:

$$Re_w = \frac{\rho V\ h}{\mu} = \frac{GD_{h,w}}{\mu} \tag{5.15}$$

$$Pr_w = \frac{\mu C_p}{\lambda_w} \tag{5.16}$$

where $G$ represents the mass flux, $D_{h,w}$ is the hydraulic diameter in the water side of test condenser, $\mu$ and $C_p$ represent the viscosity and specific heat capacity, respectively of water and $\lambda_w$ represents the thermal conductivity of water.

The derived equation for the heat transfer coefficients ($h_w$) of the DM water side for the selected serrated and wavy fin surfaces are presented in the previous chapter, given as:

$$h_w = 0.25\ (\frac{\lambda_w}{D_h})\ Re_w{}^{0.4} Pr_w{}^{0.33} \tag{5.17}$$

$$h_w = 0.168\ (\frac{\lambda_w}{D_h})\ Re_w{}^{0.43} Pr_w{}^{0.33} \tag{5.18}$$

Eq. (5.17) is derived for the Reynolds number range of 150 to 690 for serrated fin surfaces and Eq. (5.18) is derived for the Reynolds number range of 120 to 650 for wavy fin surfaces. These equations are valid only for these limited range of present water-to-water data, as the present test condensers are developed for the lower Reynolds number range. The subsequent

condensation experiments were maintained within these range of Reynolds number to determine the heat transfer and pressure drop parameters.

### 5.4.3 Pressure drop measurement

The frictional pressure drop ($\Delta P_f$) is estimated from the measured total pressure losses ($\Delta P_t$) across the test condenser, considering momentum pressure losses, gravity and manifold pressure losses. The entry and outlet manifolds pressure losses were subtracted from the total pressure losses ($\Delta P_t$), then the momentum and the gravity pressure losses were added to the $\Delta P_t$ as reported by Yan et al. (1999) and Hu and Ma (2022). The expression obtained to estimate the frictional pressure drop ($\Delta P_f$) is given as follows in Eq. (5.19):

$$\Delta P_f = \Delta P_t - \Delta P_c + \Delta P_a + \Delta P_g \tag{5.19}$$

where $\Delta P_c$ is the manifold and port pressure losses considered in the present analysis as computed by Shah and Focke (1988) empirically. $\Delta P_g$ and $\Delta P_a$ are the gravity and momentum pressure losses, respectively, which are computed using the homogeneous model of Collier (1981) for the gas-liquid flow. The expressions for these pressure losses are as follows:

$$\Delta P_c = 1.5 \frac{{G_r}^2}{2\rho_m} \tag{5.20}$$

$$\Delta P_a = {G_r}^2 (\nu_g - \nu_l)|\Delta x| \tag{5.21}$$

$$\Delta P_g = g\rho_m L_f \tag{5.22}$$

where $\nu_l$ and $\nu_g$ represent the specific volumes of the refrigerant liquid and vapour phases, respectively, $|\Delta x|$ is the change in absolute vapour quality between the entrance and exit of the test condenser, and $L_f$ represents the flow length. The two phase average density ($\rho_m$) in the test condenser is computed using a homogeneous model as follows:

$$\rho_m = \left[\frac{x_m}{\rho_g} + \frac{(1-x_m)}{\rho_l}\right]^{-1} \tag{5.23}$$

Here, $\rho_m$ is the average two phase density between the inlet and outlet of the test condenser computed using the homogeneous model of Collier (1981). $x_m$ represents the average vapour quality between the test condenser inlet and outlet. The densities of the fluid in the vapour and liquid phases are given by $\rho_g$ and $\rho_l$, respectively.

In the present study, a data reduction analysis was performed for the measured values of temperature, pressure, flow rate, and differential pressure on both the refrigerant and water circuits to predict the condensation heat transfer and pressure drop characteristics in the test condenser. The thermophysical properties of pure refrigerants were used for the analysis, and the properties were considered at the bulk mean temperature of the fluid. In the present study, lubrication oil mixed with the refrigerant was neglected because the percentage concentration of oil in the refrigerant was found to be negligible because of the usage of oil separators at the compressor outlet, which isolated the oil from the refrigerant. Considering these aspects, data reduction was performed to obtain the condensation heat transfer coefficient and frictional pressure drops of refrigerants in the serrated and wavy fin test condensers.

## 5.5 Concentration of lubricating oil in refrigerant

Bassi and Bansal (2003) and Wang et al. (2023) investigated mixtures of refrigerants and polyolester (POE) oil during condensation heat transfer. They compared their results with those of an oil-free refrigerant and found that the condensation heat transfer coefficients decreased with increase in the concentration of lubrication oil with refrigerant. This is because of the increase in the liquid film thickness and the subsequent increase in the condensation heat transfer resistance with an increase in the amount of oil mixed with the refrigerant. In this study, synthetic polyolester oil was used in the refrigerant circuit of the test facility to lubricate the reciprocating compressors. During the operation of the test facility and compressors, only a minimal amount of this lubricating oil mixed with the refrigerant, as the test facility was equipped with two levels of oil separators. Thus, in this section, the estimation of lubrication oil mixed with refrigerant is presented and discussed. Meanwhile, the test facility was always charged with the pure refrigerant.

For the analysis, an empty cylinder of refrigerant was considered, which was perfectly evacuated using the vacuum pump of the evacuating system. The weight of the empty cylinder was then measured using a digital weight balance and found to be 0.775 kg. Further, after the condensation experiment, the refrigerant was collected and transferred through the sampling port of the test facility to the empty cylinder. The weight of the cylinder with the refrigerant was then measured using a digital weight balance, and it was found 1.25 kg. Thus, the net weight of the refrigerant was estimated to be 0.475 kg. Further, the refrigerant was allowed to vent out (which easily vents out as it was in vapour form) slowly from the cylinder. However, during the process, the lubricating oil was settled at the bottom of the cylinder, due to its higher

density. The vented location (inner surface of the cylinder) was further checked with filter paper, and no oil traces or droplets were found on the filter paper. In this state, the weight of the cylinder was measured again and found to be 0.779 kg, which is the net weight of the cylinder and oil traces left at the bottom. Hence, it was found that the weight of the cylinder was slightly higher than that of an empty cylinder. Thus, the oil mixed with the refrigerant was estimated and found to be 0.85 % under this condition. The estimation of oil percentage mixed with refrigerant was repeated for the other test conditions during the experiments, and was found to be less than 1 % for all the cases. This negligible amount of oil mixed with the refrigerant was achieved due to the usage of two levels of the oil separation system, which did not degrade the heat transfer.

## 5.6 Summary

This chapter describes the experimental procedure followed to conduct the present condensation experiments in the test facility. The testing methodology employed in the test condenser is described and presented in this chapter. The data reduction performed to estimate the condensation heat transfer and pressure drop characteristics was discussed. The single-phase energy balance for the superheated vapour of the refrigerant and cold DM water was carried out and during the analysis, the heat dissipation to the surroundings during the test was found to be relatively less. In this chapter, various transducers and sensors installed in the test facility are described. The accuracies of these measuring devices are defined and the derived uncertainties obtained while estimating the refrigerant heat transfer coefficient and frictional pressure drops of the refrigerant are presented.

# Chapter 6

# Experimental Results and Discussion on Condensation Investigation

## 6.1 Preface

The present investigation was conducted to estimate the condensation heat transfer coefficient and frictional pressure drop of refrigerants R134a and R1234yf under saturated vapour conditions. In this chapter, condensation experiments performed on three test condensers with two types of serrated fin surfaces (TC1 and TC2) and one type of wavy fin surface (TC3) were presented. The effects and significance of the mass flux and saturation temperature on the condensation heat transfer coefficient and frictional pressure drop of the refrigerant are presented in this chapter. The experimental results of serrated and wavy fin test condensers using refrigerants R134a and R1234yf were compared in terms of the heat transfer coefficients and frictional pressure drops for varying mass flux and saturation temperatures. In this chapter, the effects of varying the hydraulic diameters of test condensers on heat transfer and pressure drop characteristics are also presented. Literature survey indicates that experimental investigation on condensation heat transfer of low GWP refrigerant R1234yf are not available for serrated and wavy fins test condensers. Hence, the present condensation investigation was conducted using R1234yf in these test condensers. Based on the experimental data of R1234yf, suitable correlations were developed and proposed in this chapter.

## 6.2 Test condenser considered for condensation experiments

The test condensers described in chapter 3 are considered for the present condensation experiments. The test condensers TC1 and TC2 have serrated fin surfaces, and TC3 has a wavy fin surface. The geometrical parameters of these test condensers are listed in Table 6.1.

Table 6.1. Geometrical parameters of test condensers (TC1, TC2 and TC3)

| Test unit | Flow circuit | Fin density (FPI) | Fin height (mm) | No. of fins layers | Fin thickness (mm) | Fin size (mm) | | Fin type |
|---|---|---|---|---|---|---|---|---|
| | | | | | | Flow length | Width | |
| TC1 | Refrigerant | 18 | 3.8 | 1 | 0.254 | 150 | 142 | Serrated |
| | DM water | 28 | 5 | 2 | 0.127 | 150 | 142 | |
| TC2 | Refrigerant | 28 | 3 | 1 | 0.127 | 150 | 142 | |
| | DM water | 28 | 5 | 2 | 0.127 | 150 | 142 | |
| TC3 | Refrigerant | 16 | 4.1 | 1 | 0.0762 | 150 | 142 | Wavy |
| | DM water | 18 | 10.2 | 2 | 0.152 | 150 | 142 | |

## 6.3 Testing methodology and approach

In this section, the results available in the literature on the condensation heat transfer coefficient and frictional pressure drop of R134a are considered and compared with the present results. The refrigerant heat transfer coefficient and frictional pressure drop of R134a were estimated as described by Ramana Murthy et al. (2017) and in accordance with the methodology used by the authors (Yan et al., 1999 and Longo, 2008) for plate heat exchangers. In this analysis, condensation experiments were performed using the refrigerant R134a in a test condenser installed in the test facility. A serrated fin test section (TC1), as considered by Ranganayakulu and Seetharamu (2018), was employed to estimate the condensation heat transfer and pressure drop characteristics. The present test results using R134a for the serrated fin test section (TC1) were compared with the correlations developed by Ranganayakulu and Seetharamu (2018) for refrigerant heat transfer coefficient and frictional pressure drop. The experiments were carried out for a varying refrigerant mass flux range of 15 kg/m$^2$s to 53 kg/m$^2$s and at different saturated temperatures of 38 °C and 42 °C. The energy balance between the refrigerant and the DM water in the test condenser was ensured to be within ± 5 %. The results were found to be in good agreement, as shown in Figs. 6.1 and 6.2 for the refrigerant heat transfer coefficient and frictional pressure drop, respectively. These plots also show that both heat transfer coefficient and frictional pressure drop increase with the mass flux. In addition, a reduction in the heat transfer coefficient and frictional pressure drop were observed with saturation temperature.

This is because of the increase in refrigerant vapour density with the saturation temperature. The thermophysical properties of R134a considered in the present study were obtained from the ASHRAE Fundamental Handbook (2001) and the thermophysical properties of R1234yf were evaluated from Refprop 8.0 (2008).

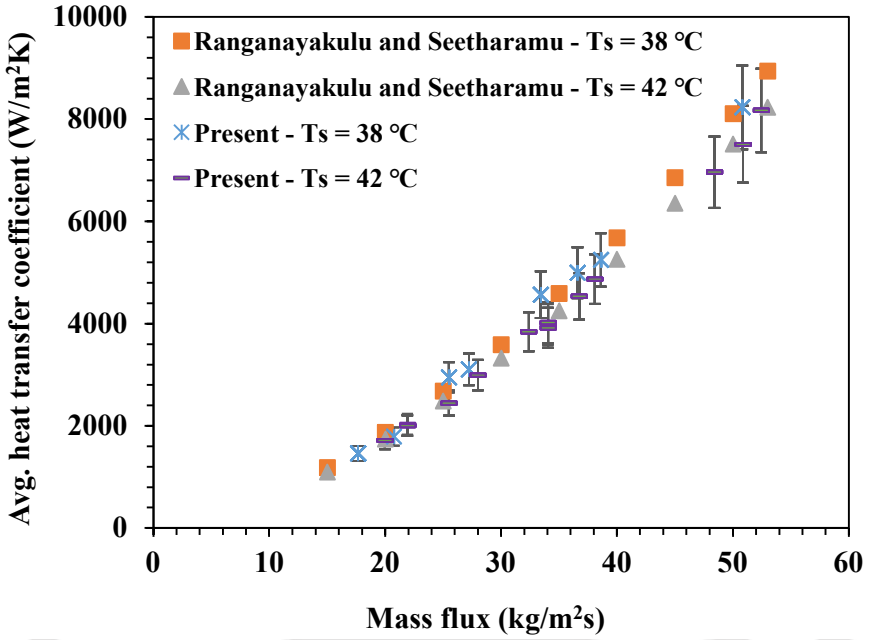


Fig. 6.1. Heat transfer coefficient with varying mass flux of R134a in TC1

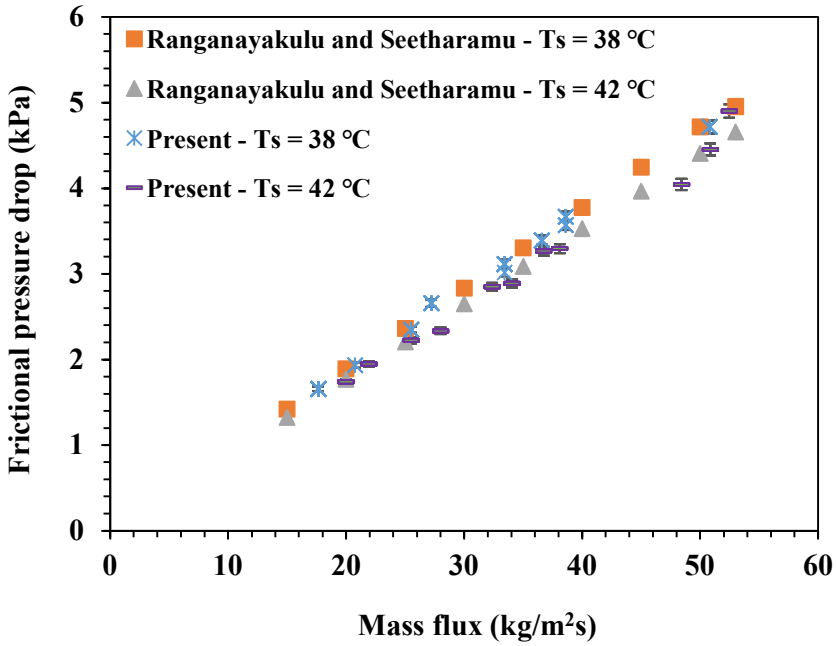


Fig. 6.2. Frictional pressure drops with varying mass flux of R134a in TC1

## 6.4 Condensation heat transfer and pressure drop of R134a and R1234yf

In the present analysis, the condensation experiments were performed using refrigerants R134a and R1234yf in test condensers with serrated fins (TC1) and wavy fins (TC3). In recent years, the HFC refrigerant R134a has been widely used by many investigators to predict the condensation heat transfer and pressure drop characteristics in tubes, herringbone fins, micro-fins, helicoidal pipes and plate heat exchangers. However, owing to the higher global warming potential (GWP) associated with R134a, many researchers have switched to environmentally friendly HFO refrigerant R1234yf, which has a lower GWP value. Thus, in the present study, the primary objective is to conduct condensation experiments in serrated and wavy fin test condensers to investigate the heat transfer and pressure drop characteristics of low GWP R1234yf, which is considered as a substitute for R134a. In this section, the condensation heat transfer coefficient ($h_r$) and frictional pressure drop ($\Delta P_f$) of R134a and R1234yf in the serrated and wavy fin test condensers are estimated and compared.

The experiments were initially conducted using R134a on a serrated fin test condenser (TC1) to determine the average condensation heat transfer coefficient ($h_r$) and frictional pressure drop ($\Delta P_f$) as described by Ramana Murthy et al. (2017). Further, the experiments using refrigerant R1234yf were performed in serrated fin test condenser (TC1). The condensation heat transfer and pressure drop results of refrigerant R1234yf were then compared with R134a as shown in Figs. 6.3 and 6.4, respectively. The experiments were performed for varying refrigerant mass flux ($G_r$) ranging from 16 to 53 kg/m$^2$s and at saturation temperatures ($T_s$) of 34 ℃, 38 ℃ and 42 ℃. Fig. 6.3 shows that the condensation heat transfer coefficient ($h_r$) of refrigerant R134a is higher than that of R1234yf by (10 - 19 %), when operated under the same conditions. The reason for the higher heat transfer coefficient of refrigerant R134a is the higher thermal conductivity than that of R1234yf.

Experiments were also performed to determine the frictional pressure drop ($\Delta P_f$) during the condensation of refrigerants R134a and R1234yf. The frictional pressure drops ($\Delta P_f$) results were compared as shown in Fig. 6.4 for the varying refrigerant mass flux ($G_r$) range of 16 to 53 kg/m$^2$s and at saturation temperatures ($T_s$) of 34 ℃, 38 ℃ and 42 ℃. It was observed that the frictional pressure drop ($\Delta P_f$) of refrigerant R134a is higher by (14 - 19 %) than that of R1234yf. The reason for the higher frictional pressure drops of R134a is its lower reduced pressure than that of R1234yf. The reduced pressure of R134a is lower than that of R1234yf

because its critical pressure is higher for a given pressure. The reduced pressure is defined as the ratio of the given pressure to the critical pressure.

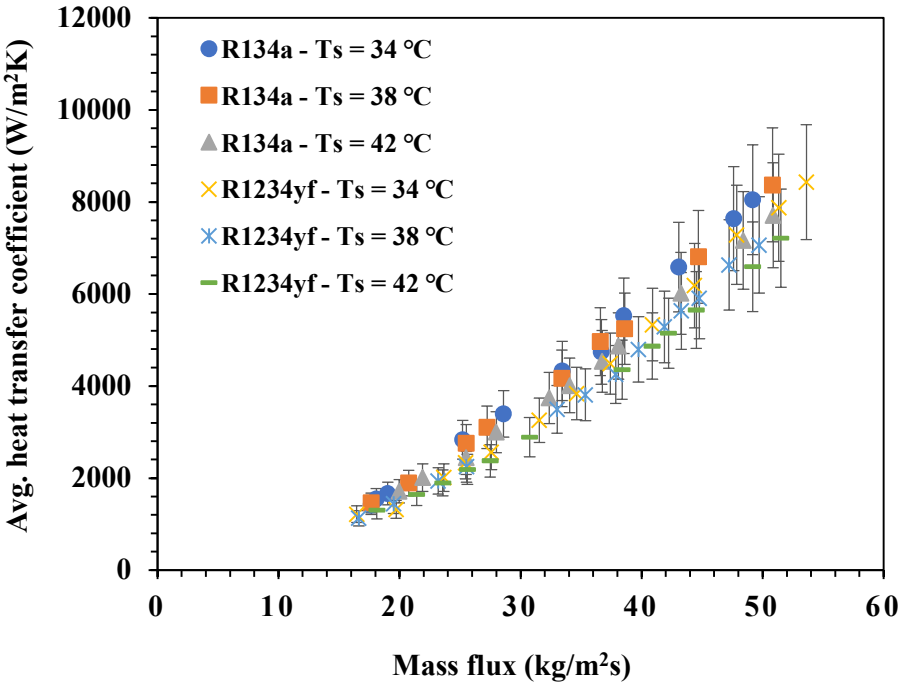


Fig. 6.3. Heat transfer coefficient of R134a and R1234yf for serrated fins surfaces

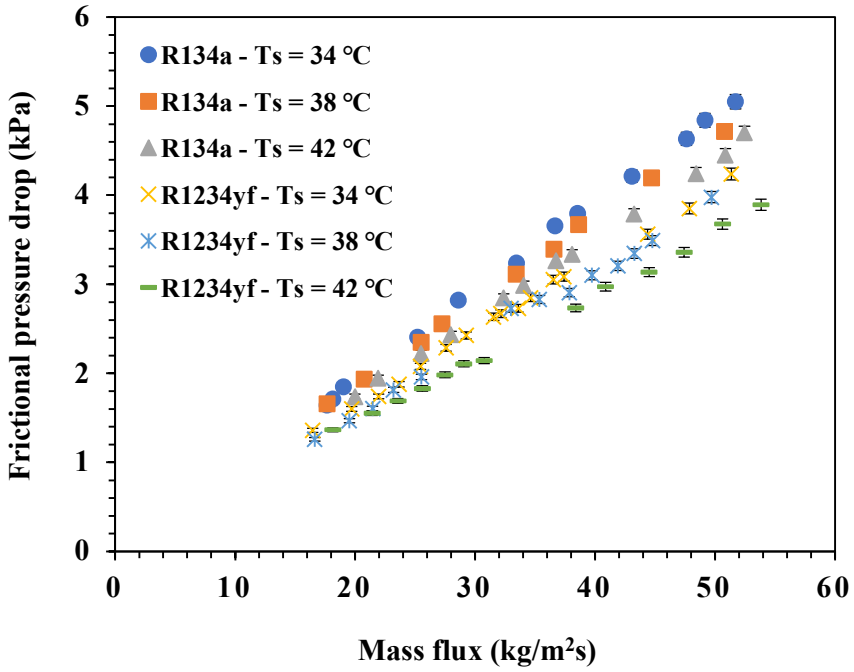


Fig. 6.4. Frictional pressure drops of R134a and R1234yf for serrated fin surfaces

Similarly, in the present study, the condensation heat transfer coefficient ($h_r$) and frictional pressure drop ($\Delta P_f$) of refrigerants R134a and R124yf were estimated in a wavy fin test condenser (TC3). The heat transfer coefficient ($h_r$) and frictional pressure drop ($\Delta P_f$) results of refrigerants R134a and R124yf were compared at the saturation temperatures ($T_s$) of 38 °C and 42 °C for the varying range of mass flux ($G_r$) from 15 to 44 kg/m$^2$s. Fig. 6.5 shows a comparison of the condensation heat transfer coefficient ($h_r$) of refrigerants R134a and R1234yf in wavy fin test condenser. The condensation heat transfer coefficient ($h_r$) of refrigerant R134a was found to be higher by 9 - 16 % than that of R1234yf for wavy fin test condenser, similar to the serrated fin test condenser. This is because the refrigerant R134a has a higher thermal conductivity than that of refrigerant R1234yf.

Fig. 6.6 shows the frictional pressure drops ($\Delta P_f$) of refrigerants R134a and R1234yf for the wavy fin test condenser (TC3) at the saturation temperatures ($T_s$) of 38 °C and 42 °C and for the varying mass flux ($G_r$) ranging from 15 to 44 kg/m$^2$s. The frictional pressure drops ($\Delta P_f$) results for refrigerants R134a and R1234yf were compared, as carried out for the serrated fin test condenser. It was found that the frictional pressure drop ($\Delta P_f$) of refrigerant R134a was higher by 10 - 17 % than that of refrigerant R1234yf, when operated under the same conditions. This is also due to the lower reduced pressure and higher critical pressure of the refrigerant R134a than those of R1234yf at a given pressure.

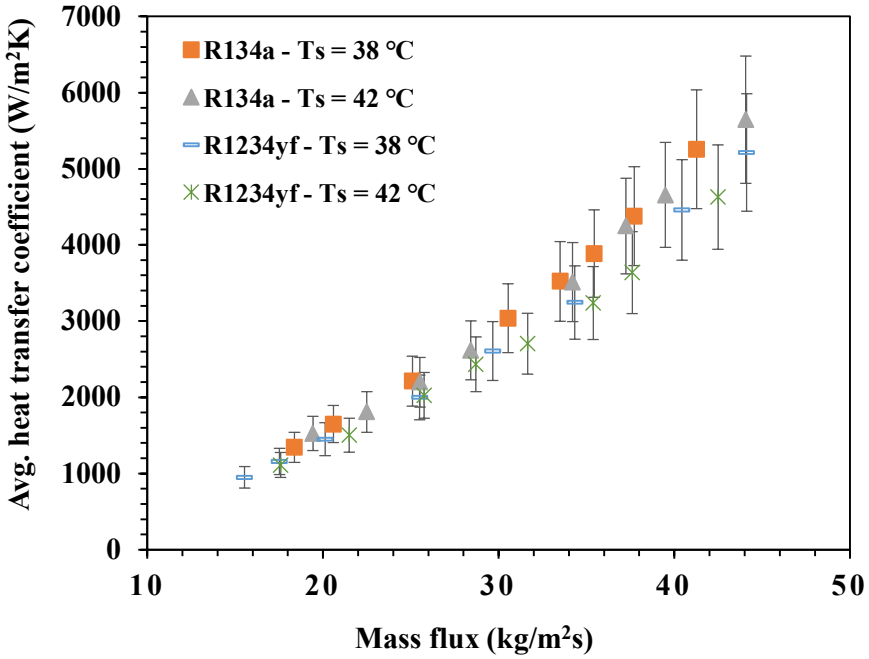


Fig. 6.5. Heat transfer coefficient of R134a and R1234yf for wavy fins surfaces

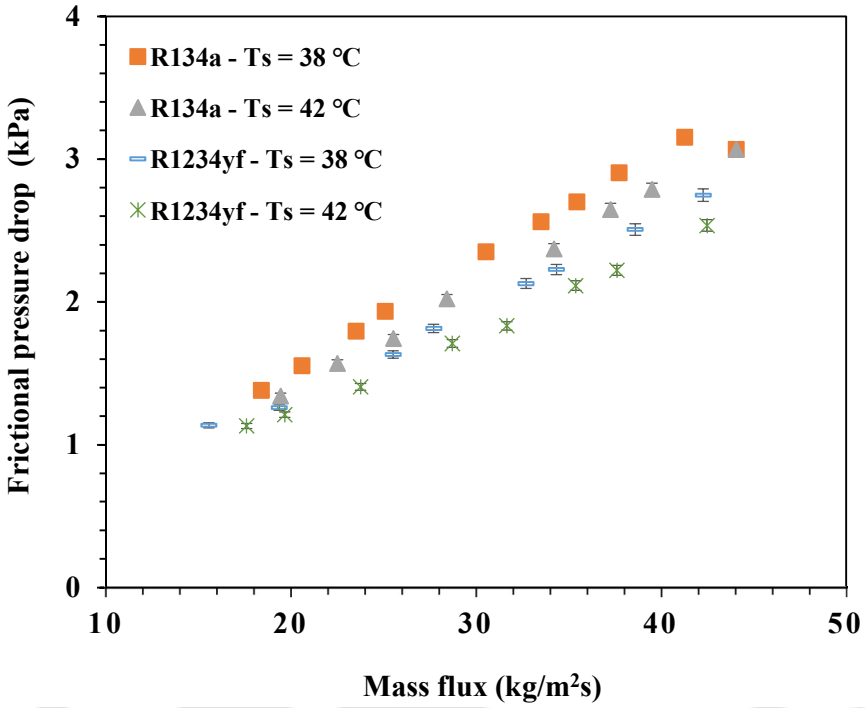


Fig. 6.6. Frictional pressure drops of R134a and R1234yf for wavy fins surfaces

## 6.5 Condensation of refrigerant R1234yf

This section presents an experimental investigation performed on the condensation of R1234yf in three test condensers (TC1, TC2, and TC3). The primary objective of this study is to estimate the condensation heat transfer coefficient ($h_r$) and frictional pressure drop ($\Delta P_f$) of R1234yf for varying refrigerant mass flux ($G_r$) and saturation temperatures ($T_s$). In the present study, different saturation conditions of the refrigerant were maintained during the experiments, which were controlled by a de-superheater installed at the upstream of the test condenser in the test facility. During the analysis, a heat balance between the refrigerant and the DM water was within ± 5 % for the entire set of experiments. The experiments on the condensation heat transfer of R1234yf carried out in three types of test condensers (TC1, TC2 and TC3) are described and presented in the subsequent sections.

### 6.5.1 Condensation in test condenser 1 (TC1)

Experiments on the condensation of refrigerant R1234yf were carried out at different saturation temperatures ($T_s$) of 30 °C to 42 °C in a test condenser (TC1) with serrated fin surfaces for varying refrigerant mass flux. The serrated fin parameters of the test condenser (TC1) are presented in Table 6.2. The significance of the mass flux ($G_r$) and saturation temperatures ($T_s$)

on the condensation heat transfer coefficient ($h_r$) and refrigerant heat flux were analysed and discussed in this section. Further, the effects of the mass flux ($G_r$), saturation temperature ($T_s$) and specific kinetic energy (γ, J/m$^3$) of the refrigerant on the frictional pressure drop ($\Delta P_f$) are also presented in this section. The required operating conditions at the inlet of the test condenser were achieved by the de-superheater by controlling the DM water flow and temperature on the de-superheater water side. The operating conditions maintained in the test condenser (TC1) during the experiments are presented in Table 6.3.

Table 6.2. Geometrical fin parameters of TC1

| Fin parameter | Unit | Refrigerant side | DM water side |
|---|---|---|---|
| Fin type | - | Serrated | Serrated |
| No. of fins layers | - | 1 | 2 |
| Fin density | FPI | 18 | 28 |
| Fin thickness | mm | 0.254 | 0.127 |
| Fin height | mm | 3.8 | 5 |
| Serration length | mm | 3.175 | 3.175 |
| Hydraulic diameter | mm | 1.745 | 1.345 |
| Heat transfer area | m$^2$ | 0.129 | 0.462 |

Table 6.3. Operating conditions during experiments on TC1

| $P_s$ (bar) | $T_s$ (°C) | $G_r$ (kg/m$^2$s) | $\dot{q}_r$ (kW/m$^2$) | $x_{in}$ | $x_{out}$ |
|---|---|---|---|---|---|
| 7.88 ± 0.1 | 30 ± 0.5 | 14-53 | 6-30 | 0.96-1 | 0-0.007 |
| 8.60 ± 0.1 | 34 ± 0.5 | 16-53 | 7-29 | 0.93-1 | 0-0.003 |
| 9.58 ± 0.1 | 38 ± 0.5 | 16-52 | 6-28 | 0.93-1 | 0-0.002 |
| 10.1 ± 0.1 | 40 ± 0.5 | 17-52 | 7-28 | 0.93-1 | 0-0.015 |
| 10.6 ± 0.1 | 42 ± 0.5 | 18-53 | 7-28 | 0.94-1 | 0-0.015 |

#### 6.5.1.1 Effect of mass flux, saturation temperature on condensation heat transfer

In this section, the significance of the refrigerant mass flux ($G_r$) and saturation temperature ($T_s$) on the condensation heat transfer coefficient ($h_r$) of R1234yf is discussed. The refrigerant mass flux ($G_r$) was varied in the test condenser from 14 to 53 kg/m$^2$s and its effects on the average

condensation heat transfer coefficient ($h_r$) for different saturation temperatures ($T_s$) from 30 ℃ to 42 ℃ are shown in Fig. 6.7. The effects of the refrigerant mass flux ($G_r$) on the heat flux ($\dot{q}_r$) are shown in Fig. 6.8 for different saturation temperatures ($T_s$).

Fig. 6.7 shows that the influence of saturation temperatures ($T_s$) on the condensation heat transfer coefficient ($h$) is found to be less than that of the refrigerant mass flux ($G_r$). As reported by Longo et al. (2017), the condensation heat transfer coefficient ($h_r$) was found to be low, in the range of 1125 to 1700 W/m$^2$K for the lower mass flux, $G_r$ < 20 kg/m$^2$s. This is because the condensation heat transfer mechanism is controlled by gravity. However, the dependency of the higher mass flux, $G_r$ > 20 kg/m$^2$s is observed to be higher as the heat transfer mechanism is associated with the forced convection as described by Longo et al. (2017) and as predicted by the classical paper of Akers et al. (1959). It was further observed that for a given saturation temperature ($T_s$) of 42 °C, the condensation heat transfer coefficient ($h_r$) improved by 83 % as the mass flux ($G_r$) increased from 18 to 53 kg/m$^2$s. It was also found that for a given mass flux ($G_r$) of 40 kg/m$^2$s, the condensation heat transfer coefficient ($h_r$) decreased by 9.2 % as the saturation temperature ($T_s$) increased from 30 °C to 42 °C. Furthermore, the condensation heat transfer coefficient ($h$) marginally decreased by 1.4 % when the refrigerant saturation temperature ($T_s$) increased from 40 ℃ to 42 ℃.

Fig. 6.8 shows the effects of the mass flux ($G_r$) on the refrigerant heat flux ($\dot{q}_r$) and it was found that with the increase in mass flux ($G_r$), the refrigerant heat flux ($\dot{q}_r$) also increases. For a given saturation temperature ($T_s$) of 42 ℃, the increase in the heat flux ($\dot{q}_r$) was up to 73.5 %, with an increase in the mass flux ($G_r$) from 18 to 53 kg/m$^2$s. However, Fig. 6.8 also shows that the effect of the saturation temperature ($T_s$) on the refrigerant heat flux ($\dot{q}_r$) is found to be marginal, compared to refrigerant mass flux ($G_r$). It was observed that, for a given refrigerant mass flux ($G_r$) of 40 kg/m$^2$s, refrigerant heat flux ($\dot{q}_r$) was decreased by 6.7 %, with the increase in saturation temperature ($T_s$) from 30 ℃ to 42 ℃. It was also found that the refrigerant heat flux ($\dot{q}_r$) was marginally decreased by 1.8 % when the saturation temperature ($T_s$) was increased from 40 ℃ to 42 ℃.

In the present analysis, it is observed that both refrigerant heat transfer coefficient ($h_r$) and heat flux ($\dot{q}_r$) decreased with saturation temperature ($T_s$), for a given mass flux. This is due to the reduction in the refrigerant vapour specific volume with an increase in the saturation temperature ($T_s$). The reduction in the specific volume of the refrigerant vapour further decreases the vapour velocity, which leads to a weaker interfacial shear stress between the

liquid and vapour. In addition, the thermal conductivity of the refrigerant liquid also decreases with the saturation temperature ($T_s$), which results in lower values of heat transfer.

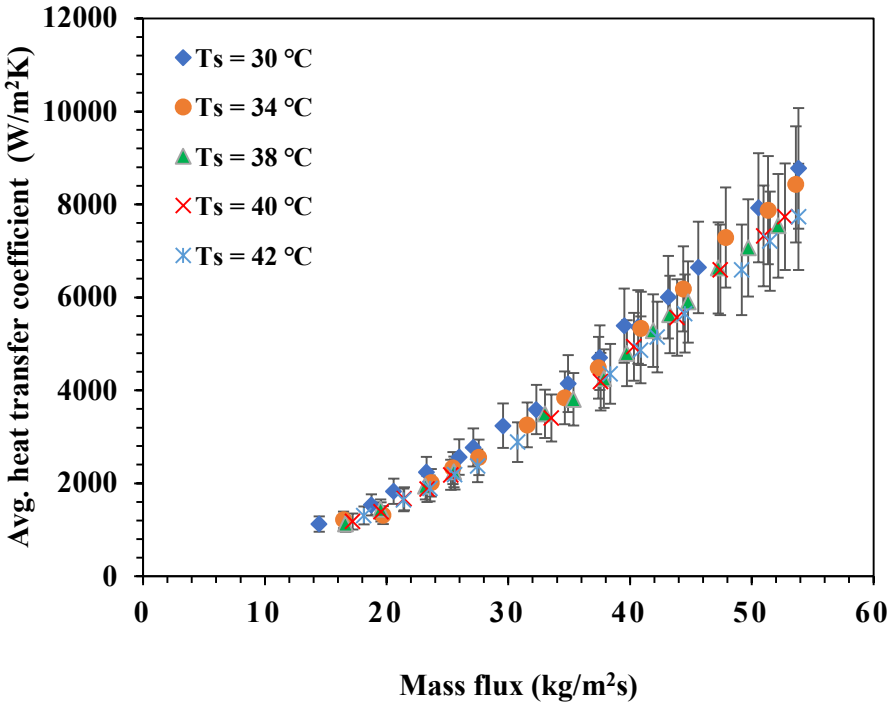


Fig. 6.7. Significance of R1234yf mass flux on heat transfer coefficient for TC1

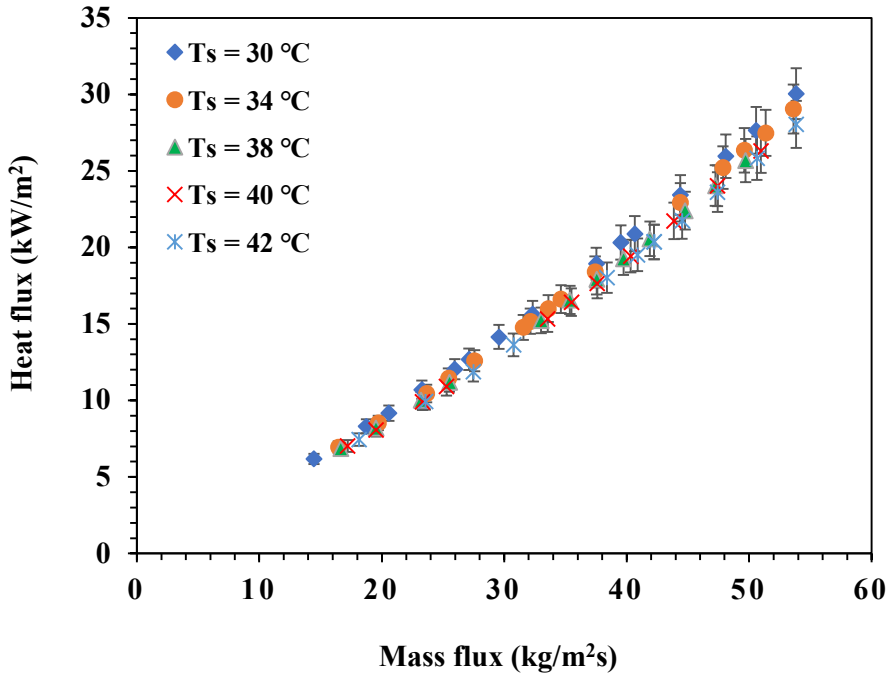


Fig. 6.8. Significance of R1234yf mass flux on heat flux for TC1

#### 6.5.1.2 Effect of mass flux and saturation temperatures on frictional pressure drop

The frictional pressure drop ($\Delta P_f$) of R1234yf was estimated from the total pressure drop measured across the test condenser (TC1) during the condensation experiments. The frictional pressure drop ($\Delta P_f$) was estimated for refrigerant mass flux ($G_r$) ranging from 14 to 53 kg/m$^2$s at the saturation temperatures ($T_s$) of 30 °C to 42 °C, and their effects on the frictional pressure drop ($\Delta P_f$) were studied, as shown in Fig. 6.9. This section also presents the significance of specific kinetic energy ($\gamma$, J/m$^3$) on frictional pressure drop ($\Delta P_f$), as shown in Fig. 6.10.

Fig. 6.9 shows the effects of the refrigerant mass flux ($G_r$) and saturation temperature ($T_s$) on the frictional pressure drop ($\Delta P_f$). It is found that the frictional pressure drop ($\Delta P_f$) increased from 1.2 to 4.8 kPa, with an increase in the mass flux ($G_r$) from 14 to 53 kg/m$^2$s. For a given refrigerant mass flux ($G_r$) of 40 kg/m$^2$s, the frictional pressure drop ($\Delta P_f$) was decreased by 17.7 % with an increase in the refrigerant saturation temperature ($T_s$) from 30 °C to 42 °C. This decrease in the frictional pressure drop is due to the increase in refrigerant vapour density and further reduction in the vapour velocity with an increase in the refrigerant saturation temperature ($T_s$), which further weakens the interfacial shear stress between the vapour and liquid. Another factor that also accounts for the lower frictional pressure drop ($\Delta P_f$) is the lower viscosity of the refrigerant liquid with saturation temperature ($T_s$).

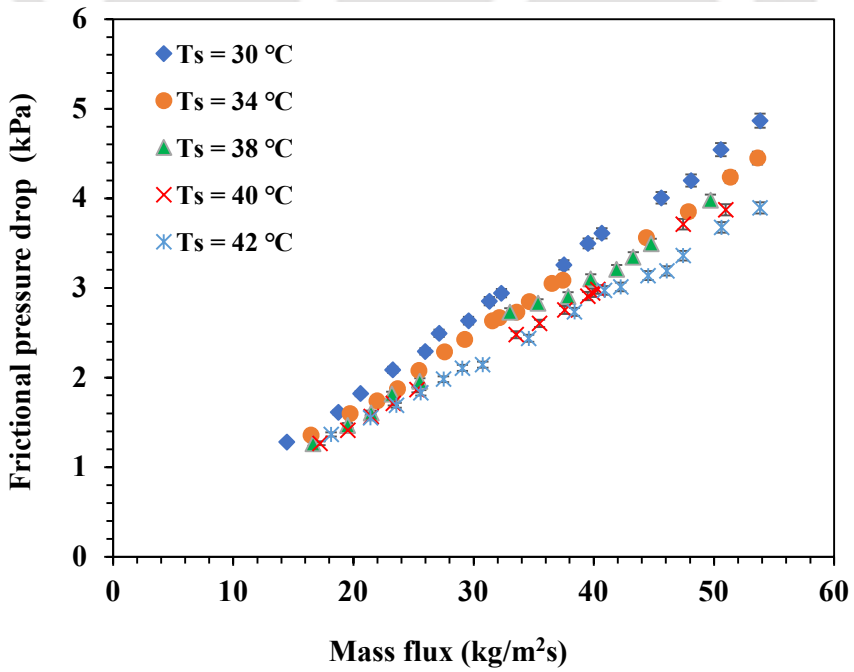


Fig. 6.9. Refrigerant frictional pressure drops with varying mass flux for TC1

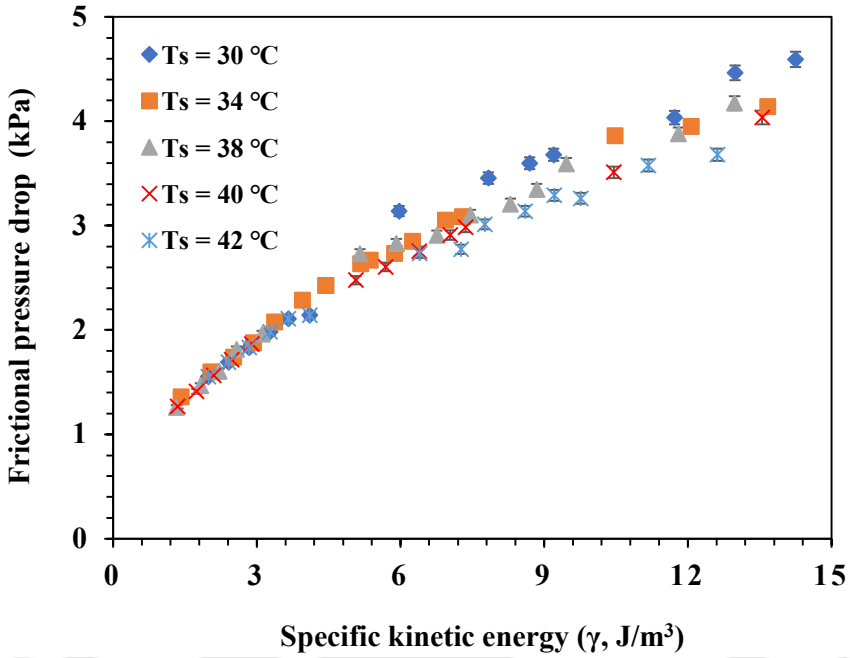


Fig. 6.10. Frictional pressure drops with varying specific kinetic energy for TC1

The significance of the specific kinetic energy ($\gamma$, J/m$^3$) of the refrigerant on the frictional pressure drop ($\Delta P_f$) is shown in Fig. 6.10. The specific kinetic energy ($\gamma$, J/m$^3$) is related to the two phase average density and the refrigerant mass flux ($G_r$). Thus, the frictional pressure drop can be studied as a function of specific kinetic energy ($\gamma$, J/m$^3$). The study was performed at saturation temperatures ($T_s$) of 30 °C to 42 °C, and it is found that the frictional pressure drop ($\Delta P_f$) increased with an increase in the specific kinetic energy ($\gamma$, J/m$^3$) of refrigerant. It is observed that the frictional pressure drop ($\Delta P_f$) increased from 1.3 to 4.5 kPa with an increase in the specific kinetic energy ($\gamma$, J/m$^3$) from 1.3 to 14 J/m$^3$, as shown in Fig. 6.10.

Similarly, in this chapter, the condensation heat transfer coefficient ($h$) and frictional pressure drop ($\Delta P_f$) of refrigerant R1234yf were also estimated and presented for the other two test condensers (TC2 and TC3). The significance of the refrigerant mass flux ($G_r$) and saturation temperature ($T_s$) on the condensation heat transfer coefficient ($h_r$) and heat flux ($\dot{q}_r$) were also discussed and presented for these test condensers. Furthermore, in this chapter, the effects of the refrigerant mass flux ($G_r$), saturation temperature ($T_s$) and specific kinetic energy ($\gamma$, J/m$^3$) of the refrigerant on the frictional pressure drop ($\Delta P_f$) for these two test condensers are also presented. The suitable correlations are also derived and proposed for the heat transfer coefficient and frictional pressure drop of refrigerant R1234yf based on the experimental data and are presented in the subsequent sections.

### 6.5.2 Condensation in test condenser 2 (TC2)

The test condenser TC2 is another brazed plate fin compact heat exchanger with serrated fin surfaces. In the test facility, the test condenser TC2 was installed after removing the test condenser TC1 for further condensation experiments using R1234yf. As described in chapter 3, the fin density of TC1 is lower than TC2 which provides higher heat transfer surface area than TC2. The geometric parameters of the test condenser TC2 are listed in Table 6.4. Condensation experiments in a test condenser TC2 were also carried out to estimate the condensation heat transfer coefficient and frictional pressure drop of R1234yf. During the experiments, an energy balance between the refrigerant and DM water was within ± 5 % for the entire set of experiments. The operating conditions as per the requirement were maintained at the inlet of the test condenser by controlling the flow rate and temperature of the de-superheater. The same testing methodology as employed for test condenser TC1 was followed for TC2. The operating conditions employed for the TC2 are listed in Table 6.5.

Table 6.4. Geometrical fin parameters of TC2

| Fin parameter | Unit | Refrigerant side | DM water side |
|---|---|---|---|
| Fin type | - | Serrated | Serrated |
| No. of fins layers | - | 1 | 2 |
| Fin density | FPI | 28 | 28 |
| Fin thickness | mm | 0.127 | 0.127 |
| Fin height | mm | 3 | 5 |
| Serration length | mm | 3.175 | 3.175 |
| Hydraulic diameter | mm | 1.227 | 1.345 |
| Heat transfer area | $m^2$ | 0.152 | 0.462 |

Table 6.5. Operating conditions during experiments on TC2

| $P_s$ (bar) | $T_s$ (°C) | $G_r$ (kg/m$^2$s) | $\dot{q}_r$ (kW/m$^2$) | $x_{in}$ | $x_{out}$ |
|---|---|---|---|---|---|
| 7.88 ± 0.1 | 30 ± 0.5 | 15-49 | 4-14 | 0.92-1 | 0-0.009 |
| 8.67 ± 0.1 | 34 ± 0.5 | 16-53 | 4-15 | 0.93-1 | 0-0.003 |
| 9.6 ± 0.1 | 38 ± 0.5 | 16-49 | 4-14 | 0.91-1 | 0-0.01 |
| 10.1 ± 0.1 | 40 ± 0.5 | 18-53 | 5-15 | 0.94-1 | 0-0.016 |
| 10.57 ± 0.1 | 42 ± 0.5 | 16-52 | 4-15 | 0.92-1 | 0-0.014 |

#### 6.5.2.1 Effect of mass flux, saturation temperature on condensation heat transfer

The experiments were performed in the test condenser (TC2) to estimate the average refrigerant heat transfer coefficient during the condensation of refrigerant R1234yf for a mass flux range of 15 to 53 kg/m$^2$s and at different saturated temperatures of 30 °C to 42 °C. In this section, the effect of the refrigerant mass flux on heat flux is analysed and presented for the test condenser TC2. Figs. 6.11 and 6.12 show the effects of the mass flux and saturation temperature on the condensation heat transfer coefficient and heat flux, respectively.

Fig. 6.11 indicates that the significance of the refrigerant mass flux on the condensation heat transfer coefficient was found to be less at lower mass flux, as the condensation heat transfer mechanism is gravity-controlled, as indicated by Longo et al. (2017). The condensation heat transfer coefficient ($h_r$) was observed to be low in the range of 1333 to 1934 W/m$^2$K for the lower refrigerant mass flux $G_r < 20$ kg/m$^2$s. However, the dependency of the higher refrigerant mass flux, $G_r > 20$ kg/m$^2$s, is observed to be greater, as the heat transfer mechanism is governed by forced convection, as indicated by Longo et al. (2017) and as predicted by the classical study of Akers et al. (1959). It was observed that for a given saturation temperature ($T_s$) of 42 °C, the condensation heat transfer coefficient ($h_r$) increased by 85 % with an increase in the refrigerant mass flux ($G_r$) from 16 to 53 kg/m$^2$s. Furthermore, it was found that the significance of the refrigerant saturation temperature ($T_s$) on the condensation heat transfer coefficient ($h_r$) was lower than that of the refrigerant mass flux ($G_r$). It was found that, for a given mass flux ($G_r$) of 40 kg/m$^2$s, the condensation heat transfer coefficient ($h$r) decreased by 12 % with an increase in the saturation temperature ($T_s$) from 30 °C to 42 °C, and the effect was found to be much lower when the saturation temperature ($T_s$) was increased from 40 ℃ to 42 ℃.

Fig. 6.12 shows the effects of the mass flux ($G_r$) on refrigerant heat flux ($\dot{q}_r$) and it was found that with an increase in the mass flux ($G_r$), the refrigerant heat flux ($\dot{q}_r$) also increases. For a given saturation temperature ($T_s$) of 42 ℃, the heat flux increased up to 69 %, when the mass flux ($G_r$) was increased from 16 to 53 kg/m$^2$s. However, as observed in the case of heat transfer coefficient, the effect of the saturation temperature ($T_s$) on heat flux ($\dot{q}_r$) was also marginal compared to mass flux ($G_r$). It was found that, for a given mass flux ($G_r$) of 40 kg/m$^2$s, the heat flux ($\dot{q}_r$) decreased by 7 %, when the saturation temperature ($T_s$) was increased from 30 ℃ to 42 ℃, and it was found to marginally decrease when the refrigerant saturation temperature ($T_s$) was increased from 40 ℃ to 42 ℃. As shown in Figs. 6.11 and 6.12, for a given refrigerant mass flux ($G_r$), both the refrigerant heat transfer coefficient ($h_r$) and heat flux ($\dot{q}_r$) decreased

with the saturation temperature ($T_s$). This is due to the reduction in the specific volume of the refrigerant vapour and the lower thermal conductivity of the refrigerant liquid with the saturation temperature ($T_s$), which leads to a lower condensation heat transfer.

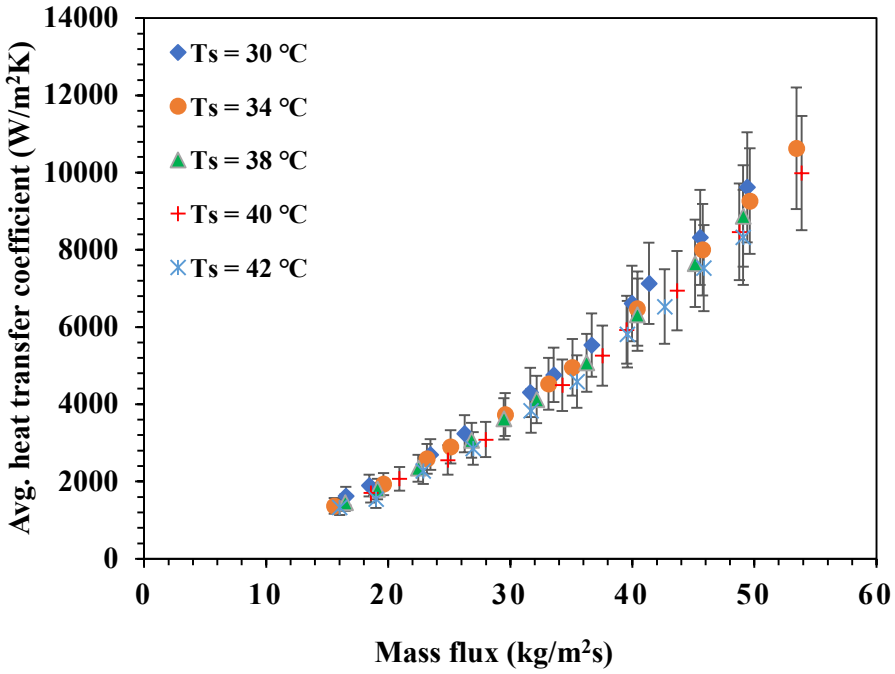


Fig. 6.11. Condensation heat transfer coefficient with varying mass flux for TC2

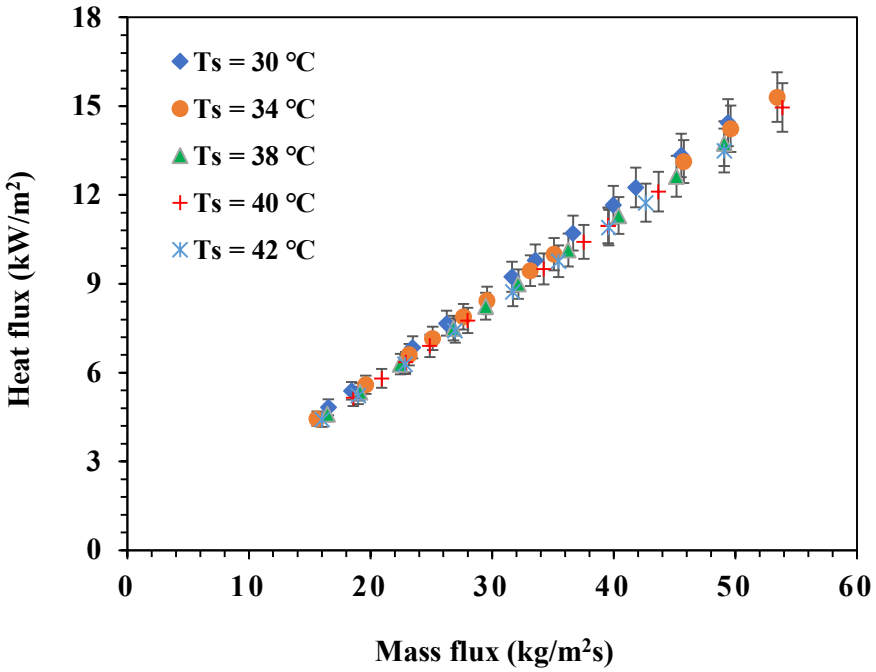


Fig. 6.12. Refrigerant heat flux with varying mass flux for TC2

#### 6.5.2.2 Effect of mass flux and saturation temperatures on frictional pressure drop

The frictional pressure drops were estimated from the total pressure drop across the test condenser TC2 for the varying mass flux ranging from 15 to 53 kg/m$^2$s and saturated temperatures ranging from 30 ℃ to 42 ℃. Fig. 6.13 shows the effect of the refrigerant mass flux and saturation temperatures on frictional pressure drop. It was observed that the effect of the mass flux on frictional pressure drop is more significant, and it decreases with an increase in the saturation temperature. It was found that the frictional pressure drop ($\Delta P_f$) increased from 1.6 to 5.6 kPa, with an increase in mass flux ($G_r$) from 15 to 53 kg/m$^2$s. Further, it was also observed that the frictional pressure drop ($\Delta P_f$) was decreased with the increase in saturation temperatures ($T_s$). For a given mass flux ($G_r$) of 40 kg/m$^2$s, the frictional pressure drop ($\Delta P_f$) was decreased by 22 % with an increase in saturation temperature ($T_s$) from 30 ℃ to 42 ℃.

In this section, the significance of the specific kinetic energy ($\gamma$, J/m$^3$) of the refrigerant on the frictional pressure drop ($\Delta P_f$) is discussed and shown in Fig. 6.14. The study was performed at refrigerant saturation temperatures ($T_s$) ranging from 30 ℃ to 42 ℃ and it was observed that the frictional pressure drop ($\Delta P_f$) was increased with an increase in the specific kinetic energy ($\gamma$, J/m$^3$) of the refrigerant. Fig. 6.14 shows that the frictional pressure drop ($\Delta P_f$) of refrigerant was found to increase from 1.8 to 5.5 kPa with the increase in specific kinetic energy ($\gamma$, J/m$^3$) of refrigerant from 1.5 to 15 J/m$^3$ in the serrated fin test condenser TC2.

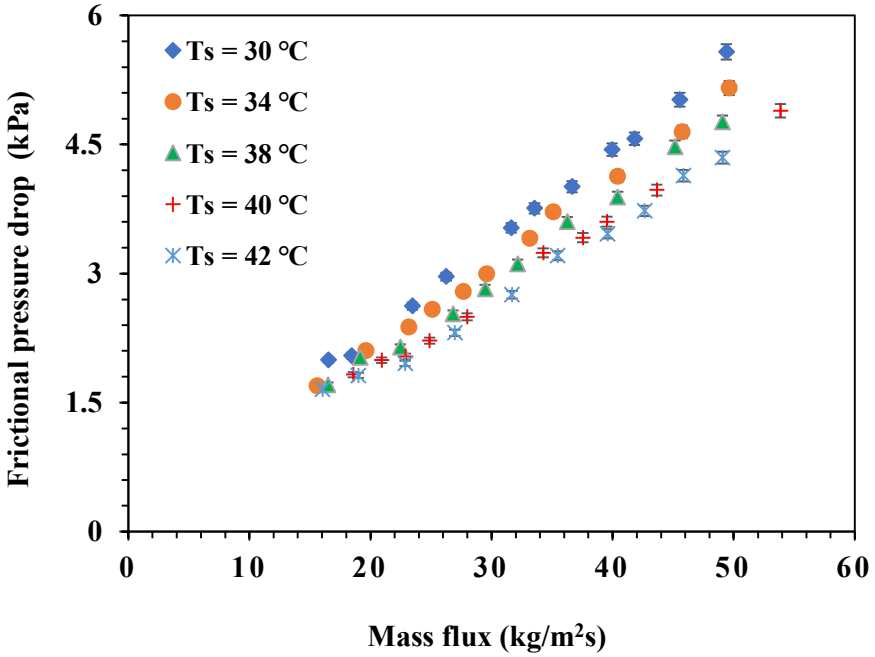


Fig. 6.13. Frictional pressure drops with varying mass flux for TC2

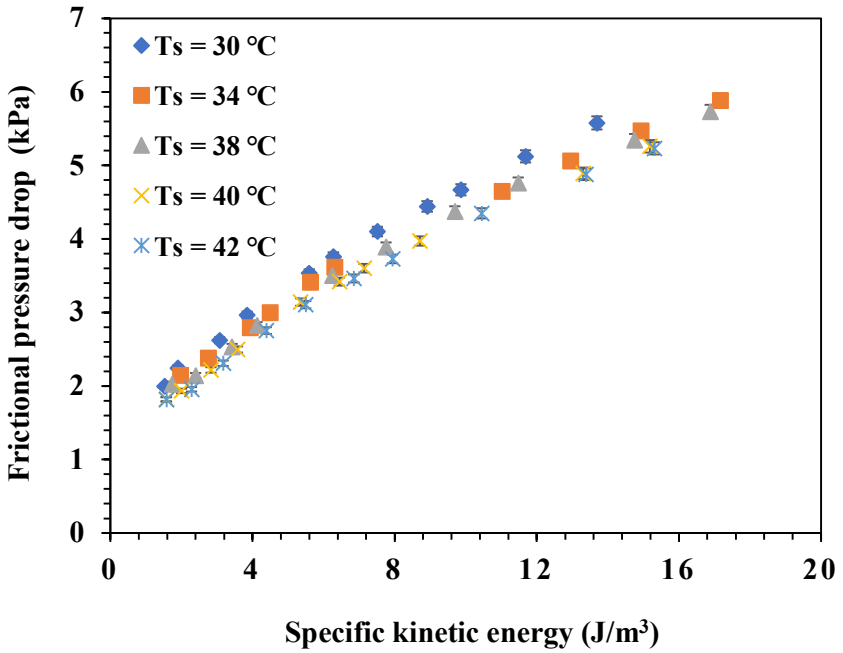


Fig. 6.14. Frictional pressure drop with varying specific kinetic energy for TC2

### 6.5.3 Condensation in test condenser 3 (TC3)

The test condenser TC3 is also a brazed plate fin compact heat exchanger with wavy fin surfaces. In this section, the investigation on condensation heat transfer coefficient and frictional pressure drops of R1234yf in a wavy fin test condenser TC3 are discussed. The geometrical parameters of the test condenser TC3 are listed in Table 6.6. The operating conditions employed in the condenser during the experiments are listed in Table 6.7.

Table 6.6. Geometrical fin parameters of TC3

| Fin parameter | Unit | Refrigerant side | DM water side |
|---|---|---|---|
| Fin type | - | Wavy | Wavy |
| No. of fins layers | - | 1 | 2 |
| Fin density | FPI | 16 | 18 |
| Fin thickness | mm | 0.0762 | 0.152 |
| Fin height | mm | 4.1 | 10.2 |
| Wave amplitude | mm | 1.95 | 1.95 |
| Wave length | mm | 9.525 | 9.525 |
| Hydraulic diameter | mm | 2.197 | 2.238 |
| Heat transfer area | $m^2$ | 0.1303 | 0.5842 |

Table 6.7. Operating conditions during experiments on TC3

| $P_s$ (bar) | $T_s$ (°C) | $G_r$ (kg/m$^2$s) | $\dot{q}_r$ (kW/m$^2$) | $x_{in}$ | $x_{out}$ |
|---|---|---|---|---|---|
| 7.88 ± 0.1 | 30 ± 0.5 | 17-48 | 8-25 | 0.95-1 | 0-0.002 |
| 8.60 ± 0.1 | 34 ± 0.5 | 15-48 | 8-25 | 0.96-1 | 0-0.008 |
| 9.55 ± 0.1 | 38 ± 0.5 | 15-48 | 8-25 | 0.96-1 | 0-0.08 |
| 10.1 ± 0.1 | 40 ± 0.5 | 17-49 | 9-24 | 0.95-1 | 0-0.08 |
| 10.6 ± 0.1 | 42 ± 0.5 | 17-49 | 9-24 | 0.95-1 | 0-0.003 |

#### 6.5.3.1 Effects of mass flux and saturation temperature on condensation heat transfer

The condensation heat transfer coefficient ($h_r$) of refrigerant R1234yf was estimated in test condenser TC3 for varying refrigerant mass flux ($G_r$) ranging from 15 to 49 kg/m$^2$s and for saturation temperatures ($T_s$) ranging from 30 °C to 42 °C. The effects of varying refrigerant mass flux ($G_r$) and saturation temperatures ($T_s$) on the average refrigerant heat transfer coefficient ($h_r$) and heat flux ($\dot{q}_r$) during the condensation of refrigerant R1234yf are shown in Figs. 6.15 and 6.16, respectively.

As shown in Fig. 6.15, the significance of the saturation temperatures ($T_s$) on the refrigerant heat transfer coefficient ($h_r$) is much lower than that of refrigerant mass flux ($G_r$). As indicated by Longo et al. (2017), for a refrigerant mass flux ($G_r$) of lesser than 20 kg/m$^2$s, the refrigerant heat transfer coefficient ($h_r$) was found to be lower, in the range of 963 to 1300 W/m$^2$K, as the condensation heat transfer mechanism is gravity controlled. Longo et al. (2017) also reported that for a refrigerant mass flux ($G_r$) greater than 20 kg/m$^2$s, the condensation heat transfer coefficient ($h_r$) is more dominant. This is because the condensation heat transfer mechanism is governed by forced convection as predicted in the classical study of Akers et al. (1959). It was further observed that for a given saturation temperature ($T_s$) of 42 °C and an increase in the refrigerant mass flux ($G_r$) from 17 to 49 kg/m$^2$s, the condensation heat transfer coefficient ($h_r$) was increased by 81 %. Further, it was also found that for a given refrigerant mass flux ($G_r$) of 40 kg/m$^2$s, the condensation heat transfer coefficient ($h_r$) was decreased by 11.2 % (from 4600 to 4082 W/m$^2$K) when the saturation temperature ($T_s$) increased from 30 °C to 42 °C. It was also observed that when the saturation temperature ($T_s$) was increased from 40 °C to 42 °C, the condensation heat transfer coefficient ($h_r$) was decreased by only 1.6 %.

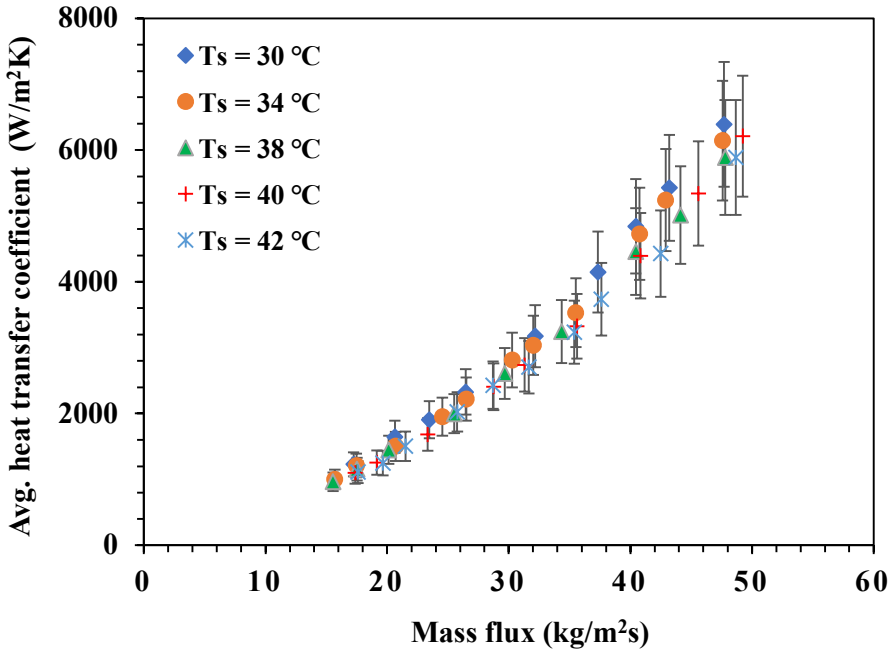


Fig. 6.15. Refrigerant heat transfer coefficient with varying mass flux for TC3

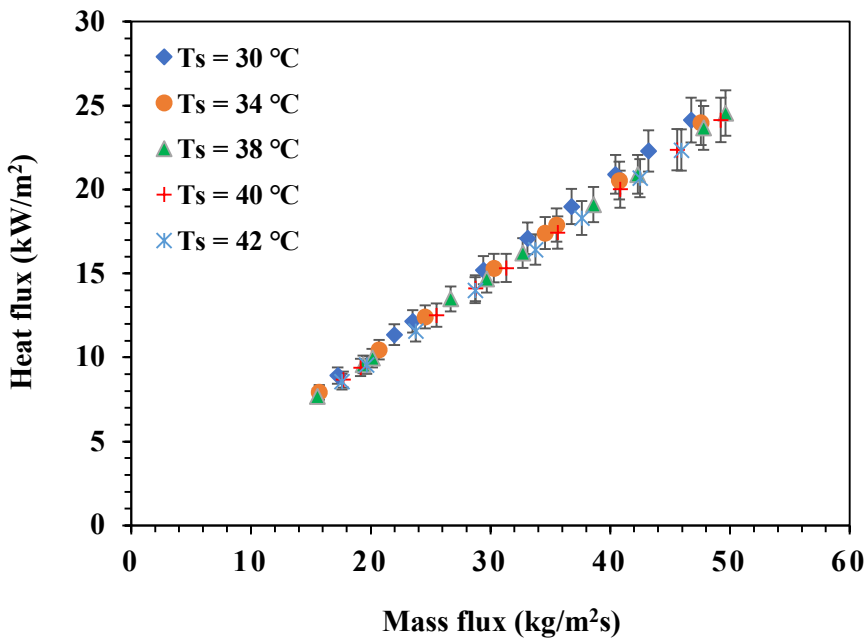


Fig. 6.16. Refrigerant heat flux with varying mass flux for TC3

Fig. 6.16 shows the significance of the refrigerant mass flux ($G_r$) on the heat flux ($\dot{q}_r$) and it is evident that the increase in mass flux ($G_r$) also increases the heat flux ($\dot{q}_r$). It was observed that for a given saturation temperature ($T_s$) of 42 °C, an increase in the refrigerant mass flux ($G_r$) from 17 to 49 kg/m$^2$s increased the heat flux by 61 %. Further, it was also found that, for a

given refrigerant mass flux of 40 kg/m$^2$s, the heat flux decreased by 6.7 %, as the saturation temperature ($T_s$) increased from 30 °C to 42 °C, and when the saturation temperature ($T_s$) was increased from 40 °C to 42 °C, the refrigerant heat flux was found to marginally decrease by 1.7 %. Figs. 6.15 and 6.16 also indicate that for a constant refrigerant mass flux ($G_r$), both the refrigerant heat transfer coefficient ($h_r$) and heat flux ($\dot{q}_r$) decreased with saturation temperature ($T_s$). This is due to the fact that the density of the refrigerant vapour increases with saturation temperatures ($T_s$), that further decreases the vapour velocity of the refrigerant. This results in a lower interfacial shear stress between the refrigerant vapour and the liquid phase. Another factor contributing to the decrease in the condensation heat transfer coefficient ($h_r$) with saturation temperature ($T_s$) is the lower thermal conductivity of the refrigerant liquid.

#### 6.5.3.2 Effects of mass flux and saturation temperatures on frictional pressure drop

In this section, the effects of the mass flux, saturation temperature, and refrigerant specific kinetic energy ($\gamma$, J/m$^3$) on frictional pressure drops are presented for a wavy fin test condenser TC3. The total pressure drops ($\Delta P_t$) of refrigerant R1234yf across the test condenser TC3 were measured for varying mass flux ($G_r$) ranging from 15 to 49 kg/m$^2$s and at saturation temperatures ($T_s$) of 30 ℃ to 42 ℃. The frictional pressure drop ($\Delta P_f$) were estimated from the measured total pressure drops ($\Delta P_t$) across the wavy fin test condenser (TC3). The influences of the refrigerant mass flux ($G_r$) and saturation temperature ($T_s$) on frictional pressure drop ($\Delta P_f$) are shown in Fig. 6.17, and the dependence of specific kinetic energy ($\gamma$, J/m$^3$) of refrigerant on frictional pressure drop ($\Delta P_f$) is shown in Fig. 6.18.

Fig. 6.17 shows that the influence of the refrigerant mass flux ($G_r$) and saturation temperature ($T_s$) on the frictional pressure drop ($\Delta P_f$). It was found that the dependence of refrigerant mass flux ($G_r$) on frictional pressure drop ($\Delta P_f$) is very significant. It was observed that with the increase in mass flux ($G_r$) from 15 to 49 kg/m$^2$s, the frictional pressure drop ($\Delta P_f$) of the refrigerant was increased from 1.13 to 3.71 kPa. It was also found that the frictional pressure drop ($\Delta P_f$) of the refrigerant decreased with an increase in saturation temperature ($T_s$). This is because the interfacial shear stress between the liquid and vapour phases decreases with an increase in the saturation temperature ($T_s$). In addition, the viscosity of the refrigerant liquid decreases with the saturation temperature ($T_s$), which further lowers the pressure drop of the refrigerant. Furthermore, it was also found that as the saturation temperature ($T_s$) increased from 30 °C to 42 °C, the refrigerant frictional pressure drop ($\Delta P_f$) was decreased by 20.5 % for a given mass flux ($G_r$) of 40 kg/m$^2$s.

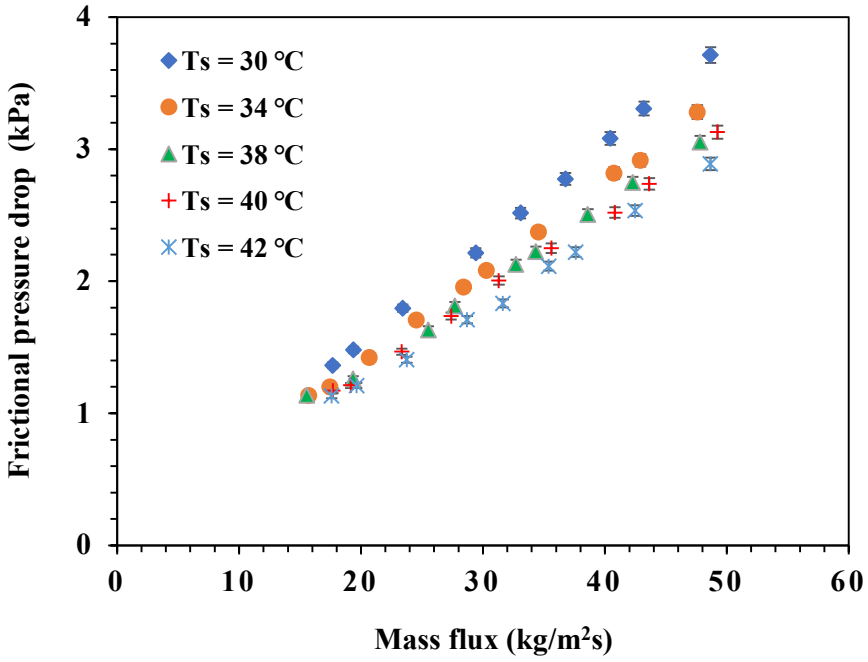


Fig. 6.17. Frictional pressure drops with varying mass flux for TC3

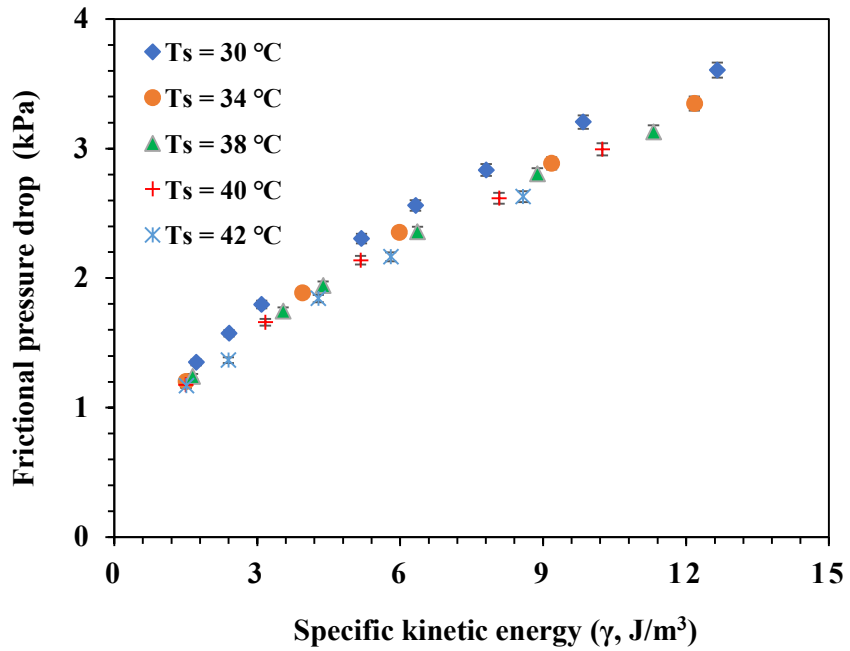


Fig. 6.18. Frictional pressure drops with varying specific kinetic energy for TC3

Fig. 6.18 shows the dependency of specific kinetic energy ($\gamma$, J/m$^3$) of refrigerant on frictional pressure drop ($\Delta P_f$) at different saturation temperatures ($T_s$) ranging from 30 °C to 42 °C. The refrigerant specific kinetic energy ($\gamma$, J/m$^3$) was varied from 1.5 to 13 J/m$^3$ in the test condenser, and the frictional pressure drop ($\Delta P_f$) was found to increase from 1.16 to 3.6 kPa. The specific

kinetic energy ($\gamma$, J/m$^3$) of the refrigerant is dependent on the mass flux ($G_r$) and two phase average density ($\rho_m$). Further, the frictional pressure drop ($\Delta P_f$) also depends on the specific kinetic energy ($\gamma$, J/m$^3$); thus, as the specific kinetic energy ($\gamma$, J/m$^3$) increases, the frictional pressure drop ($\Delta P_f$) also increases. It was found that for a given refrigerant specific kinetic energy of 5 J/m$^3$, the frictional pressure drop ($\Delta P_f$) was decreased by 15 % as the saturation temperature ($T_s$) increased from 30 ℃ to 42 ℃.

## 6.6 Heat transfer and pressure drop correlations

Using the condensation experimental results, the refrigerant heat transfer coefficient ($h_r$) and frictional pressure drop ($\Delta P_f$) of R1234yf were estimated for the three selected test condensers (TC1, TC2, and TC3). The experimental data generated during the condensation experiments for varying refrigerant mass flux and saturation temperatures ($T_s$) ranging from 30 ℃ to 42 ℃ were used to derive the suitable correlations for heat transfer and pressure drop. In this section, the development of correlations for the average condensation heat transfer coefficient ($h_r$) and frictional pressure drop ($\Delta P_f$) of R1234yf are discussed and presented. The experimental results are then expressed and plotted in terms of the proposed correlations.

### 6.6.1 Condensation heat transfer correlations

In this section, the development of a correlation for the condensation heat transfer coefficient ($h_r$) of R1234yf from the experimental data is discussed. The correlation is derived for the test condenser (TC1) with serrated fin surfaces for the saturation temperatures ranging from 30 ℃ to 42 ℃. The power law expression is used to derive a suitable correlation for the refrigerant heat transfer coefficient ($h_r$), as a function of equivalent Reynolds number ($Re_{eq}$), liquid Prandtl number ($Pr_l$), liquid thermal conductivity ($\lambda_l$), and hydraulic diameter ($D_h$), as described by Ramana Murthy et al. (2017). The condensation heat transfer coefficient ($h_r$) represented in terms of ($\lambda_l/D_h$), $Re_{eq}$ and $Pr_l$ is shown in Eq. (6.1).

$$h_r = B\left(\frac{\lambda_l}{D_h}\right)^{a1}\left(Re_{eq}\right)^{a2}(Pr_l)^{a3} \tag{6.1}$$

where *B, a1, a2* and *a3* are the constants determined from the experimental data.

Thus, the equation for condensation heat transfer coefficient ($h_r$) of refrigerant R1234yf is derived for the Reynolds number range of 500 to 2000 using the experimental data of the serrated fin test condenser (TC1), which is expressed as follows in Eq. (6.2):

$$h_r = 2.96 * 10^{-9} \left(\frac{\lambda_l}{D_h}\right)^{5.49} \left(Re_{eq}\right)^{1.66} (Pr_l)^{-2.8} \quad (6.2)$$

$$Re_{eq} = G\left[(1 - x_m) + x_m \left(\frac{\rho_l}{\rho_g}\right)^{\frac{1}{2}}\right] \frac{D_h}{\mu_l} \quad (6.3)$$

$$Pr_l = \mu_l \frac{Cp_l}{\lambda_l} \quad (6.4)$$

where $x_m$ is the average vapour quality between the inlet and outlet of the test condenser, $\rho_l$ and $\rho_g$ are the densities of the refrigerant liquid and vapour phase, respectively, $\mu_l$ is the refrigerant viscosity in the liquid phase and $Cp_l$ is the specific heat of the refrigerant in the liquid phase. The heat transfer correlation given in Eq. (6.2) for the serrated fin test condenser (TC1) correctly predicted the present experimental results within a mean absolute deviation of ± 15 % as shown in Fig. 6.19. Eq. (6.2) is valid for the Reynolds number range of 500 to 2000 and for the saturation temperatures ($T_s$) range of 30 °C to 42 °C.

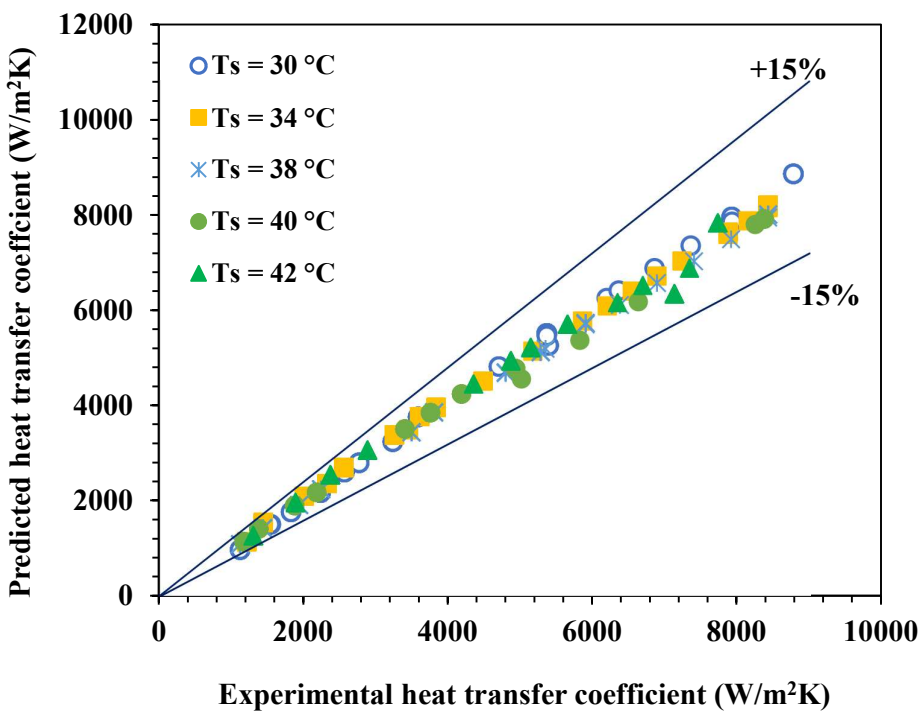


Fig. 6.19. Experimental and predicted average heat transfer coefficient for TC1

Similar to the condensation experiments performed on the test condenser (TC1) for varying refrigerant mass flux and saturation temperature ($T_s$) ranging from 30 °C to 42 °C, experiments using R1234yf were also carried out for the other two test condensers (TC2 having serrated fin

surfaces and TC3 having wavy fin surfaces). The effects of the refrigerant mass flux ($G_r$) and saturation temperature ($T_s$) on refrigerant heat transfer coefficient were also studied for these test condensers. Based on the experimental data for refrigerant R1234yf, the correlations for the refrigerant heat transfer coefficient ($h_r$) for these two test condensers (TC2 and TC3) are also proposed as follows:

a) The derived equation for the condensation heat transfer coefficient ($h_r$) for the Reynolds number range of 400 to 1300 in the serrated fin test condenser (TC2) is given below:

$$h_r = 9.39 * 10^{-6} \left(\frac{\lambda_l}{D_h}\right)^{1.5} \left(Re_{eq}\right)^{1.67} (Pr_l)^{2.46} \tag{6.5}$$

b) The derived equation for the condensation heat transfer coefficient ($h_r$) for the Reynolds number range of 700 to 2200 in the wavy fin test condenser (TC2) is as follows:

$$h_r = 1.343 * 10^{-5} \left(\frac{\lambda_l}{D_h}\right)^{1.38} \left(Re_{eq}\right)^{1.64} (Pr_l)^{2.3} \tag{6.6}$$

The heat transfer correlations given in Eqs. (6.5) and (6.6) predict the present experimental data within a mean absolute deviation of ± 15 %, as shown in Fig. 6.20 for the serrated test condenser (TC2) and Fig. 6.21 for the wavy fin test condenser (TC3).

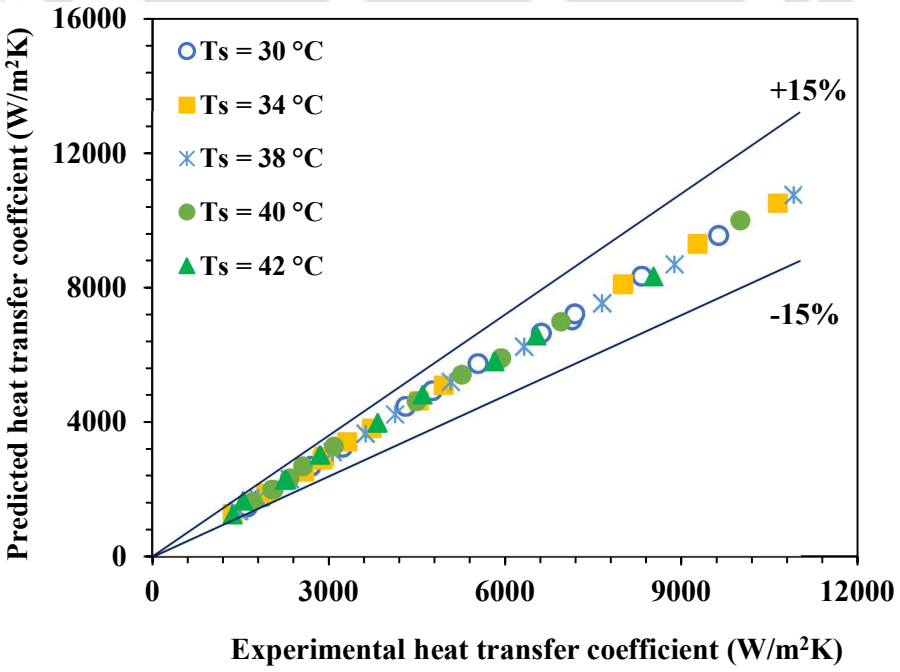


Fig. 6.20. Experimental and predicted average heat transfer coefficient for TC2

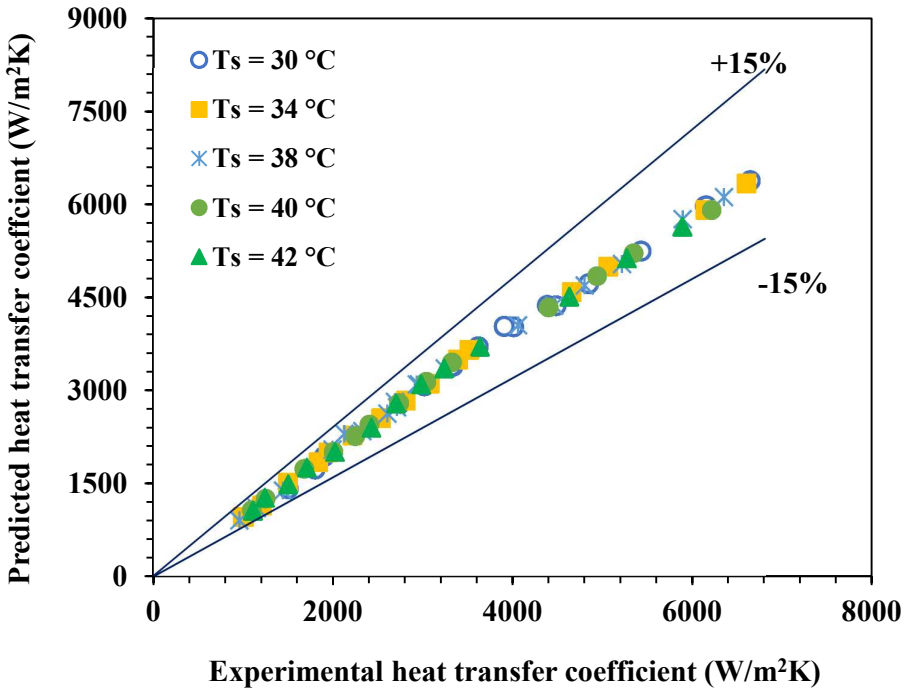


Fig. 6.21. Experimental and predicted average heat transfer coefficient for TC3

### 6.6.2 Frictional pressure drop correlations

In this section, the frictional pressure drop ($\Delta P_f$) estimated from the measured pressure drops across the serrated and wavy fin test condensers (TC1, TC2, and TC3) are defined as functions of the specific kinetic energy ($\gamma$, J/m$^3$) of the refrigerant, as indicated by Longo et al. (2017) and Ramana Murthy et al. (2017). The power law expression is used to develop a suitable correlation for the frictional pressure drop ($\Delta P_f$) of refrigerant from the experimental data, obtained for serrated and wavy fin test condensers (TC1, TC2, and TC3). The proposed correlation as indicated by Longo et al. (2017) for the frictional pressure drop ($\Delta P_f$) of refrigerant in terms of the specific kinetic energy ($\gamma$, J/m$^3$) is represented as follows:

$$\Delta P_f = C(\gamma)^{b1} \tag{6.7}$$

where $C$ and $b1$ are the constants determined from experimental data.

The best-fitting equation is derived for the frictional pressure drop ($\Delta P_f$) as a function of refrigerant specific kinetic energy ($\gamma$, J/m$^3$) using the experimental data of R1234yf in serrated fin test condenser TC1. The proposed equation is derived for the varying specific kinetic energy ($\gamma$, J/m$^3$) and for the saturation temperatures ($T_s$) ranging from 30 °C to 42 °C. The suitable

correlation proposed for the frictional pressure drop ($\Delta P_f$) of the refrigerant R1234yf in the test condenser TC1 is expressed as follows:

$$\Delta P_f = 1.12 * (\gamma)^{0.51} \tag{6.8}$$

The correlation given in Eq. (6.8) for the frictional pressure drop ($\Delta P_f$) of the refrigerant predicts the experimental data within a mean absolute percentage deviation of ± 15 %, as shown in Fig. 6.22. The proposed equation given in Eq. (6.8) is derived and valid for the specific kinetic energy ($\gamma$, J/m$^3$) of the refrigerant ranging from 1 to 14 J/m$^3$ and a saturation temperature ($T_s$) range of 30 °C to 42 °C.

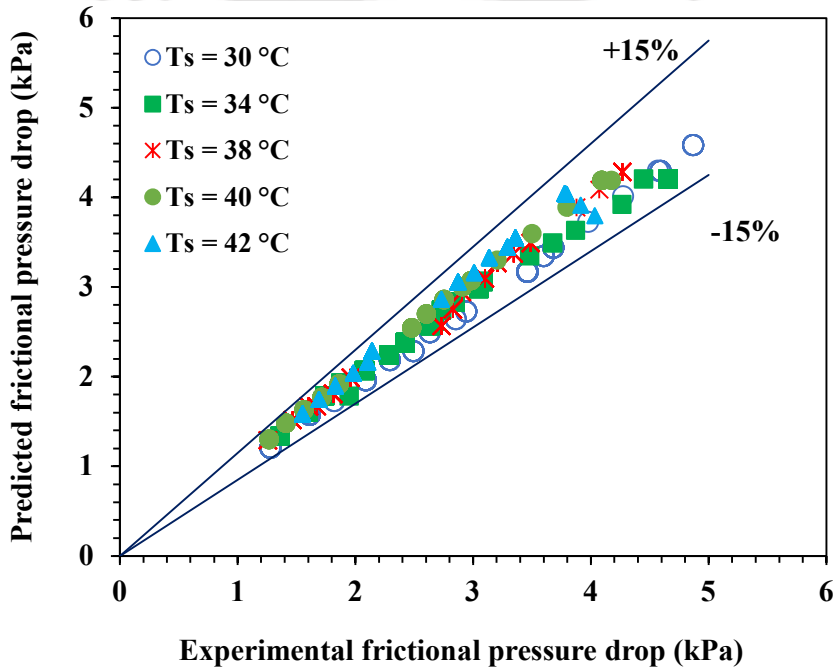


Fig. 6.22. Experimental and predicted frictional pressure drop for TC1

Similarly, the condensation experiments were also performed at saturation temperature ($T_s$) range of 30 °C to 42 °C for the serrated and wavy fin test condensers (TC2 and TC3) to estimate the frictional pressure drop of refrigerant R1234yf. The effects of the mass flux ($G_r$), saturation temperature, and specific kinetic energy ($\gamma$, J/m$^3$) on the frictional pressure drop ($\Delta P_f$) of the refrigerant R1234yf were analysed. Based on the experimental data obtained during condensation experiments at saturation temperatures ($T_s$) ranging from 30 °C to 42 °C, suitable correlations are proposed for the frictional pressure drop ($\Delta P_f$) of R1234yf for these two test condensers (TC2 and TC3). The proposed correlations are expressed as follows:

a) The derived equation for the frictional pressure drop ($\Delta P_f$) of the refrigerant is expressed as a function of the specific kinetic energy ($\gamma$, J/m$^3$) using the experimental data of serrated fin test condenser (TC2). The proposed equation for frictional pressure drop of refrigerant, in the specific kinetic energy ($\gamma$, J/m$^3$) range of 1.5 to 15 J/m$^3$ is given in Eq. (6.9), as follows:

$$\Delta P_f = 1.46 * (\gamma)^{0.48} \tag{6.9}$$

b) The proposed equation for the frictional pressure drop ($\Delta P_f$) of the refrigerant in the specific kinetic energy ($\gamma$, J/m$^3$) range of 1 to 13 J/m$^3$ using experimental data of wavy fin test condenser (TC3) is given in Eq. (6.10), as follows:

$$\Delta P_f = 0.96 * (\gamma)^{0.5} \tag{6.10}$$

The pressure drop correlations given in Eqs. (6.9) and (6.10) for the serrated and the wavy fin test condensers (TC2 and TC3) correctly predict the present experimental data within a mean absolute deviation of ± 15 %, as shown in Figs. 6.23 and 6.24, respectively. The proposed equations of the refrigerant frictional pressure drop ($\Delta P_f$), as expressed in Eqs. (6.9) and (6.10) are derived and valid for the specific kinetic energy ($\gamma$, J/m$^3$) of the refrigerant ranging from 1.5 to 15 J/m$^3$ and 1.5 to 13 J/m$^3$, respectively.

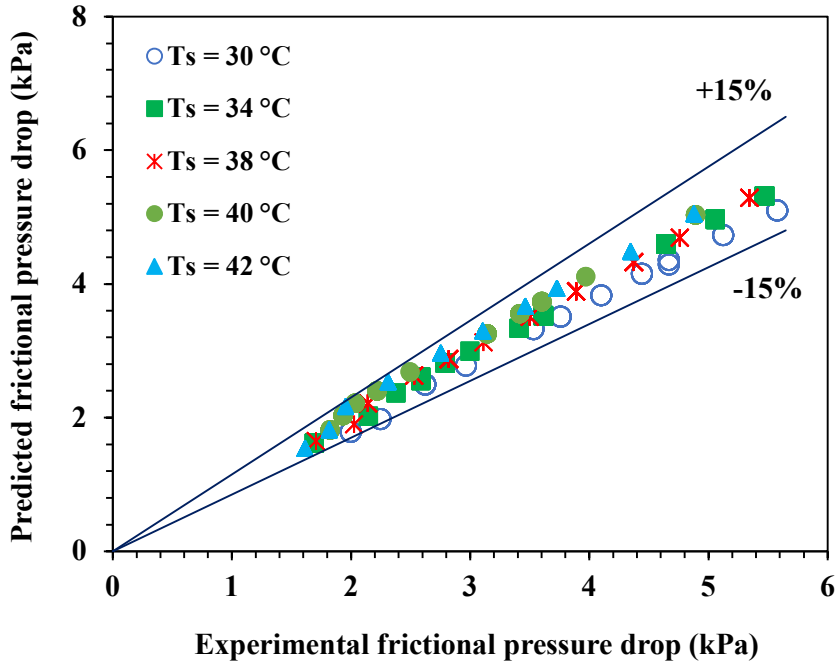


Fig. 6.23. Experimental and predicted frictional pressure drop for TC2

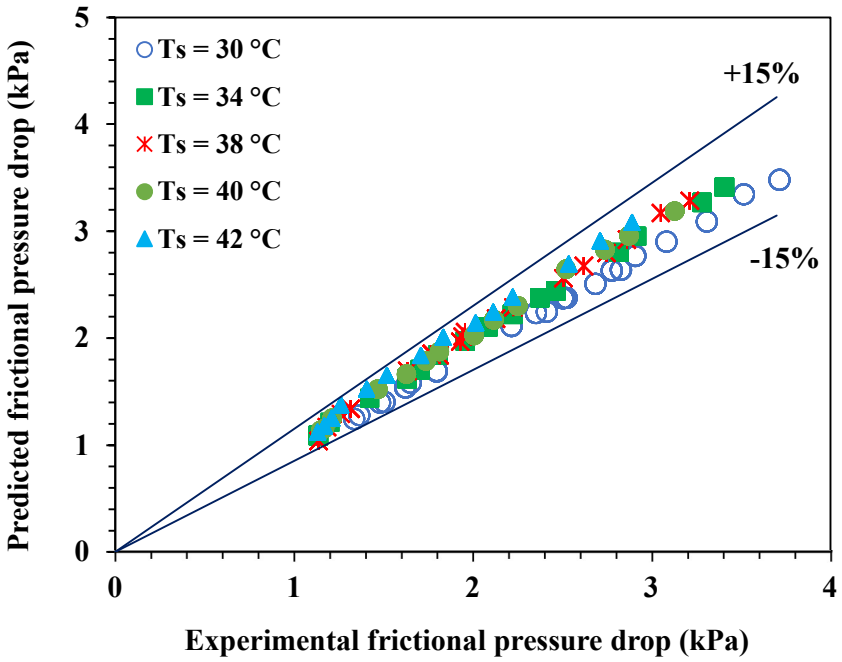


Fig. 6.24. Experimental and predicted frictional pressure drop for TC3

### 6.6.3 Combined heat transfer and pressure drop correlations for serrated fin surfaces

In this section, the experimental data of two serrated fin test condensers, TC1 and TC2 are employed to derive suitable correlations for the condensation heat transfer coefficient ($h_r$) and frictional pressure drop ($\Delta P_f$) of refrigerant R1234yf at saturation temperatures ($T_s$) range of 30 °C to 42 °C. A power law expression is used to derive the combined correlation for the refrigerant heat transfer coefficient ($h_r$), which is defined as a function of equivalent Reynolds number ($Re_{eq}$), liquid Prandtl number ($Pr_l$), liquid thermal conductivity ($\lambda_l$), and fin hydraulic diameter ($D_h$), as described by Ramana Murthy et al. (2017). The proposed relationship is represented by Eq. (6.11).

$$h_r = B\left(\frac{\lambda_l}{D_h}\right)^{a1}\left(Re_{eq}\right)^{a2}(Pr_l)^{a3} \tag{6.11}$$

where *B, a1, a2* and *a3* are the constants determined from the experimental data.

The best-fitting equation is derived using the combined experimental data of the serrated fin test condensers, TC1 and TC2. The correlation derived for the refrigerant heat transfer coefficient ($h_r$) for the Reynolds number range of 400 to 1900 is expressed in Eq. (6.12):

$$h_r = 1.75 * 10^{-6}\left(\frac{\lambda_l}{D_h}\right)^{2.3}\left(Re_{eq}\right)^{1.67}(Pr_l)^{1.27} \tag{6.12}$$

Similarly, the combined correlations for the frictional pressure drop ($\Delta P_f$) are derived in terms of specific kinetic energy ($\gamma$, J/m$^3$) of the refrigerant, as indicated by Longo et al. (2017). The power law expression is used to develop a suitable correlation using the combined experimental data of serrated fin test condensers (TC1) and (TC2). The correlation for the refrigerant frictional pressure drop ($\Delta P_f$) as indicated by Longo et al. (2017) is expressed as follows:

$$\Delta P_f = C(\gamma)^{b1} \tag{6.13}$$

where $C$ and $b1$ are constants determined from experimental data.

The derived equation of frictional pressure drop ($\Delta P_f$) for the specific kinetic energy ($\gamma$, J/m$^3$) range of 1 to 16 J/m$^3$ is expressed as follows:

$$\Delta P_f = 1.12 * (\gamma)^{0.55} \tag{6.14}$$

Eqs. (6.12) and (6.14) for the condensation heat transfer coefficient ($h_r$) and frictional pressure drop ($\Delta P_f$), respectively, predict the combined experimental data of TC1 and TC2 within a mean absolute deviation of ± 20 %, as shown in Figs. 6.25 and 6.26. The correlations given in Eqs. (6.12) and (6.14) are valid for the Reynolds number range of 400 to 1900 and the specific kinetic energy ($\gamma$, J/m$^3$) range of 1 to 16 J/m$^3$, respectively.

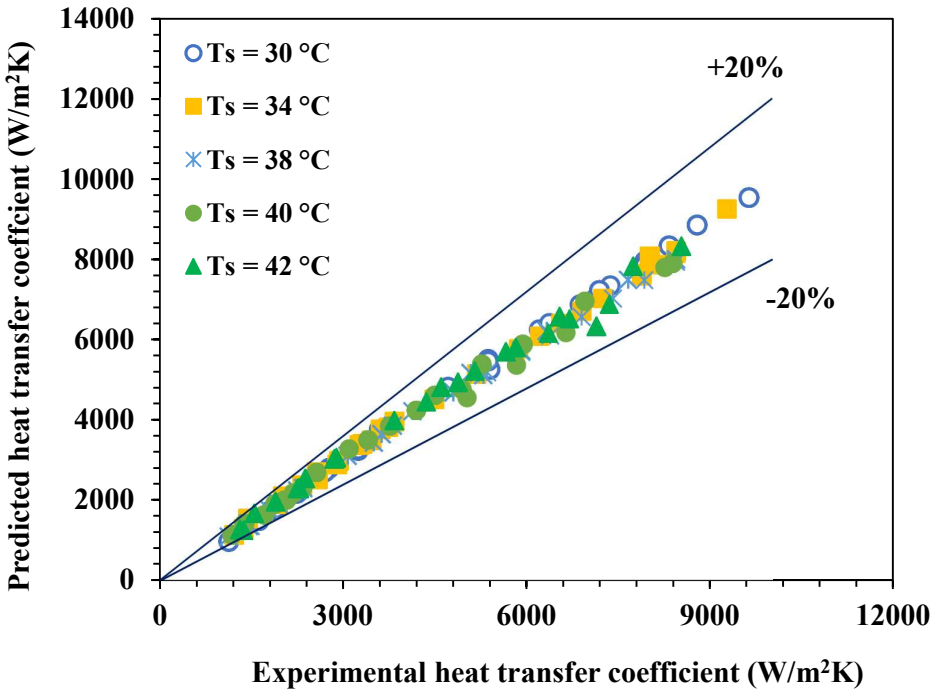


Fig. 6.25. Experimental and predicted heat transfer coefficient for combined TC1 and TC2

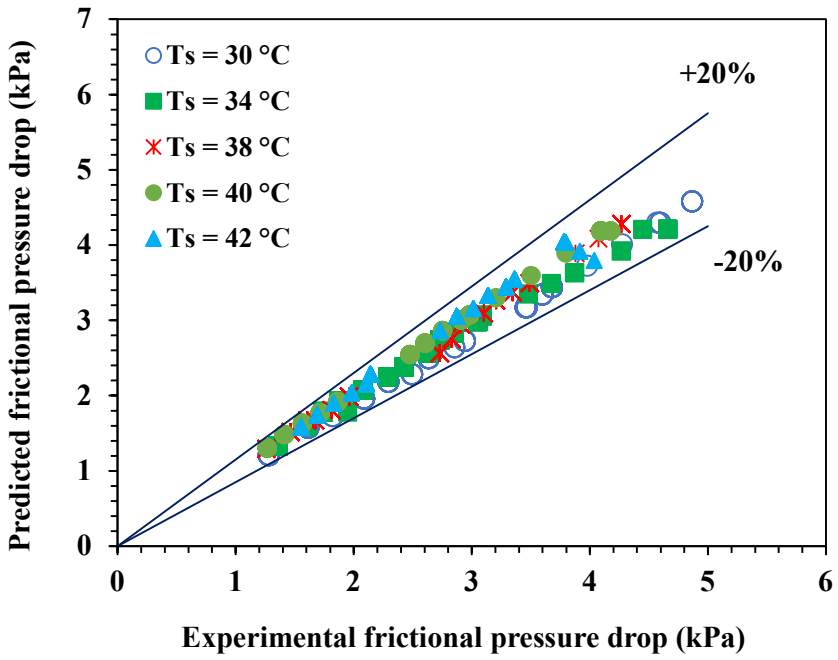


Fig. 6.26. Experimental and predicted frictional pressure drop for combined TC1 and TC2

In the open literature, no one has reported the condensation heat transfer coefficient and frictional pressure drop of R1234yf in a brazed plate fin type of compact heat exchanger with serrated and wavy fin surfaces. The present experimental results on the condensation heat transfer and pressure drop of R1234yf follow a similar trend to that reported by many investigators for different test sections, that are available in the literature. Longo and Zilio (2013), Longo et al. (2018 and 2019) and Shah (2019) and many other authors have used the correlations proposed by Akers et al. (1959) for comparing their investigation and results. In the present study, the condensation heat transfer coefficient ($h_r$) of refrigerant obtained experimentally is also compared with the correlation of condensation heat transfer coefficient for the tubes, proposed by Akers et al. (1959). A deviation as expected is observed as shown in Fig. 6.27 between the predicted heat transfer values of the tubes and the experimental values of the test condensers. A similar deviation was also reported by Zhang et al. (2019), when they compare their results with the equation of Akers et al. (1959). The main reason for this deviation in the present study is due to the geometrical variation in the fluid flow passage. In addition, the interruptions in the flow passage, due to the serrated and wavy nature of the fin surfaces used in the present experimental studies, give comparatively higher heat transfer than tubes. Further, the present condensation investigation of R1234yf in a brazed plate fin compact heat exchanger with serrated fin and wavy fin surfaces will be helpful in compact condenser development and its usage in thermal fluid systems for various applications and industries.

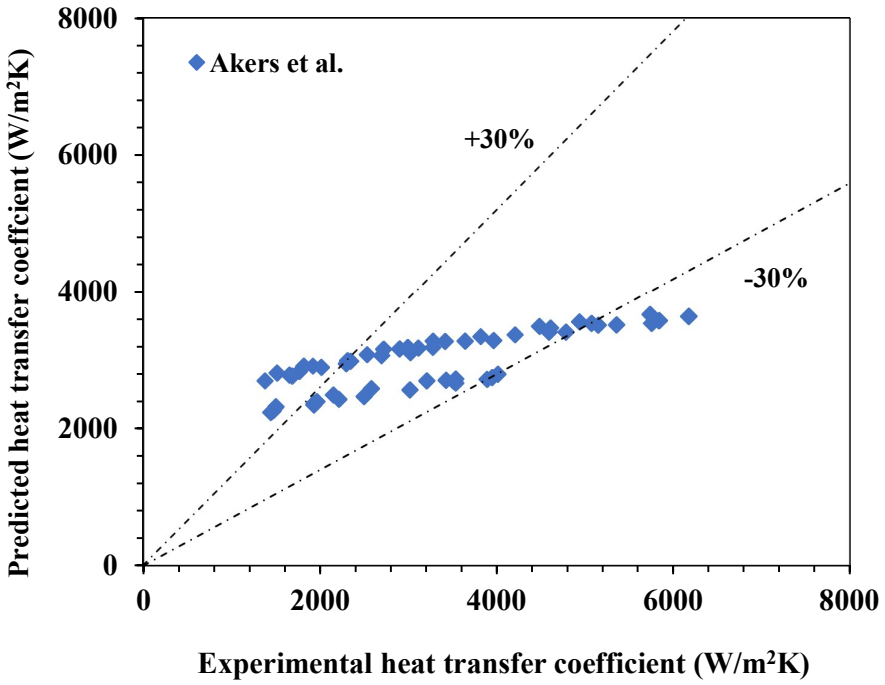


Fig. 6.27. Experimental results compared to equation of Akers et al. (1959)

## 6.7 Effect of fin geometrical parameters on heat transfer and pressure drop

In this section, the effects of the fin geometrical parameters of the test condensers on condensation heat transfer coefficient ($h_r$) and frictional pressure drop ($\Delta P_f$) are discussed. The effects of fin geometries are studied in terms of hydraulic diameters for varying refrigerant mass flux and saturation temperatures. Two serrated fin test condensers (TC1 and TC2) with hydraulic diameters ($D_h$) of 1.745 mm and 1.227 mm, respectively, are considered to study the influence of geometrical fin parameters on the condensation $h_r$ and $\Delta P_f$. The geometrical parameters of these two serrated fin test condensers are presented in Table 6.8.

Table 6.8. Fin geometries of test condensers TC1 and TC2

| Test unit | Flow circuit | Fin density (FPI) | Height (mm) | No. of fins layers | Fin size (mm) | | | Hydraulic diameter (mm) | Fin type |
|---|---|---|---|---|---|---|---|---|---|
| | | | | | Flow length | Width | Thickness | | |
| TC1 | Refrigerant | 18 | 3.8 | 1 | 150 | 142 | 0.254 | 1.745 | Serrated |
| | DM Water | 28 | 5 | 2 | 150 | 142 | 0.127 | 1.345 | |
| TC2 | Refrigerant | 28 | 3 | 1 | 150 | 142 | 0.127 | 1.227 | |
| | DM Water | 28 | 5 | 2 | 150 | 142 | 0.127 | 1.345 | |

### 6.7.1 Influence of hydraulic diameter on condensation heat transfer

In the present test facility, condensation experiments were performed as described in the previous sections in serrated fin test condensers, TC1 and TC2. The investigation was extended to study the influence of the hydraulic diameter on the condensation heat transfer coefficient and frictional pressure drop of refrigerant R1234yf. During the experiments, the energy balance between the refrigerant and the DM water was maintained within ± 5 %. The de-superheater, installed at the upstream of the test condenser, was used to achieve the desired inlet conditions. In this section, the influence of the hydraulic diameter ($D_h$) on condensation heat transfer coefficient ($h_r$) is presented for the two serrated fin test condensers, TC1 and TC2. The hydraulic diameters ($D_h$) of test condensers TC1 and TC2 on the refrigerant side are 1.745 mm and 1.227 mm, respectively, and the hydraulic diameter ($D_h$) on the DM water side is 1.345 mm, which is same for both test condensers. Fig. 6.28 shows the influence of the hydraulic diameter ($D_h$) on the condensation heat transfer coefficient ($h_r$) for the saturation temperature ($T_s$) range of 38 °C to 42 °C. The refrigerant mass flux ($G_r$) was varied from 16 to 53 kg/m$^2$s and the effect of mass flux ($G_r$) on condensation $h_r$ was observed for both TC1 and TC2.

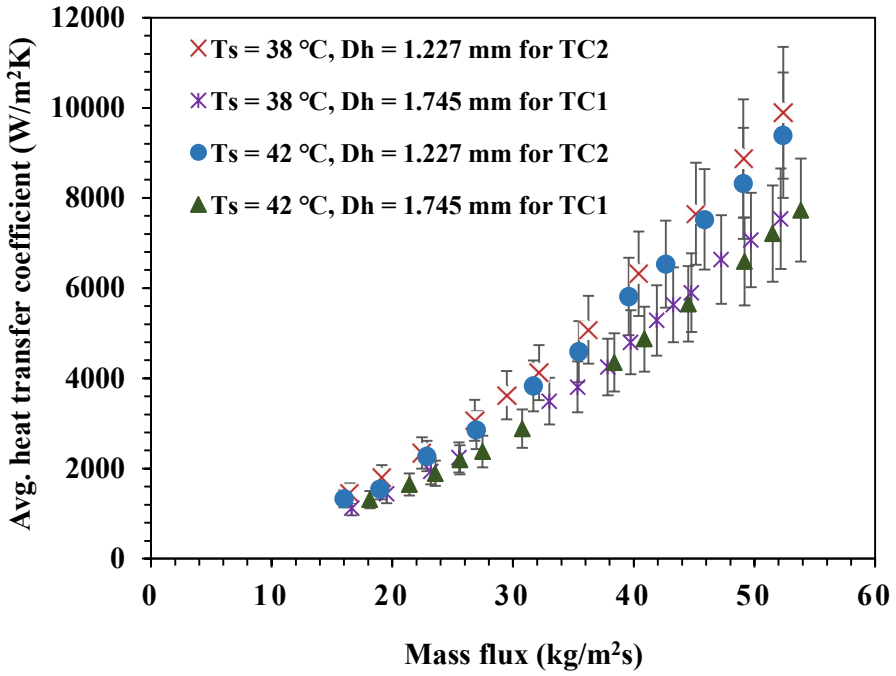


Fig. 6.28. Influence of hydraulic diameter on heat transfer coefficient

As shown in Fig. 6.28, when the hydraulic diameter ($D_h$) was increased for a given mass flux ($G_r$), the condensation heat transfer coefficient ($h_r$) was found to decrease. This is because with

an increase in the hydraulic diameter ($D_h$), the film thickness in the flow path is increased, which led to the increase in the thermal resistance. As a result, the heat transfer coefficient ($h_r$) is decreased with an increase in the hydraulic diameter ($D_h$). Further, it is also observed that the condensation heat transfer coefficient ($h_r$) of the serrated fin test condenser TC2 was 18 - 23 % higher than that of test condenser TC1, as the hydraulic diameter ($D_h$) of the test condenser TC2 was 30 % lower than that of test condenser TC1, for the mass flux ($G_r$) range of 16 to 53 kg/m$^2$s and saturation temperatures ($T_s$) range of 38 ℃ and 42 ℃.

### 6.7.2 Influence of hydraulic diameter on frictional pressure drop

The frictional pressure drop of R1234yf was estimated from the total pressure drop measured across the test condenser during the experiment. Fig. 6.29 shows the influence of the hydraulic diameter ($D_h$) on the frictional pressure drop for the two serrated fin test condensers (TC1 and TC2) and for the saturation temperature ($T_s$) range of 38 to 42 °C. The hydraulic diameters ($D_h$) of test condensers TC1 and TC2 are 1.745 mm and 1.227 mm, respectively. It is observed in Fig. 6.29 that the frictional pressure drop ($\Delta P_f$) was increased as the hydraulic diameter ($D_h$) was decreased, due to reduction in the free flow area. It is observed that the frictional pressure drop ($\Delta P_f$) in the serrated fin test condenser TC2 was 7 - 17 % higher for test condenser TC1, as the $D_h$ of test condenser TC2 was 30 % lower than that of test condenser TC1, for the mass flux ($G_r$) range of 16 to 53 kg/m$^2$s and saturation temperature ($T_s$) range of 38 ℃ and 42 ℃.

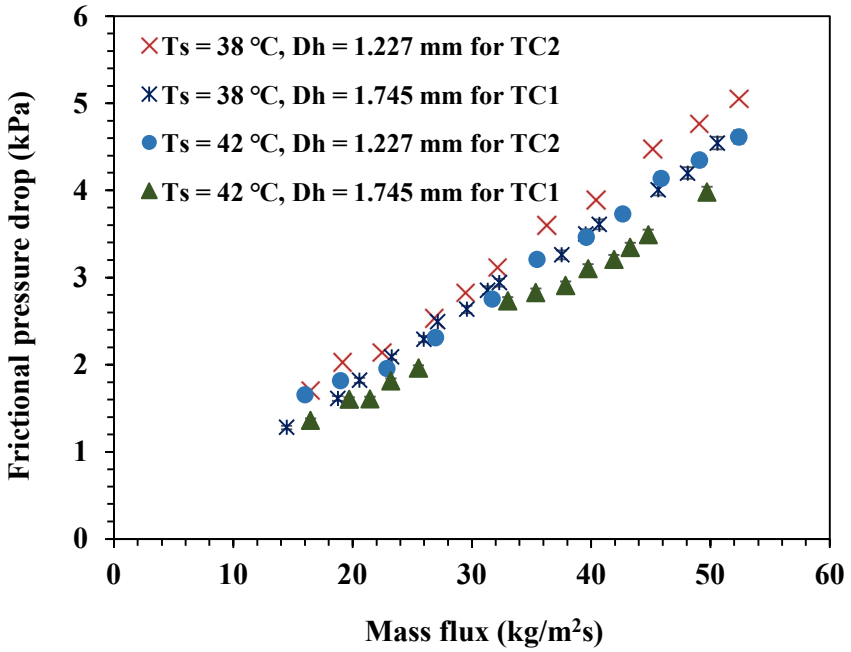


Fig. 6.29. Influence of hydraulic diameter on frictional pressure drop

## 6.8 Summary

The condensation heat transfer coefficient ($h_r$) and frictional pressure drop of R134a and R1234yf estimated for serrated and wavy fins test condensers are presented. The effects of mass flux and saturation temperatures on the condensation heat transfer coefficient and frictional pressure drop are presented in this chapter for three test condensers having two numbers serrated fins and one number wavy fins. Further, the effects of serrated fin geometrical parameters on the condensation heat transfer coefficient and frictional pressure drop are also presented. In this chapter, the condensation heat transfer coefficient and frictional pressure drop of R134a and R1234yf are compared, and it is found that both heat transfer and pressure drop of R134a are higher than R1234yf under the same operating conditions. Further, suitable heat transfer and pressure drop correlations are derived which fit the present experimental results within a mean absolute deviation of ± 15 %. The equations derived for $h_r$ are as follows:

a) Serrated fin test condenser TC1 for Reynolds number range of 500 to 2000

$$h_r = 2.96 * 10^{-9} \left(\frac{\lambda_l}{D_h}\right)^{5.49} \left(Re_{eq}\right)^{1.66} (Pr_l)^{-2.8} \quad (6.15)$$

b) Serrated fin test condenser TC2 for Reynolds number range of 400 to 1300

$$h_r = 9.39 * 10^{-6} \left(\frac{\lambda_l}{D_h}\right)^{1.5} \left(Re_{eq}\right)^{1.67} (Pr_l)^{2.46} \quad (6.16)$$

c) Wavy fin test condenser TC3 for Reynolds number range of 700 to 2200

$$h_r = 1.343 * 10^{-5} \left(\frac{\lambda_l}{D_h}\right)^{1.38} \left(Re_{eq}\right)^{1.64} (Pr_l)^{2.3} \quad (6.17)$$

Similarly, the equations derived for frictional pressure drop ($\Delta P_f$) are as follows:

a) Serrated fin test condenser TC1 for specific kinetic energy (J/m$^3$) range of 1 to 14 J/m$^3$

$$\Delta P_f = 1.12 * (\gamma)^{0.51} \quad (6.18)$$

b) Serrated fin test condenser TC2 for specific kinetic energy (J/m$^3$) range of 1 to 15 J/m$^3$

$$\Delta P_f = 1.46 * (\gamma)^{0.48} \quad (6.19)$$

c) Wavy fin test condenser TC3 for specific kinetic energy (J/m$^3$) range of 1 to 13 J/m$^3$

$$\Delta P_f = 0.96 * (\gamma)^{0.5} \quad (6.20)$$

# Chapter 7
# Conclusion and Future Scope

The major conclusions drawn from the present single-phase numerical and experimental investigations are presented in this chapter. The findings on experimental investigations using refrigerants R134a and R1234yf are also discussed in this chapter. A summary of the key findings on the heat transfer coefficient ($h_r$) and frictional pressure drop ($\Delta P_f$) during condensation in brazed plate fin compact heat exchanger with serrated and wavy fin surfaces is presented. The effects of the refrigerant mass flux, saturation temperatures, and geometrical serrated fin parameters on the condensation heat transfer coefficient and frictional pressure drop of refrigerant R1234yf are also presented.

The condensation heat transfer and pressure drop of the low-GWP refrigerant R1234yf were estimated in a brazed plate compact heat exchanger with serrated and wavy fin surfaces. In recent years, studies on condensation heat transfer of refrigerant R1234yf have been performed by many investigators, mostly in tubes, channels, micro-fins, micro-channels, and plate heat exchangers. However, these studies using refrigerant R1234yf in brazed plate fin compact heat exchangers with serrated fin or wavy fin surfaces are not available in the literature. Considering these literature gaps, the objectives of the present study were defined and condensation experiments using R1234yf were performed as a substitute for refrigerant R134a.

## 7.1 Major conclusions

The major conclusions drawn from the present investigations are as follows:

- A comparison of the experimental and numerical heat transfer coefficients ($h_w$) of water for serrated fin surfaces was found to be within 15 % for the lower Reynolds number range up to 160 and less than 10 % for the higher range of Reynolds numbers up to 690. Similarly, for wavy fin surfaces, the comparison of experimental and numerical heat transfer coefficients ($h_w$) of water was found to be within 11 % for Reynolds numbers ranging from 120 to 650.

- The condensation heat transfer coefficient ($h_r$) of refrigerants R134a in serrated fin test condenser under the same operating conditions was found to be higher than that of R1234yf by 10 - 19 % for the mass flux ($G_r$) range of 16 to 53 kg/m$^2$s. The frictional pressure drop ($\Delta P_f$) of R134a was also observed to be higher by 14 - 19 % than that of R1234yf in serrated fin test condenser.

- Similarly, for the wavy fin test condenser, it was observed that the condensation heat transfer coefficient ($h_r$) and frictional pressure drop ($\Delta P_f$) of refrigerant R134a were higher than those of R1234yf by 9 - 16 % and 10 - 17 %, respectively for a mass flux ($G_r$) ranging from 15 to 44 kg/m$^2$s.

- For test condenser TC1, the condensation heat transfer coefficient ($h_r$) was found to be low, ranging from 1125 to 1700 W/m$^2$K for a lower mass flux ($G_r$) < 20 kg/m$^2$s, as the heat transfer mechanism is gravity-controlled. In addition, for a given saturation temperature ($T_s$) of 42 °C, the condensation heat transfer coefficient ($h_r$) was found to increase by 83 % with an increase in the mass flux ($G_r$) from 18 to 53 kg/m$^2$s. The significance of the saturation temperature ($T_s$) on condensation heat transfer coefficient ($h_r$) was found to be less than that of the mass flux ($G_r$).

- For the test condenser TC1, it was found that for a given saturation temperature ($T_s$) of 42 °C, the heat flux of refrigerant R1234yf was increased up to 73.5 %, with an increase in the refrigerant mass flux ($G_r$) from 18 to 53 kg/m$^2$s.

- For the test condenser TC1, it was observed that frictional pressure drop ($\Delta P_f$) of refrigerant R1234yf was increased from 1.2 to 4.8 kPa, with the increase in mass flux ($G_r$) from 14 to 53 kg/m$^2$s. Further, it was found that for a given refrigerant mass flux ($G_r$) of 40 kg/m$^2$s, the frictional pressure drop ($\Delta P_f$) of refrigerant was decreased by 17.7 % with the increase in the saturation temperature ($T_s$) from 30 °C to 42 °C.

- For the test condenser TC1, it was noticed that the frictional pressure drop ($\Delta P_f$) of refrigerant R1234yf was increased from 1.3 to 4.5 kPa with the increase in refrigerant specific kinetic energy ($\gamma$, J/m$^3$) from 1.3 to 14 J/m$^3$ for the saturation temperature ($T_s$) of 30 ℃ to 42 ℃

- The present experimental results and the proposed correlations for average condensation heat transfer coefficient ($h_r$) and frictional pressure drop ($\Delta P_f$) of refrigerant R1234yf were found to be within ± 15 % for the saturation temperature ($T_s$) range of 30 ℃ to 42 ℃ in TC1, TC2 and TC3 test condensers.

- Further, the condensation heat transfer coefficient in the test condenser TC2 was observed to be 18 - 23 % higher than that of TC1, as the hydraulic diameter ($D_h$) of TC2 was 30 % lower than that of TC1, for the mass flux range of 16 to 53 kg/m$^2$s and saturation temperatures ($T_s$) of 38 °C and 42 °C.

- It was also observed that the frictional pressure drop of refrigerant R1234yf in test condenser TC2 was 7 - 17 % higher than that of TC1, as the hydraulic diameter ($D_h$) of TC2 was 30 % lower than that of TC1.

## 7.2 Scope for future work

The investigations carried out in the present study provide several practical prospects and opportunities to extend and broaden the research on phase change heat transfer in compact heat exchangers. The scope for future work is listed as follows:

- Different types of test condensers with different fin configurations, such as plain fins, louvered fins, and perforated fins, can be considered to study the condensation characteristics using the refrigerant R1234yf.

- Studies on the effect of vapour quality on condensation heat transfer coefficient and frictional pressure drop of R1234yf in a test condenser with both serrated and wavy fins could be considered.

- The experimental investigation on boiling heat transfer of R1234yf inside the test evaporator for both serrated and wavy fin surfaces could be extended.

- Investigations of the boiling and condensation of other environmentally friendly refrigerants could also be studied and extended.

## References

**Akers W.W., Deans H.A., Crosser O.K.,** (1959) Condensing heat transfer within horizontal tubes, Chemical Engineering Progress Symposium Series, 55, 171-176.

**Amaranatha Raju M., Ashok Babu T.P., Ranganayakulu C.,** (2015) Development of single phase heat transfer correlations for water & R134a in rectangular channel with smooth wavy fin, Journal of Physical Science and Application, 5, 199-208. doi:10.17265/2159-5348/2015.03.006

**Amaranatha Raju M., Ashok Babu T.P., Ranganayakulu C.,** (2017) Flow boiling heat transfer and pressure drop analysis of R134a in a brazed heat exchanger with offset strip fins, Heat and Mass Transfer, 53, 3167-3180. https://doi.org/10.1007/s00231-017-2060-1

**Anderson J.D.,** (1995) Computational fluid dynamics-The basic with applications. McGraw-Hill Companies Inc, New York.

**ASHRAE Fundamental Handbook**, (2001) American society of heating, refrigerating and air-conditioning engineers, Inc, USA.

**Ayub Z.H**., (2003) Plate heat exchanger literature survey and new heat transfer and pressure drop correlations for refrigerant evaporators, Heat Transfer Engineering 24, 3-16. https://doi.org/10.1080/01457630304056

**Bandhauer T.M., Agarwal A., Garimella S.,** (2006) Measurement and modelling of condensation heat transfer coefficients in circular micro channels, Journal of Heat Transfer, 128, 1050-1059. https://doi.org/10.1115/1.2345427

**Bashar M.K., Nakamura K., Kariya K., Miyara A.,** (2020) Condensation heat transfer of R1234yf in a small diameter smooth and microfin tube and development of correlation, International Journal of Refrigeration, 120, 331-339. https://doi.org/10.1016/j.ijrefrig.2020.09.002

**Bassi R., Bansal P.K.,** (2003) In-tube condensation of mixture of R134a and ester oil: empirical correlations, International Journal of Refrigeration, 26, 402-409. https://doi.org/10.1016/S0140-7007(02)00152-4

**Bohdal T., Charon H., Sikora M.,** (2011) Comparative investigations of the condensation of R134a and R404A refrigerants in pipe mini-channels, International Journal of Heat and Mass Transfer, 54, 1963-1974. https://doi.org/10.1016/j.ijheatmasstransfer.2011.01.005

**Briggs D.E., Young E.H.,** (1969) Modified Wilson plot techniques for obtaining heat transfer correlations for shell and tube heat exchangers, Chemical Engineering Progress Symposium Series, 65, 35-45.

**Bromley L.A.,** (1952), Effect of heat capacity of condensate, Industrial and Engineering Chemistry, 44, 2966-2969.

**Cavallini A., Del Col D., Doretti L., Longo G.A., Rossetto L.,** (2000) Heat transfer and pressure drop during condensation of refrigerants inside horizontal enhanced tubes, International Journal of Refrigeration, 23, 4-25.
https://doi.org/10.1016/S0140-7007(99)00032-8

**Chen M.,** (1961) An analytical study of laminar film condensation: Part I – Flat plates, Journal of Heat Transfer, 83, 48–54.
https://doi.org/10.1115/1.3680467

**Chennu R., Paturu P.,** (2011) Development of heat transfer coefficient and friction factor correlations for offset fins using CFD, International Journal of Numerical Methods for Heat & Fluid Flow, 21, 935-951.
https://doi.org/10.1108/09615531111177732

**Collier J.G.,** (1981) Convective boiling and condensation, Second edition, McGraw Hill Book Company, New York

**Del Col D., Cavallini A., Thome J.R.,** (2005) Condensation of zeotropic mixtures in horizontal tubes: New simplified heat transfer model based on flow regimes, Journal of Heat Transfer, 127, 221-230.
https://doi.org/10.1115/1.1857951

**Del Col D., Torresin D., Cavallini A.,** (2010) Heat transfer and pressure drop during condensation of low GWP refrigerant R1234yf, International Journal of Refrigeration, 33, 1307-1318.
https://doi.org/10.1016/j.ijrefrig.2010.07.020

**Eckels S.J., Pate M.B.,** (1991) An experimental comparison of evaporation and condensation heat transfer coefficients for HFC-134a and CFC-12, International Journal of Refrigeration, 14, 70-77.
https://doi.org/10.1016/0140-7007(91)90078-U

**Eldeeb R., Aute V., Radermacher R**., (2016) A survey of correlations for heat transfer and pressure drop for evaporation and condensation in plate heat exchangers, International Journal of Refrigeration 65, 12-26.
https://doi.org/10.1016/j.ijrefrig.2015.11.013

**Fernández-Seara J., Rubén Diz, Uhía F.J.,** (2013) Pressure drop and heat transfer characteristics of a titanium brazed plate-fin heat exchanger with offset strip fins, Applied Thermal Engineering, 51, 502-511. https://doi.org/10.1016/j.applthermaleng.2012.08.066

**Han D., Lee K.S., Kim Y.,** (2003) The characteristics of condensation in brazed plate heat exchangers with different chevron angles, Journal of the Korean Physical Society, 43, 66-73.

**Han J.T., Lin C.X., Ebadian M.A**., (2005) Condensation heat transfer and pressure drop characteristics of R-134a in an annular helical pipe, International Communications in Heat and Mass Transfer, 32, 1307-1316. https://doi.org/10.1016/j.icheatmasstransfer.2005.07.009

**Hu S., Ma X.,** (2022) Experimental study of pressure drop during water-ethanol condensation in a vertical plate heat exchanger, Heat and Mass Transfer, 58, 1289-1302. https://doi.org/10.1007/s00231-022-03175-5.

**Hwang S.D., Jang I.H., Cho H.H.,** (2006) Experimental study on flow and local heat/mass transfer characteristics inside corrugated duct, International Journal of Heat and Fluid Flow, 27, 21-32. https://doi.org/10.1016/j.ijheatfluidflow.2005.07.001

**Illán-Gómez F., López-Belchí A., García-Cascales J.R., Vera-García F.,** (2015) Experimental two-phase heat transfer coefficient and frictional pressure drop inside mini-channels during condensation with R1234yf and R134a, International Journal of Refrigeration, 51, 12-23. https://doi.org/10.1016/j.ijrefrig.2014.11.014

**Ji Zhang., Martin Ryhl Kærn., Torben Ommen., Brian Elmegaard., Fredrik Haglind.,** (2019) Condensation heat transfer and pressure drop characteristics of R134a, R1234ze(E), R245fa and R1233zd(E) in a plate heat exchanger, International Journal of Heat and Mass Transfer, 128, 136-149. https://doi.org/10.1016/j.ijheatmasstransfer.2018.08.124.

**Joshi H.M., and Webb R.L.,** (1987) Heat transfer and friction in the offset strip fin heat exchanger, International Journal of Heat and Mass Transfer, 30, 6235-6242. https://doi.org/10.1016/0017-9310(87)90061-5

**Kang H.J., Lin C. X., Ebadian M.A.,** (2000) Condensation of R134a flowing inside helicoidal pipe, International Journal of Heat and Mass Transfer, 43, 2553-2564. https://doi.org/10.1016/S0017-9310(99)00296-3

**Kays W.M., London A.L.,** (1964) Compact heat exchangers, Reprint Third Edition, Krieger Publishing, Malabar, FL, 1998; First Edition, McGraw Hill, New York.

**Kays W.M.,** (1972) Compact Heat Exchangers, AGARD Lecture Series No 57 on Heat Exchangers, AGARD-LS-75-72, NATO, Paris.

**Kline S.J., McClintock F.A.,** (1953) Describing uncertainties in single-sample experiments. Mechanical Engineering, 75, 3-8.

**Kim B., Sohn B.,** (2006) An experimental study of flow boiling in a rectangular channel with offset strip fins, International Journal of Heat and Fluid flow, 27, 514-521. https://doi.org/10.1016/j.ijheatfluidflow.2005.11.008

**Kumar R., Varma H.K., Agrawal K.N., Mohanty B.,** (2001) A comprehensive study of modified Wilson plot technique to determine the heat transfer coefficient during condensation of steam and R-134a over single horizontal plain and finned tubes, Heat Transfer Engineering, 22, 3-12. https://doi.org/10.1080/014576301462218

**Kuo W.S., Lie Y.M., Hsieh Y.Y., Lin T.F.**, (2005) Condensation heat transfer and pressure drop of refrigerant R-410A flow in a vertical plate heat exchanger, International Journal of Heat and Mass Transfer, Volume 48, 5205-5220. https://doi.org/10.1016/j.ijheatmasstransfer.2005.07.023

**Kwon O.J., Shon B., Kang Y.T.,** (2019) Experimental investigation on condensation heat transfer and pressure drop of a low GWP refrigerant R-1233zd(E) in a plate heat exchanger, International Journal of Heat and Mass Transfer, 131, 1009-1021. https://doi.org/10.1016/j.ijheatmasstransfer.2018.11.114

**London, A. L., Shah, R.K.,** (1968) Offset Rectangular Plate-Fin Surfaces-Heat Transfer and Flow Friction Characteristics, Journal of Engineering for Gas Turbines and Power 90, 218-228. https://doi.org/10.1115/1.3609175

**Longo G.A., Gasparella A., Sartori R.,** (2004) Experimental heat transfer coefficients during refrigerant vaporisation and condensation inside herringbone-type plate heat exchangers with enhanced surfaces, International Journal of Heat and Mass Transfer, 47, 4125-4136. https://doi.org/10.1016/j.ijheatmasstransfer.2004.05.001

**Longo G.A., Gasparella A**., (2007) Heat transfer and pressure drop during HFC refrigerant vaporisation inside a brazed plate heat exchanger, International Journal of Heat and Mass Transfer, 50, 5194-5203.

https://doi.org/10.1016/j.ijheatmasstransfer.2007.07.001

**Longo G.A.,** (2008) Refrigerant R134a condensation heat transfer and pressure drop inside a small brazed plate heat exchanger, International Journal of Refrigeration, 31, 780-789. https://doi.org/10.1016/j.ijrefrig.2007.11.017

**Longo G.A.,** (2009) R410A condensation inside a commercial brazed plate heat exchanger, Experimental Thermal and Fluid Science, 33, 284-291. https://doi.org/10.1016/j.expthermflusci.2008.09.004

**Longo G.A., Zilio C.,** (2013) Condensation of the low GWP refrigerant HFC1234yf inside a brazed plate heat exchanger, International Journal of Refrigeration, 36, 612-621. https://doi.org/10.1016/j.ijrefrig.2012.12.018

**Longo G.A., Mancin S., Righetti G., Zilio C.,** (2017) HFC404A condensation inside a small brazed plate heat exchanger: Comparison with the low GWP substitutes propane and propylene, International Journal of Refrigeration, 81, 41-49. https://doi.org/10.1016/j.ijrefrig.2017.05.017

**Longo G.A., Mancin S., Righetti G., Zilio C.,** (2018) Saturated vapour condensation of R410A inside a 4 mm ID horizontal smooth tube: Comparison with the low GWP substitute R32, International Journal of Heat and Mass Transfer, 125, 702-709. https://doi.org/10.1016/j.ijheatmasstransfer.2018.04.109

**Longo G.A., Mancin S., Righetti G., Zilio C.,** (2019) Saturated vapour condensation of R134a inside a 4 mm ID horizontal smooth tube: Comparison with the low GWP substitutes R152a, R1234yf and R1234ze(E), International Journal of Heat and Mass Transfer, (133) 461-473. https://doi.org/10.1016/j.ijheatmasstransfer.2018.12.115.

**Mancin S., Del Col D., Rossetti, L.,** (2012) Condensation of superheated vapour of R410A and R407C inside plate heat exchangers: experimental results and simulation procedure, International Journal of Refrigeration, 35, 2003-2013. https://doi.org/10.1016/j.ijrefrig.2012.06.001

**Mancin S., Del Col D., Rossetto L.,** (2013) R32 partial condensation inside a brazed plate heat exchanger, International Journal of Refrigeration, 36, 601–611. https://doi.org/10.1016/j.ijrefrig.2012.10.019

**Maiti D.K.,** (2002) Heat transfer and flow friction characteristics of plate-fin heat exchanger surfaces - a numerical study, PhD Thesis, IIT Kharagpur, India.

**Manglik R.M., Bergles A.E.,** (1995) Heat transfer and pressure drop correlations for the rectangular offset strip fin compact heat exchanger, Experimental Thermal and Fluid Science, 10, 171–180.

https://doi.org/10.1016/0894-1777(94)00096-Q

**Mattiuzzo N., Azzolin M., Berto A., Bortolin S., Del Col D.,** (2023) Condensation heat transfer and pressure drop of R1234yf/HFC mixtures inside small diameter channels, International Journal of Thermal Sciences, 189, 108258. https://doi.org/10.1016/j.ijthermalsci.2023.108258

**Mochizuki S., Yagi Y., Yang W.J.,** (1987) Transport phenomena in stacks of interrupted parallel-plate surfaces, Experimental Heat Transfer, 1, 127-140. https://doi.org/10.1080/08916158708946336

**Mota-Babiloni A., Navarro-Esbrí J., Barragán Á., Molés F., Peris, B.,** (2014) Drop-in energy performance evaluation of R1234yf and R1234ze(E) in a vapor compression system as R134a replacements, Applied Thermal Engineering, 71, 259-265. https://doi.org/10.1016/j.applthermaleng.2014.06.056

**Mueller A.C.,** (1973) Heat exchangers, in Handbook of Heat Transfer, edited by Rohsenow W.M, and Hartnett J.P, McGraw-Hill Book Co.

**Muley A., Manglik R.M.,** (1999) Experimental study of turbulent flow heat transfer and pressure drop in a plate heat exchanger with chevron plates, Journal of Heat Transfer. 121, 110–121. https://doi.org/10.1115/1.2825923

**Nalbandian H., Yang C., Chen K.,** (2020) Effect of channel size and shape on condensation heat transfer of refrigerants HFO-1234yf and HFC-134a in rectangular microchannels, International Journal of Heat and Mass Transfer, 161, 120314. https://doi.org/10.1016/j.ijheatmasstransfer.2020.120314

**Navarro-Esbrí J., Mendoza-Miranda J.M., Mota-Babiloni A., Barragán-Cervera A., Belman-Flores J.M.,** (2013) Experimental analysis of R1234yf as a drop-in replacement for R134a in a vapor compression system. International Journal of Refrigeration, 36, 870-880. https://doi.org/10.1016/j.ijrefrig.2012.12.014

**Nusselt W.,** (1916) Die Oberflaechenkondensation des Wasserdampes, Zeitschrift des Vereines Deutscher Ingenieure, 60, 541-546, 569-575.

**Park J.E., Vakili-Farahani F., Consolini L., Thome J.R.,** (2011) Experimental study on condensation heat transfer in vertical minichannels for new refrigerant R1234ze(E) versus R134a and R236fa, Experimental Thermal and Fluid Science, (35), 442-454. https://doi.org/10.1016/j.expthermflusci.2010.11.006

**Patankar S.V., Liu C.H., Sparrow, E.,** (1977). Fully developed flow and heat transfer in ducts having stream wise-periodic variations of cross-sectional area, Journal of Heat Transfer, 99, 180-186. https://doi.org/10.1115/1.3450666

**Patankar S.V.,** (1980) Numerical heat transfer and fluid flow, Hemisphere Publication Corporation, USA.

**Pham Q.V., Oh J.,** (2021) Condensation heat transfer characteristics of R1234yf inside multiport mini-channel tube, International Journal of Heat and Mass Transfer, 170, 121029. https://doi.org/10.1016/j.ijheatmasstransfer.2021.121029

**Ramana Murthy K.V., Ranganayakulu C., Ashok Babu T.P.,** (2015) Development of Heat Transfer Coefficient and friction factor correlations for serrated fins in water medium using CFD, Journal of Physical Science Application, 5, 238-248. doi:10.17265/2159-5348/2015.03.010

**Ramana Murthy K.V., Ranganayakulu C., Ashok Babu T.P.,** (2017) Condensation heat transfer and pressure drop of R-134a saturated vapour inside a brazed compact plate fin heat exchanger with serrated fin, Heat and Mass Transfer, 53, 331–341. DOI:10.1007/s00231-016-1827-0

**Ranganayakulu Ch., Seetharamu K.N., Sreevatsan K.V.,** (1997) The effects of inlet fluid flow non-uniformity on thermal performance and pressure drops in cross flow plate-fin heat exchangers, International Journal of Heat and Mass Transfer 40, 27–38. https://doi.org/10.1016/S0017-9310(96)00087-7

**Ranganayakulu Ch., Seetharamu K.N.,** (1999) The combined effects of longitudinal heat conduction, flow nonuniformity and temperature nonuniformity in cross flow plate-fin heat exchangers, International Communications in Heat and Mass Transfer 26, 669–678. https://doi.org/10.1016/S0735-1933(99)00053-6

**Ranganayakulu C., Seetharamu K.N**., (2018) Analysis, design and optimization using FEM and CFD approach, ASME Press and John Wiley & Sons Ltd.

**Ranganayakulu C., Kabelac S.,** (2015) Boiling of R134a in a plate-fin heat exchanger having offset fins, Journal of Heat Transfer, 137, 121002. https://doi.org/10.1115/1.4030910

**Refprop 8.0, (2008)** NIST, Standard Reference Database.

**Rohsenow W.M.,** (1956) Heat transfer and temperature distribution in laminar-film condensation, Transactions of the American Society of Mechanical Engineers, 78, 1645–1648.
https://doi.org/10.1115/1.4014125

**Shah M.M.,** (2019) Improved correlation for heat transfer during condensation in conventional and mini/micro channels, International Journal of Refrigeration, 98, 222-237. https://doi.org/10.1016/j.ijrefrig.2018.07.037.

**Shah M.,** (1979) A general correlation for heat transfer during film condensation inside pipes, International Journal of Heat and Mass Transfer, 22, 547– 556.
https://doi.org/10.1016/0017-9310(79)90058-9

**Shah R.K., Focke W.W.,** (1988) Plate heat exchangers and their design theory, in eds. Shah R.K., Subbarao E.C., and Mashelkar R.A., Heat transfer design, Hemisphere Publishing, Washington D.C. Hemisphere, Washington, 227-254.

**Shah R.K., Sekulic D.P.,** (2003) Fundamentals of heat exchanger design, John Wiley & Sons, Hoboken, New Jersey.

**Sheik Ismail L., Ranganayakulu C., Shah R.K.,** (2009) Numerical study of flow patterns of compact plate-fin heat exchangers and generation of design data for offset and wavy fins, International Journal of Heat and Mass Transfer, 52, 3972–3983.
https://doi.org/10.1016/j.ijheatmasstransfer.2009.03.026

**Sparrow E.M., Baliga B.R., Patankar S.V.,** (1977) Heat transfer and fluid flow analysis of interrupted-wall channel, with application to heat exchangers, Journal of Heat Transfer, 99, 4-11.
https://doi.org/10.1115/1.3450654

**Vaisi A., Javaherdeh K., Moosavi R.,** (2022) Condensation heat transfer performance in multi-fluid compact heat exchangers with wavy and strips fins, International Journal of Heat and Mass Transfer, 182, 121968.
https://doi.org/10.1016/j.ijheatmasstransfer.2021.121968

**Vakili-Farahani F., Agostini B., Thome J.R.,** (2013) Experimental study on flow boiling heat transfer of multiport tubes with R245fa and R1234ze(E), International Journal of Refrigeration, 36, 335-352
https://doi.org/10.1016/j.ijrefrig.2012.12.007

**Versteeg H.K., Malalasekera W.,** (1995) An Introduction to Computational Fluid Dynamics, the Finite Volume Method. Prentice Hall, New York, 62-146.

**Wang L.K., Sunden B., Yang Q.S.,** (1999) Pressure drop analysis of steam condensation in a plate heat exchanger, Heat Transfer Engineering, 20, 71-77. https://doi.org/10.1080/014576399271727

**Wang L., Dang C., Hihara E.,** (2012) Experimental study on condensation heat transfer and pressure drop of low GWP refrigerant HFO1234yf in a horizontal tube, International Journal of Refrigeration, 35, 1418-1429. https://doi.org/10.1016/j.ijrefrig.2012.04.006

**Wang Z., Xu Z., Luo L., Xia X., Li X., He J., Chen Y., (2023)** Experimental investigation of condensation heat transfer of zeotropic refrigerant/oil mixtures in plate heat exchanger, International Journal of Thermal Sciences, 185, 108067 https://doi.org/10.1016/j.ijthermalsci.2022.108067

**Wieting A.R.,** (1975) Empirical correlation for heat transfer and flow friction characteristics of rectangular offset-fin plate-fin heat exchangers, Journal of Heat Transfer, 97, 488-490. https://doi.org/10.1115/1.3450412

**Wilson E.E.,** (1915) A basis for rational design of heat transfer apparatus, Journal of Heat Transfer, 37, 47-70.

**Yan Y.Y., Lin T.,** (1999) Condensation heat transfer and pressure drop of refrigerant R-134a in a small pipe. International Journal of Heat and Mass Transfer, 42, 697-708. https://doi.org/10.1016/S0017-9310(98)00195-1

**Yan Y.Y., Lio H.C., Lin. T.F.,** (1999) Condensation heat transfer and pressure drop of refrigerant R-134a in a plate heat exchanger, International Journal of Heat and Mass Transfer, 42, 993-1006. https://doi.org/10.1016/S0017-9310(98)00217-8.

**Yang C., Nalbandian H.,** (2018) Condensation heat transfer and pressure drop of refrigerants HFO-1234yf and HFC-134a in small circular tube, International Journal of Heat and Mass Transfer, 127, 218-227. https://doi.org/10.1016/j.ijheatmasstransfer.2018.07.093

# Appendix A

# Sample Calculation

Estimation of refrigerant heat transfer coefficient ($h_r$) and frictional pressure drop ($\Delta P_f$):

Refrigerant mass flow rate ($m_r$) = 0.017 kg/s

Condenser inlet pressure ($P_{r,in}$) = 10.15 bar a

Condensing temperature ($T_s$) = 40.7 ℃

Water Inlet Temperature ($T_{wo}$) = 28.0 ℃

Water Outlet Temperature ($T_{wi}$) = 32.11 ℃

Water flow rate ($\dot{m}_w$) = 7.939 lpm

Refrigerant side heat transfer area ($A_r$) = 0.114734 $m^2$

Water side heat transfer area ($A_w$) = 0.47412 $m^2$

Refrigerant side free flow area ($A_{fr}$) = 0.000413 $m^2$

Water side free flow area ($A_{fw}$) = 0.001191 $m^2$

Water side hydraulic diameter ($D_{hw}$) = 0.001345 m

Plate area = 0.0213 $m^2$

Water side heat load is calculated as follows:

$$\dot{Q} = \dot{m}_w C_{pw}(T_{wo} - T_{wi}) = 7.939 \times 4.18 \times \frac{32.11 - 28.0}{60} = 2.274 \text{ kW}$$

$$\dot{Q} = UA_r\Delta T_{ln}$$

$$\Delta T_{ln} = \frac{T_{wo} - T_{wi}}{ln\frac{T_s - T_{wi}}{T_s - T_{wo}}} = \frac{32.11 - 28.0}{ln\frac{40.7 - 28.0}{40.7 - 32.11}} = 10.5112\ ℃$$

$$U = \frac{2.274 \times 1000}{10.5112 \times 0.114734} = 1885.326\ \text{W/m}^2\text{K}$$

The average condensation heat transfer coefficient ($h_r$) is determined by:

$$\frac{1}{U} = \frac{1}{\eta_{or} h_r} + \frac{t}{\lambda\left(\frac{A_p}{A_r}\right)} + \frac{1}{\eta_{ow} h_w \left(\frac{A_w}{A_r}\right)}$$

Water side heat transfer coefficient ($h_w$) is given by

$$h_w = 0.25 \left(\frac{\lambda_w}{D_{hw}}\right) Re_w^{0.4} Pr_w^{0.33}$$

Water mass flux ($G_w$) = $\frac{m_w}{60 \times Afw} = \frac{7.939}{60 \times 0.001191} = 111.187\ \text{kg/m}^2\text{s}$

Water Reynolds number ($Re_w$) = $\frac{G_w\, D_{hw}}{\mu_w} = \frac{111.187 \times 0.001345}{0.001003} = 149.099$

Water side heat transfer coefficient ($h_w$) $= 0.25 \left(\frac{0.6}{0.001345}\right) \times 149.099^{0.4} \times 6.99^{0.33}$

$= 1568.329\ \text{W/m}^2\text{K}$

Overall fin surface efficiency ($\eta_o$) is given by:

$$\eta_{ow} = 1 - a(1 - \eta_f)$$

$$\eta_f = \frac{tanh(ml)}{ml}$$

$$m = \sqrt{\frac{2h\left(1 + \frac{t}{l}\right)}{\lambda t}}$$

Water side overall fin surface efficiency ($\eta_{ow}$) = 1- 0.882 × (1 - 0.8305) = 0.8505

$$\text{m} = \sqrt{\frac{2 \times 1568.329 \times \left(1 + \frac{0.152}{150}\right)}{202.4 \times 0.000152}} = 319.468$$

$$\eta_f = \frac{tanh\left(319.468 \times \frac{5}{2} \times 0.001\right)}{\left(319.468 \times \frac{5}{2} \times 0.001\right)} = 0.8305$$

And refrigerant side overall fin surface efficiency on refrigerant side ($\eta_{or}$) is given by:

$$\eta_{or} = 1 - a(1 - \eta_f) = 0.6738$$

The average condensation heat transfer coefficient ($h_r$) is determined by:

$$\frac{1}{U} = \frac{1}{\eta_{or} h_r} + \frac{t}{\lambda\left(\frac{A_p}{A_r}\right)} + \frac{1}{\eta_{ow} h_w \left(\frac{A_w}{A_r}\right)}$$

$$h_r = 5018.52 \text{ W/m}^2\text{K}$$

Frictional Pressure drop ($\Delta P_f$) is given by:

$$\Delta P_f = \Delta P_t - \Delta P_c + \Delta P_a + \Delta P_g$$

Total Pressure drop ($\Delta P_t$) = 0.407 psi = 2.806 kPa

Manifolds and ports pressure losses ($\Delta P_c$) = $1.5 \frac{{G_r}^2}{2\rho_m}$ = 11.0341 Pa

Refrigerant mass flux ($G_r$) = $\frac{m_r}{Afr} = \frac{0.01665}{0.000413}$ = 40.323 kg/m$^2$s

Mean density ($\rho_m$) = $\left[\frac{x_m}{\rho_g} + \frac{(1-x_m)}{\rho_l}\right]^{-1}$ = 110.527 kg/m$^3$

Momentum pressure losses ($\Delta P_a$) = $G_r^2$ ($\nu_g$ - $\nu_l$)|$\Delta x$| = 26.274 Pa

Gravity pressure losses ($\Delta P_g$) = $g\rho_m L_f$ = 162.6412 Pa

Frictional Pressure drop ($\Delta P_f$) = 2.806-11.0341 × 0.001+26.274 × 0.001 + 162.6412 × 0.001

Frictional Pressure drop ($\Delta P_f$) = 2.984 kPa

# Appendix B

# Uncertainty Analysis

Estimation of uncertainty in heat transfer coefficient ($h_r$) and frictional pressure drop ($\Delta P_f$):

Uncertainty analysis for estimating the uncertainty of dependent parameter, depends on the measured independent parameter. Kline and McClintock (1953) method was used to estimate the derive uncertainties of dependent parameter, which is describes as follow:

Let the function N is given as a function of all the independent variables

$$N = N(x_1, x_2, x_3 \ldots\ldots\ldots\ldots\ldots\ldots\ldots\ldots x_n)$$

The derived uncertainty from all these independent measured variables is given by:

$$\Delta N = \sqrt{\left(\frac{\partial N}{\partial x_1}\Delta x_1\right)^2 + \left(\frac{\partial N}{\partial x_2}\Delta x_2\right)^2 + \cdots + \left(\frac{\partial N}{\partial x_n}\Delta x_n\right)^2}$$

where $\Delta x_1$, $\Delta x_2$, $\Delta x_3$…….....$\Delta x_n$ are the errors in the measured quantities.

The estimation of the derived uncertainties is performed using Engineering Equation Solver (EES) software and the parameters that are considered while estimating refrigerant heat transfer coefficient are given below:

Temperature difference ($\Delta T$) is given by:

$$\Delta T = T_{wo} - T_{wi} = 4.1\ ^\circ\text{C}$$

$$\Delta(\Delta T) = \sqrt{\left(\frac{\partial \Delta T}{\partial T_{wo}}\ \Delta T_{wo}\right)^2 + \left(\frac{\partial \Delta T}{\partial T_{wi}}\ \Delta T_{wi}\right)^2}$$

$$\Delta(\Delta T) = \sqrt{(1 \times 0.15)^2 + (-1 \times 0.15)^2} = \pm 0.2121$$

$$\frac{\Delta(\Delta T)}{\Delta T} = \frac{\pm 0.2121}{4.1} = \pm 5.2\ \%$$

Heat transfer in water side ($Q_w$) is given by:

$$Q_w = m_w C_{pw} \Delta T = 2.274 \text{ kW}$$

$$\Delta Q_w = \sqrt{\left(\frac{\partial Q_w}{\partial m_w} \Delta m_w\right)^2 + \left(\frac{\partial Q_w}{\partial \Delta T} \Delta(\Delta T)\right)^2} = \pm 0.1175$$

$$\frac{\Delta Q_w}{Q_w} = \frac{\pm 0.1175}{2.274} = \pm 5.2\ \%$$

Logarithmic mean temperature difference ($\Delta T_{ln}$):

$$\Delta T_{ln} = \frac{(DT1 - DT2)}{ln\left(\frac{DT}{DT2}\right)} = 10.5\ ^\circ\text{C}$$

$$DT1 = T_s - T_{wi} = 8.6\ ^\circ\text{C}$$

$$DT2 = T_s - T_{wo} = 12.7\ ^\circ\text{C}$$

$$\Delta\ (\Delta T_{\ln}) = \sqrt{\left(\frac{\partial(\Delta T_{ln})}{\partial DT1} \Delta DT1\right)^2 + \left(\frac{\partial(\Delta T_{ln})}{\partial DT2} \Delta DT2\right)^2} = \pm 0.1532$$

$$\frac{\Delta\ (\Delta T_{\ln})}{\Delta T_{\ln}} = \frac{\pm 0.1532}{10.51} = \pm 1.5\ \%$$

Overall heat transfer coefficient ($U$) is given by:

$$Q_w = UA\Delta T_{ln}$$

$$U = 1885.326 \text{ W/m}^2\text{K}$$

$$\Delta U = \sqrt{\left(\frac{\partial U}{\partial Q_w} \Delta Q_w\right)^2 + \left(\frac{\partial U}{\partial \Delta T_{ln}} \Delta(\Delta T_{ln})\right)^2} = \pm 103.6$$

$$\frac{\Delta U}{U} = \frac{\pm 103.6}{1885.326} = \pm 5.5\ \%$$

Water heat transfer coefficient ($h_w$) is given by:

$$h_w = 0.25 \frac{\lambda_w}{D_{hw}} {Re_w}^{0.4} Pr^{0.3} = 1568.329 \text{ W/m}^2\text{K}$$

$$\Delta h_w = \sqrt{\left(\frac{\partial h_w}{\partial m_w}\,\Delta m_w\right)^2 + \left(\frac{\partial h_w}{\partial D_{hw}}\,\Delta D_{hw}\right)^2 + + \left(\frac{\partial h_w}{\partial A_{fr}}\,\Delta A_{fr}\right)^2} = \pm 55.15$$

$$\frac{\Delta h_w}{h_w} = \frac{\pm 55.15}{1568.329} = \pm 3.5\ \%$$

Refrigerant heat transfer coefficient ($h_r$) is given by:

$$\frac{1}{U} = \frac{1}{\eta_{or} h_r} + \frac{t}{\lambda\left(\frac{A_p}{A_r}\right)} + \frac{1}{\eta_{ow} h_w \left(\frac{A_w}{A_r}\right)}$$

$$h_r = 5018.52\ \text{W/m}^2\text{K}$$

$$\Delta h_r = \sqrt{\left(\frac{\partial h_r}{\partial U}\,\Delta U\right)^2 + \left(\frac{\partial h_w}{\partial h_w}\,\Delta h_w\right)^2} = \pm 506.7$$

$$\frac{\Delta h_r}{h_r} = \frac{\pm 506.7}{5018.82} = \pm 10.1\ \%$$

Frictional Pressure drop ($\Delta P_f$) is given by:

$$\Delta P_f = \Delta P_t - \Delta P_c + \Delta P_a + \Delta P_g = 2.984\ \text{kPa}$$

$$\Delta\,(\Delta P_f) = \sqrt{\left(\frac{\partial \Delta P_f}{\partial m_r}\,\Delta m_r\right)^2 + \left(\frac{\partial \Delta P_f}{\partial \Delta P_t}\,\Delta(\Delta P_t)\right)^2} = \pm 0.04834$$

$$\frac{\Delta\,(\Delta P_f)}{\Delta P_f} = \frac{\pm 0.04834}{2.984} = \pm 1.6\ \%$$

**List of publications**

The major outcomes from the present thesis work have been published in renowned international journals and presented in reputed conference. The list of all the publications is shown below.

**International Journal Publications**

1. P.P. Kemprai, K.V. Ramana Murthy, C. Ranganayakulu, P. Muthukumar, Experimental investigation on condensation heat transfer coefficient and frictional pressure drop of low GWP refrigerant R1234yf on a wavy fin surface, Thermal Science and Engineering Progress, 47 (2024) 102300. https://doi.org/10.1016/j.tsep.2023.102300.

2. P.P. Kemprai, K.V. Ramana Murthy, P. Muthukumar, C. Ranganayakulu, Estimation of condensation heat transfer coefficient and pressure drop of R1234yf inside a brazed plate serrated fin heat exchanger, Thermal Science and Engineering Progress, 59 (2025) 103311. https://doi.org/10.1016/j.tsep.2025.103311.

**International Conference Publications**

3. P.P. Kemprai, K.V. Ramana Murthy, P. Muthukumar, C. Ranganayakulu, Experiments on condensation heat transfer and pressure drop of low GWP refrigerant R1234yf inside a brazed plate serrated fin heat exchanger presented at 8$^{th}$ National and 2$^{nd}$ International Conference on Refrigeration and Air Conditioning (NCRAC 2024), March 13-15, IIT Madras.

4. P.P. Kemprai, C. Ranganayakulu, P. Muthukumar, Numerical and experimental investigation in compact heat exchanger surfaces with wavy Fins, presented at 25$^{th}$ National and 3$^{rd}$ International ISHMT-ASTFE Heat and Mass Transfer Conference (IHMTC 2019), December 28-31, IIT Roorkee.